The Effects of a Protein Osmolyte, Detergent Headgroup, and Detergent Chain Length on the Stability of the Integral Membrane Protein Glycerol Facilitator

by

Simon Baturin

A Thesis submitted to the Faculty of Graduate Studies of

The University of Manitoba

in partial fulfilment of the requirements of the degree of

MASTER OF SCIENCE

Department of Chemistry

University of Manitoba

Winnipeg

THE UNIVERSITY OF MANITOBA

FACULTY OF GRADUATE STUDIES

*****

COPYRIGHT PERMISSION

The Effects of a Protein Osmolyte, Detergent Headgroup, and Detergent Chain Length on the Stability of the Integral Membrane Protein Glycerol Facilitator

BY

Simon Baturin

A Thesis/Practicum submitted to the Faculty of Graduate Studies of The University of Manitoba in partial fulfillment of the requirement of the degree

Of

Master of Science

"Success is the ability to go from one failure to another with no loss of enthusiasm"

- Winston Churchill

Table of Contents:

THE EFFECTS OF PROTEIN OSMOLYTES, DETERGENT HEADGROUP, AND DETERGENT CHAIN LENGTH ON THE STABILITY OF THE INTEGRAL MEMBRANE PROTEIN GLYCEROL FACILITATOR 1

TABLE OF CONTENTS: 3

LIST OF FIGURES: 6

ABBREVIATIONS: 12

ABSTRACT: 13

CHAPTER I: INTRODUCTION 14

1.1 The Cellular Membrane: 14

1.1.1 Membrane Composition *14*

1.1.3 Membrane Proteins *17*

1.1.3.1 Aquaporins *20*

1.1.3.2 Glycerol Facilitator *22*

1.2 Protein Folding: 27

1.3 Membrane Protein Insertion: 29

1.4 Membrane Protein Folding: 30

1.5 Osmolytes: 31

1.6 Dynamic Light Scattering: 33

1.8 Goals of the Research: 34

CHAPTER II: MATERIALS AND METHODS 35

2.1 MATERIALS: 35

2.2 METHODS: 36

2.2.1 Glycerol Facilitator Expression and Purification 36

2.2.2 Electrophoresis: 37

2.2.3 Dynamic Light Scattering Studies: 39

2.2.4 Gel Scanning and Curve Fitting 39

2.2.5 Error Calculation 40

CHAPTER III: RESULTS 41

3.1 GLPF IN DODECYL-B-D MALTOSIDE 41

3.1.1 SDS Denaturations at Various Temperatures 42

3.1.2 GlpF Renaturation Experiments. 49

3.1.3 SDS Denaturations at Various Temperatures in the Presence of a Protein Osmolyte. 52

3.1.4 Thermal Denaturations in the Presence and Absence of TMAO. 58

3.1.5 Kinetic Studies at Various Temperatures. 62

3.1.6 Dynamic Light Scattering Heat Denaturations of GlpF in Absence and Presence of TMAO. 66

3.2 GLPF IN N-TETRADECYL-B-D MALTOSIDE 80

3.2.1 SDS Denaturations at 40°C in the Presence and Absence of 4 M TMAO. 81

3.2.2 Concentration Dependence of TMAO 84

3.2.3 Thermal Denaturations in the Presence and Absence of TMAO. 88

3.2.4 Dynamic Light Scattering Heat Denaturations on GlpF in Presence and Absence of TMAO. *91*

3.3 GLPF IN 1-LAUROYL-2-HYDROXY-SN-GLYCERO-3-PHOSPHOCHOLINE 99

3.3.1 SDS Denaturations at 40°C in the Presence and Absence of 4 M TMAO. *99*

3.3.2 Concentration Dependence of TMAO. *102*

3.3.3 Thermal Denaturations in the Presence and Absence of TMAO. *107*

3.3.4 Dynamic Light Scattering Heat Denaturations on GlpF in Presence and Absence of TMAO. *110*

3.4 GLPF IN 1-MYRISTOYL-2-HYDROXY-SN-GLYCERO-3-PHOSPHOCHOLINE 117

3.4.1 SDS Denaturations at 40°C in the Presence and Absence of 4 M TMAO. *117*

3.4.2 Concentration Dependence of TMAO. *119*

3.4.3 Thermal Denaturations in the Presence and Absence of TMAO. *124*

3.4.4 Dynamic Light Scattering Heat Denaturations on GlpF in the Absence and Presence of TMAO. *127*

CHAPTER IV: DISCUSSION 135

4.1 CHEMICAL STABILITY OF MEMBRANE PROTEINS. 135

4.2 CHEMICAL STABILITY OF GLPF IN THE PRESENCE AND ABSENCE OF TMAO 140

4.4 THERMAL STABILITY OF MEMBRANE PROTEINS. 146

4.4 THERMAL STABILITY OF GLPF IN THE PRESENCE AND ABSENCE OF TMAO 148

4.5 DYNAMIC LIGHT SCATTERING INVESTIGATIONS OF GLPF 151

4.6 FUTURE WORK 157

List of Figures:

Figure 1: Joint ribbon diagram and space-filling model of the AQP1 monomer viewed parallel to the membrane..... 22

Figure 2: The GlpF tetramer. 23

Figure 3: The transmission of Glycerol-2, (G2) Glycerol-3 (G3), and water through the GlpF selectivity filter. 26

Figure 4: Schematic illustration of a dimeric protein folding pathway. 28

Figure 5: SDS-PAGE showing a 22°C SDS denaturation of GlpF in DDM. 43

Figure 6: SDS-PAGE showing a 22°C SDS denaturation of GlpF in DDM. 44

Figure 7: Mathematica graph showing the dissociation of tetramer to monomer at 22°C. 45

Figure 8: SDS-PAGE showing a 40°C SDS denaturation of GlpF in DDM. 46

Figure 9: SDS-PAGE showing a 40°C SDS denaturation of GlpF in DDM. 47

Figure 10: Mathematica graph showing the dissociation of tetramer to monomer at 40°C. 48

Figure 11: SDS-PAGE showing GlpF renaturation experiment in DDM. 50

Figure 12: SDS-PAGE showing GlpF renaturation experiment in DDM. 51

Figure 13: SDS-PAGE showing a 22°C SDS denaturation of GlpF in DDM in the presence of 0.6 M TMAO. 53

Figure 14: SDS-PAGE showing a 22°C SDS denaturation of GlpF in DDM in the presence of 0.6 M TMAO. 54

Figure 15: SDS-PAGE showing a 40°C SDS denaturation of GlpF in DDM in the presence of 4 M TMAO. 55

Figure 16: SDS-PAGE showing a 40°C SDS denaturation of GlpF in DDM in the presence of 4 M TMAO. 56

Figure 17: Mathematica graph showing the dissociation of tetramer to monomer. 57

Figure 18: SDS-PAGE showing a temperature denaturation of GlpF in DDM. 59

Figure 19: SDS-PAGE showing a temperature denaturation of GlpF in DDM in the presence of 0.6 M TMAO. 60

Figure 20: SDS-PAGE showing a temperature denaturation of GlpF in DDM in the presence of 4 M TMAO. 61

Figure 21: Mathematica graph showing the thermal dissociation of tetramer to monomer. 62

Figure 22: SDS-PAGE showing a kinetic stability experiment of GlpF in DDM in the presence and absence of 0.6 M TMAO after 48 hours. 63

Figure 23: SDS-PAGE showing a kinetic stability experiment of GlpF in DDM in the presence and absence of 0.6 M TMAO after 26 days. 65

Figure 24: SDS-PAGE showing a kinetic stability experiment of GlpF in DDM in the presence and absence of 0.6 M TMAO after 55 days. 66

Figure 26: DLS of DDM at several temperatures. 68

Figure 27: DLS in the presence of GlpF in DDM at several temperatures 69

Figure 28: DLS of 4 M TMAO in DDM at several temperatures. 72

Figure 29: DLS of GlpF in 4 M TMAO and DDM at several temperatures. 74

Figure 30: DLS thermal renaturation in the presence of GlpF in DDM. 77

Figure 31: DLS thermal renaturation in the presence of GlpF in DDM. 78

Figure 32: DLS thermal renaturation in the presence of GlpF and 4 M TMAO in DDM. 79

Figure 34: SDS-PAGE showing a 40°C SDS denaturation of GlpF in TDM. 82

Figure 35: Mathematica graph showing the dissociation of tetramer to monomer in TDM at 40°C. 83

Figure 36: SDS-PAGE showing a 40°C SDS denaturation of GlpF dissolved in TDM in the presence of 4 M TMAO. 84

Figure 37: SDS-PAGE showing a 40°C SDS denaturation of GlpF in TDM in the presence of 0.5 M TMAO. 85

Figure 38: SDS-PAGE showing a 40°C SDS denaturation of GlpF in TDM in the presence of 1 M TMAO. 86

Figure 39: SDS-PAGE showing a 40°C SDS denaturation of GlpF in TDM in the presence of 2 M TMAO. 87

Figure 40: Mathematica graph showing the dissociation of tetramer to monomer in TDM. 88

Figure 41: SDS-PAGE showing a temperature denaturation of GlpF in TDM. 89

Figure 42: SDS-PAGE showing a temperature denaturation of GlpF in TDM in the presence of 4 M TMAO. 90

Figure 43: DLS of TDM at several temperatures. 92

Figure 44: DLS of GlpF in TDM at several temperatures. 93

Figure 45: DLS of TDM in the presence of 4 M TMAO at several temperatures. 96

Figure 46: DLS thermal denaturation in the presence of GlpF and 4 M TMAO in TDM at several temperatures..... 97

Figure 47: SDS-PAGE showing a 40°C SDS denaturation of GlpF in LLPC..... 100

Figure 48: Mathematica graph showing the dissociation of tetramer to monomer in LLPC at 40°C..... 101

Figure 49: SDS-PAGE showing a 40°C SDS denaturation of GlpF in LLPC in the presence of 4 M TMAO..... 102

Figure 50: SDS-PAGE showing a 40°C SDS denaturation of GlpF in LLPC in the presence of 0.5 M TMAO..... 103

Figure 51: SDS-PAGE showing a 40°C SDS denaturation of GlpF in LLPC in the presence of 1 M TMAO..... 104

Figure 52: SDS-PAGE showing a 40°C SDS denaturation of GlpF in LLPC in the presence of 2 M TMAO..... 105

Figure 53: Mathematica graph showing the dissociation of GlpF tetramer to monomer in LLPC..... 106

Figure 54: SDS-PAGE showing a temperature denaturation of GlpF in LLPC..... 108

Figure 55: SDS-PAGE showing a temperature denaturation of GlpF in LLPC in the presence of 4 M TMAO..... 109

Figure 56: DLS of LLPC at several temperatures..... 110

Figure 57: DLS of GlpF in LLPC at several temperatures..... 111

Figure 58: DLS of LLPC in 4 M TMAO at several temperatures..... 114

Figure 59: DLS of GlpF in LLPC and 4 M TMAO at several temperatures..... 115

Figure 60: SDS-PAGE showing a 40°C SDS denaturation of GlpF in LMPC..... 118

Figure 61: SDS-PAGE showing a 40°C SDS denaturation of GlpF in LMPC in the presence of 4 M TMAO. 119

Figure 62: SDS-PAGE showing a 40°C SDS denaturation of GlpF in LMPC in the presence of 0.5 M TMAO. 120

Figure 63: SDS-PAGE showing a 40°C SDS denaturation of GlpF in LMPC in the presence of 1 M TMAO. 121

Figure 64: SDS-PAGE showing a 40°C SDS denaturation of GlpF in LMPC in the presence of 2 M TMAO. 122

Figure 65: Mathematica graph showing the SDS-induced dissociation of GlpF tetramer in LMPC at 40°C. 123

Figure 66: SDS-PAGE showing a temperature denaturation of GlpF in LMPC. 125

Figure 67: SDS-PAGE showing a temperature denaturation of GlpF in LMPC in the presence of 4 M TMAO. 126

Figure 68: DLS of LMPC at various temperatures. 128

Figure 69: DLS of GlpF in LMPC at several temperatures. 130

Figure 70: DLS of LMPC in the presence of 4 M TMAO. 131

Figure 71: DLS thermal denaturation in the presence of GlpF and 4 M TMAO in LMPC. 132

List of Tables:

Table 1: SDS_{half} values at given temperatures in DDM calculated from Mathematica 49

Table 2: DDM Small Particle Diameters at Different Temperatures 70

Table 3: DDM Large Particle Diameters at Different Temperatures 70

Table 4: DDM Intermediate Particle Diameter at Different Temperatures 71

Table 5: Small Particle Diameters at Different Temperatures in DDM with 4 M TMAO 72

Table 6: Large Particle Diameters at Different Temperatures in DDM with 4 M TMAO 72

Table 7: Small Particle Diameters at Different Temperatures in DDM with 4 M TMAO 75

Table 8: Large Particle Diameters at Different Temperatures in DDM with 4 M TMAO 75

Table 9: Particle Diameters at Different Temperatures in First Peak in DDM with 4 M TMAO 77

Table 10: TDM Small Particle Diameters at Different Temperatures 94

Table 11: TDM Large Particle Diameters at Different Temperatures 95

Table 12: Small Particle Diameters at Different Temperatures in TDM with 4 M TMAO 98

Table 13: Large Particle Diameters at Different Temperatures in TDM with 4 M TMAO 98

Table 13: LLPC Small Particle Diameters at Different Temperatures 112

Table 14: LLPC Large Particle Diameters at Different Temperatures 113

Table 15: Small Particle Diameters at Different Temperatures in LLPC with 4 M TMAO 116

Table 16: Large Particle Diameters at Different Temperatures in LLPC with 4 M TMAO 116

Table 17: SDS_{half} Values for GlpF Tetramer Dissociation all Detergents at Specific TMAO Concentrations 124

Table 18: T_m values in different concentrations of TMAO 127

Table 19: LMPC Small Particle Diameters at Different Temperatures 130

Table 20: LMPC Large Particle Diameters at Different Temperatures 130

Table 21: Small Particle Diameters at Different Temperatures in LMPC with 4 M TMAO 133

Table 22: Intermediate Particle Diameters at Different Temperatures in LMPC with 4 M TMAO 133

Table 23: Large Particle Diameters at Different Temperatures in LMPC with 4 M TMAO 134

Abbreviations:

AQP, aquaporin; Bis-Tris, Bis(2-hydroxyethyl)-amino-tris(hydroxymethyl)methane; CD, circular dichroism; DDM, dodecyl-β-D-maltoside; TDM, tetradecyl-β-D-maltoside; GlpF, glycerol facilitator; kDa, kilodalton; LMPC, lyso-myristoylphosphatidyl choline; LLPC, lyso-lauroylphosphatidyl choline; M_r, relative mass; NMR, Nuclear Magnetic Resonance; NTA, nitrilotriacetic acid; OG, octyl-β-D-glucopyranoside; PAGE, polyacrylamide gel electrophoresis; SDS sodium dodecyl sulphate; SRP, signal-recognition particle; Tris, tris(hydroxymethyl)aminomethane; UV, ultra-violet; TMAO, trimethylamine N-oxide; DLS, dynamic light scattering; ND, not determinable.

Abstract:

One of the main impediments to membrane protein research is the lower stability of the proteins following their removal from the lipid bilayer. Osmolytes are naturally-occurring molecules used by a wide variety of organisms to stabilize proteins under conditions of high salinity, high hydrostatic pressure, desiccation, and high and low temperatures. Osmolytes have also been shown to protect proteins from chemical denaturants such as urea in kidney cells. The results of studies to determine the effects of the osmolyte trimethylamine N-oxide (TMAO) on the stability of the *E. coli* integral membrane protein glycerol facilitator (GlpF) are presented. TMAO promoted the association of the normally tetrameric α-helical protein into an octameric species in dodecyl-maltoside (DDM), but not in tetradecyl-maltoside (TDM), lyso-lauroylphosphatidyl choline (LLPC), or lyso-myristoylphosphatidyl choline (LMPC). Both the tetramer and octamer are significantly more heat stable in the presence of TMAO. The osmolyte also stabilizes the protein against denaturation by sodium dodecyl sulphate (SDS). A concentration-dependence of TMAO in stabilizing against SDS denaturation was also observed in all detergents, with high levels of octamer in DDM only being found at high TMAO concentrations. Protein structure was monitored by sodium dodecyl sulphate-polyacrylamide gel electrophoresis (SDS-PAGE) and dynamic light scattering (DLS). The latter technique was applied to a membrane protein for the first time.It is also found that the protein is more stable in detergents with the phosphatidylcholine head group (LLPC and LMPC), and the least stable in TDM. These results may contribute to improved methodology for studying membrane proteins and a better understanding of membrane protein structure, folding and dynamics.

Chapter I: Introduction

1.1 The Cellular Membrane:

All cells in nature are surrounded by a lipid bilayer that contains many different proteins. It functions to define the peripheral boundaries of cells and internal lipid bilayers define the cells internal compartments. It also controls the molecular traffic that flows across those boundaries. These lipid bilayers are the scaffold that participates in and houses all the cellular machinery which is responsible for the formation of electrochemical gradients across the membrane (e.g. cellular energy development), cell to cell communication, and assisting in the transport of essential materials across the membrane (e.g. water, ions, DNA, protein). The membrane also forms a structure to allow for membrane associated proteins to assist in maintaining the cell's shape whilst being flexible and self-sealing, thus allowing for the shape changes that accompany cellular growth and movement.

1.1.1 Membrane Composition

The membrane composition and structure have been described by a 'fluid mosaic model' [1]. This model depicts cellular membranes as fluid bilayers with a mosaic of lipids and embedded proteins, which exhibit both structural and functional asymmetry. Typical biological membranes are about 30 Å to 50 Å thick with a hydrophobic region about 20 Å wide [2]. The fluidity aspect of the model is that membrane proteins are

allowed to freely diffuse laterally throughout the membrane, unless their movements have been restricted through association with other cellular components.

The relative amounts of specific lipids on the inner and outer leaflets of the membrane can vary widely, although the asymmetry is not absolute and the composition varies depending on the organism [3, 4]. Membrane proteins called flipases specifically function to flip phospholipids across the membrane bilayer to cause the asymmetric distribution in the two membrane leaflets. In some cells the presence of high levels of a specific type of lipid on the exterior of a cell can induce a particular cellular response (e.g. phosphatidylserine on the outside of many cells induces blood clotting in higher organisms) [5]. Lipids can also be organized in a membrane into two or more types of individual domains where there are specific segments of the membrane that contain large numbers of a particular type of lipid. These lipid sections can persist for a period of time, and have a related function to lipid-anchored proteins. Membrane domains have been shown in certain cases to coordinate membrane activities by either concentrating interacting molecules in particular areas of the surface, or by excluding molecules and so preventing their interaction. An example of this is a 'lipid raft' in which there is a subdomain of the membrane that is composed of tightly packed glycosphingolipids, cholesterol, protein receptors, and signalling molecules [6].

There are several molecules that are able to cross the membrane without any type of transport mechanism: oxygen, nitrogen, and methane, which are all relatively non-polar molecules and biologically significant. Water, despite its polarity can permeate the membrane most likely because of its very high concentration (55 M), but only very

slowly and facilitated diffusion is required in membranes that necessitate the rapid transit of water molecules (e.g. kidney cells) [7].

1.1.2 Lipids

Lipids are the basic structural element of membranes, and they form the fourth major group of molecules found in all cells by relative mass. They are an extensive family of amphipathic biological molecules that are predominantly hydrophobic and therefore tend to self-associate in water. There are several major classes of lipids that are found in cellular membranes. The first of these are fatty acids, which are carboxylic acids with long alkyl chains that are typically found in an esterified form within the membrane. Glycerophospholipids are the second class and comprise the principal component of cellular membranes. They are composed of a glycerol-3-phosphate in which the C1 and C2 positions are esterified with fatty acids. Sphingolipids are the third large class membrane lipids and they are similar to Glycerophospholipids in that they have two non-polar alkyl chains, but they do not include a glycerol backbone. Sphingolipids possess one molecule of sphingosine or one of its derivatives (a long-chain amino alcohol), to which a long alkyl chain and a polar head group (phosphocholine or sugars) are attached. Sterols are the last major group of lipids in cellular membranes and they serve as structural lipids due to their fused ring system which provides it with greater rigidity than other membrane lipids [8].

1.1.3 Membrane Proteins

There are two distinct families of membrane proteins that are found in all cells: integral and peripheral. Integral proteins are situated directly in the membrane and can only be removed from the membrane by detergents and/or organic solvents. Peripheral proteins are associated with the membrane through electrostatic interactions and hydrogen bonding to the charged lipid headgroups, and polar and charged amino acid residues from the interfacial hydrophilic sections of integral membrane proteins. Peripheral membrane proteins can easily be dissociated from the membrane, and are essentially soluble proteins that have an affinity for the membrane. Integral membrane proteins have two distinct structural motifs; α-helical bundles and β-barrels, and they are held in the membrane by hydrophilic and hydrophobic interactions between the protein and the lipid bilayer. The interior amino acids are almost exclusively non-polar and are packed just as tightly as soluble proteins [9]. There is very little H-bonding in between the α-helices of integral membrane proteins except in the participating helices of the pore in pore-forming proteins. The surface amino acids that face the hydrophobic portion of the membrane are less polar in transmembrane α-helices and β-barrels than in their soluble counterparts. Because of the 30 Å membrane that needs to be traversed, the average length of the secondary structural elements are longer in membrane proteins than soluble proteins, with membrane proteins possessing α-helices that are more than 20 amino acids in length and β-strands that are more than 10 amino acids [10]. Hydropathy plots have been very useful in predicting the topology of α-helical membrane proteins [11, 12]. One of the most distinguishable characteristics of membrane proteins is the preference for certain amino acids at specific positions in the protein. Examples of this

situation are arginine and lysine being much more abundant on the cytoplasmic face of the protein (giving rise to the 'positive-inside' rule to predict membrane topology) [13], and the very large inclination for aromatic residues (specifically tryptophan and tyrosine), to be located in interfacial positions in the protein.

There are several different functions that are carried out by specific groups of membrane proteins involving both passive and active transport. In passive transport a substance that is too large or polar to freely diffuse across the lipid bilayer can flow from high concentration to low concentration via membrane proteins that are variously called carriers, permeases, porins, channels, facilitators, and transporters. These proteins lower the activation energy required to transport polar or large molecules across the membrane by supplying an alternative path for these molecules to cross the membrane without any chemical modification. In active transport the process is thermodynamically unfavourable (endergonic) because a molecule is transported against the chemical and/or electrostatic gradient (the electrochemical gradient). This requires the transport to be coupled to an acceptable exergonic process to make the transport achievable such as the absorption of light, the breakdown of ATP, or the simultaneous flow of another molecule down its electrochemical gradient [8].

There are various types of passive transport that are worth discussing. The first of these is ionophores, which are of bacterial origin and increase the permeability of the membrane to ions such as potassium and sodium. There are two different kinds of ionophores: carrier ionophores which transport ions by diffusing through the membrane with the bound ion (e.g. valinomycin – transport of K^+), and channel-forming ionophores which form a channel across the membrane to allow the free diffusion of specific ions

(e.g. gramicidin A – transport of K^+ and Na^+) [14]. Porins are the next group of passive transporters and they consist of α-helices and β-barrel structures with a central aqueous channel. Porins regulate the type of molecules that they transport by controlling the size of the channel and the residues that form its walls. A few examples of a porin membrane protein are OmpF (which is a weakly cation selective outer membrane protein), OmpX (a family of outer membrane virulence factors that control the ability of pathogenic Gram-negative bacteria to oppose the host defence system)[15], maltoporin (an outer membrane protein that allows the diffusion of maltodextrins across the membrane), GluT1 (a 12 transmembrane α-helical glucose transporter in erythrocytes), and aquaporins (a family of membrane proteins that allow the rapid passage of water in many different tissues and organisms, and will be discussed in more detail in the following section).

Ion channels comprise a large group of intrinsic membrane proteins that are found in every cell and allow the rapid passage of ions such as Cl^-, K^+, and Na^+ across the membrane. The movement of ions through the membrane is essential for maintaining the electrochemical balance, osmotic pressure, and several cellular pathways such as neurotransmission. An example of a well studied ion channel is the potassium channel KcsA in *Streptomyces lividans*, which is an α-helical tetrameric integral membrane protein that has a selectivity filter allowing the passage of K^+ ions and not Na^+ ions [16, 17].

Transport proteins are the final group of membrane protein passive transporters worth discussing. These proteins undergo conformational changes to allow the passage of substances across the membrane. An example of a transport protein is the glucose transporter GLUT1 in humans, which binds glucose on one side of the membrane causing

a conformational change in the protein that exposes the binding site on the other side of the membrane. This allows the glucose molecule to dissociate from GLUT1 on the other side of the membrane and GLUT1 reverts back to its original conformation completing the transport cycle [8].

1.1.3.1 Aquaporins

The aquaporins (AQPs) are a large family of intrinsic membrane proteins that allow the rapid transit of water, glycerol, and several linear alcohols across the cellular membrane. The first aquaporin (AQP1) was discovered by Peter Agre in 1991 [18], and subsequently was characterized in his lab [18-20]. There are now more than 150 different aquaporin sequences that are known from bacteria, yeast, humans, and plants [21]. They are known to be involved with many different illnesses such as kidney abnormalities, loss of eyesight, arsenic toxicity, and the beginning of brain edema in their wild-type and/or variant forms [22]. There are two distinct subgroups in this protein family: the aquaporins and the aquaglyceroporins. The aquaporins transport only water, whereas the aquaglyceroporins transport water, glycerol, urea, and several alditols (linear sugars/alcohols) [23]. They form homo-tetramers in which each monomer is composed of six transmembrane spanning α-helices that form an hour-glass pore, and two half-membrane spanning loops in which one half of the loop contains a highly conserved Asn-Pro-Ala (NPA) motif and the other is α-helical. The non-helical section of the loops containing the NPA motif defines a curvilinear conduction pathway in the pore through the organization of the carbonyl groups of the peptide backbone. The α-helical sections of the half-spanning loops are arranged in a head-to-head fashion that allows the NPA

motifs to come in close proximity to each other and the macro-dipoles of the helices to point their positive ends towards the selectivity filter and centre of the channel (Figure 1).

Molecular dynamics studies have shown that AQP1 and glycerol facilitator (GlpF – a member of the AQP family), can house nine water molecules in their narrow pores and that the orientation of the water molecules is closely related to their transportation across the membrane [24, 25]. The water molecules are arranged in a hydrogen bonded chain, and as the water molecules transfer through the membrane their orientation changes at the NPA motifs. The first five water molecules have their hydrogen atoms pointing towards the extracellular side, the sixth water molecule donating hydrogen bonds to water molecules on both sides, and the remaining three water molecules with their hydrogen atoms facing the cytoplasmic side of the membrane. Transfer of the orientation of the water molecules at the selectivity filter is due to the polarity of the half-spanning helices and the two amide groups in the NPA motifs [24-26]. The actual width of the selectivity filter (also known as the constriction region), is about 2.8 Å wide, which is the van der Waals diameter of a water molecule [27]. This process allows the specific bipolar passage of water through the pore without allowing any H^+ or OH^- through the pore that would eliminate the electrochemical membrane potential and kill the cell [28].

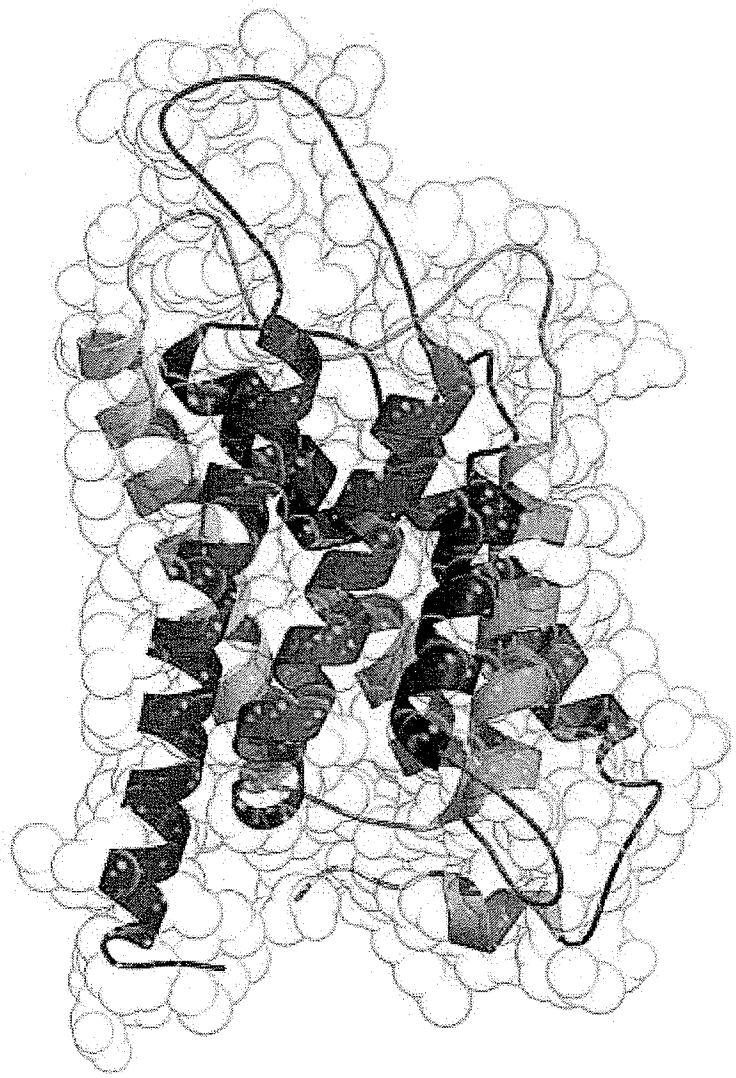

Figure 1: Joint ribbon diagram and space-filling model of the AQP1 monomer viewed parallel to the membrane. Each α-helix in the seven transmembrane monomer is shown in a different colour. Reprinted from [29] with permission.

1.1.3.2 Glycerol Facilitator

As stated in the previous section, glycerol facilitator (GlpF – Figure 2) is a selective integral membrane protein in the aquaporin super-family, and aquaglyceroporin

sub-family that allows the transfer of glycerol, water, urea, glycine, DL-glyceraldehyde, and numerous alditols across the membrane [30]. The structure of GlpF in *E. coli* was confirmed to a resolution of 2.2 Å [21, 29, 31], and the monomer is approximately 60 Å from the periplasmic to the cytoplasmic side of the membrane and 40 Å wide [29]. Each monomer consists of a right-handed helical bundle of six transmembrane and two half-spanning α-helices referred to as M1 through M8, and it is these helices that surround the glycerol conducting pore. The inter-monomer helix angles between M1 and M2 of one monomer, and M5 and M6 of the neighbouring monomer are about -20° [21].

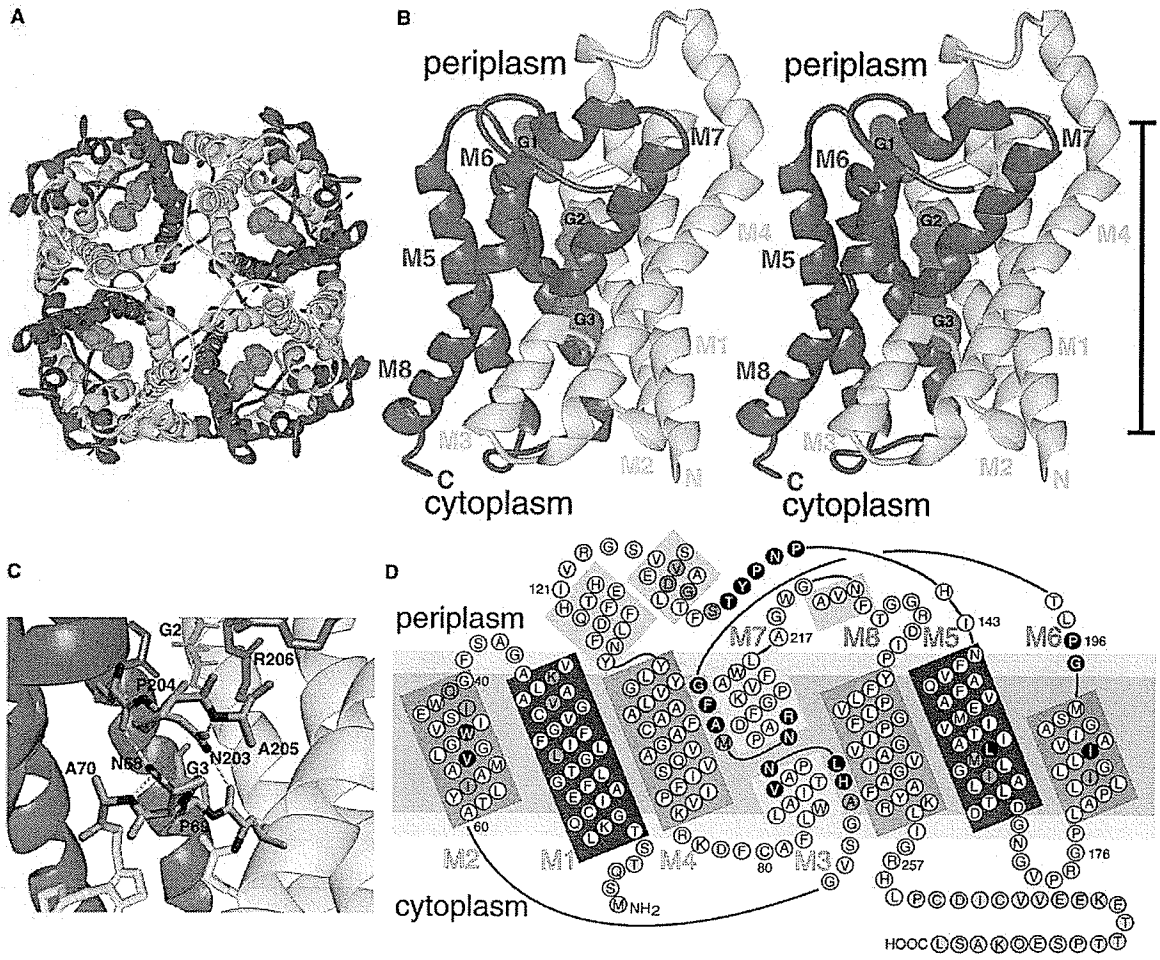

Figure 2: The GlpF tetramer with glycerol molecules G1, G2, and G3 coloured magenta in **A** and **B**. (**A**) Ribbon diagram of the GlpF tetramer viewed from the periplasmic side

of the membrane. (**B**) Stereo view of the GlpF monomer with the vertical bar corresponding to the size of the membrane (35 Å). (**C**) Intersection of the NPA motifs. (**D**) Topographical diagram of the GlpF amino acid sequence. Helices M1 and M5, M2 and M6, and so forth are boxed in similar colours to signify their similar roles in the structure. Residues in black circles interact with glycerol. Residues in red circles contribute carbonyl oxygen or amide NHs to the channel. Residues in purple circles supply hydrocarbon to the channel. Gray circles represent residues that are not seen in the structure. The presumed location of the cell membrane is shown in gray. Reprinted from [21] with permission.

The pore of GlpF is slightly dumbbell shaped when viewed along the membrane. This is due to the fact that it has a large cytoplasmic vestibule about 15 Å in diameter, a narrow pore about 40 Å long containing the selectivity filter and constriction region, and a large periplasmic vestibule about 15 Å wide [23]. About half of the pore wall, observed vertically, can be regarded as hydrophobic and the other half as hydrophilic. This is because GlpF has evolved to align the OH groups attached to the glycerol backbone with the carbonyl oxygens of residues on one side of the pore, and the hydrophobic glycerol backbone with the hydrophobic residues on the other side of the pore. This allows for the displacement of certain waters of hydration by a selectivity filter in the protein as glycerol moves through the pore. Approximately 20 Å from the periplasmic vestibule, the pore narrows to a size of about 3.8 Å and comprises the constriction region [29]. After the constriction region lies the selectivity filter that is approximately 28 Å long. In the crystal structure [21], there are three glycerol binding sites in the pore labelled G1,

G2, and G3, which are numbered in order from the periplasmic to the cytoplasmic side of the membrane [31]. G1 is hydrogen bonded to one water molecule and a tyrosine in the periplasmic vestibule. G2 and G3 are located in the selectivity filter of the pore (Figure 3), and there is a hydrogen bond to water bridging the two glycerol molecules suggesting that there is co-transportation of glycerol and water molecules [21, 31]. The selectivity filter at G2 has been termed 'tripathic' because it is made up of two aromatic groups on one side of the pore that form a corner (Trp48 and Phe200), two amino hydrogens from Arg206 on the second side, and two main strand carbonyl oxygens from Gly199 and Phe200 on the third side [21, 23, 29, 31] (Figure 3). It is at this section of the protein that G2 accepts hydrogen bonds from the Arg206 NH groups and donates hydrogen bonds to carbonyl oxygens, at the Trp48 and Phe200 corner. This orientation leaves no added room around G2 such that the van der Waals forces, hydrogen bonding, and electrostatic forces all contribute to the stabilization of G2 and therefore its passage through the pore. It is also at this constriction point that there is a key difference between GlpF and AQP1; in GlpF there is a substitution of His182 for glycine, and Cys191 for phenylalanine. This increases the size and hydrophobicity of the GlpF pore, allowing larger molecules such as glycerol and alditols to be transported across the membrane. At the junction between the two NPA motifs (helices M3 and M7 – Figure 2), G3 is hydrogen bonded to the asparagine from both motifs and a highly conserved His66 residue allowing only the single file movement of glycerol and water through the pore. The NPA motifs are found in both water- and glycerol-selective channels, which suggests that they do not play a role in determining the selectivity of the pore [29]. In the region following the NPA motifs there is a similar hydrophobic and hydrophilic side to the pore, as found on the

periplasmic end of GlpF, which aligns the glycerol molecules as they leave the pore. The pore then begins to gradually widen for the next 10 Å, until the cytoplasmic vestibule is reached.

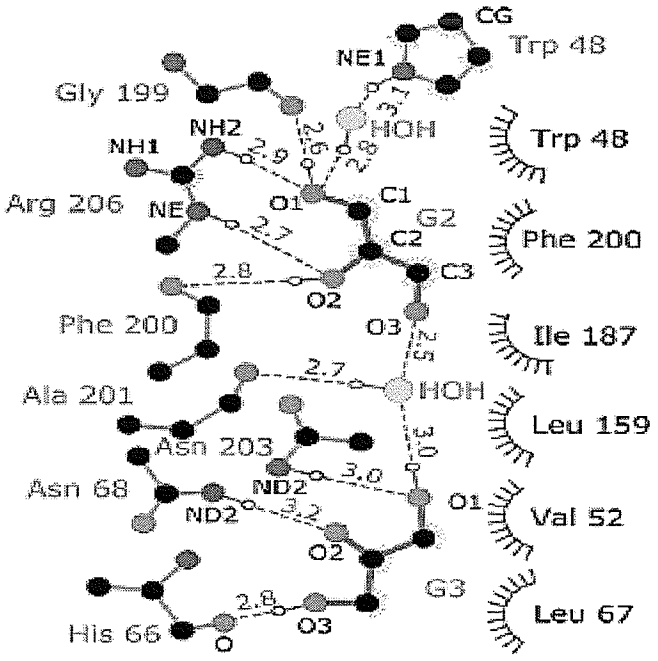

Figure 3: The transmission of Glycerol-2, (G2) Glycerol-3 (G3), and water through the GlpF selectivity filter. The hydrophobic residues are shown with radial lines on the right side of the figure, the red circles are side chain hydroxyl groups, the blue circles are side chain amine groups, and the distances (in Å) between atoms are shown by dotted lines. The top of the figure is the periplasmic side of the pore. Reprinted from [21] with permission.

1.2 Protein Folding:

The amino acid sequence of a protein determines its structure and this was first observed through denaturation experiments on ribonuclease by Anfinsen et al. in 1957 [32]. The "thermodynamic hypothesis" and several other supporting investigations [33-35] explaining that all the information for the folding of a protein is encoded in its amino acid sequence [36], were the first attempts to explain the reversible denaturation observations. This research paved the way for modern concepts of protein folding.

Folding is thought to begin in the formation of local secondary structure segments of α-helices and β-sheets. This first folding event happens very rapidly on the order of microseconds due to the close proximity of the amino acids involved in these structures, although the stability of these intermediates is quite low due to the small number of residues involved [37]. The next step involves the interaction of different secondary structural elements to form a partially collapsed protein termed a 'molten globule' (Figure 4), which has most of the secondary structure of a native protein, but little tertiary structure [38]. The large hydrophobic interactions in the core of proteins also contribute to the formation of the molten globule among the non-polar residues in a process that has been termed 'hydrophobic collapse' [39]. The final steps involve the tightening of the intra-protein secondary structures (or domains), and expulsion of the final water molecules from the hydrophobic core to form a well folded monomer [8]. In multimeric proteins, well folded monomers may interact with each other to form the native multimeric form of the protein, or molten globule-like monomers interact may with one another and cause the tertiary and quaternary constraints to adjust and become more rigid forming the native protein (Figure 4).

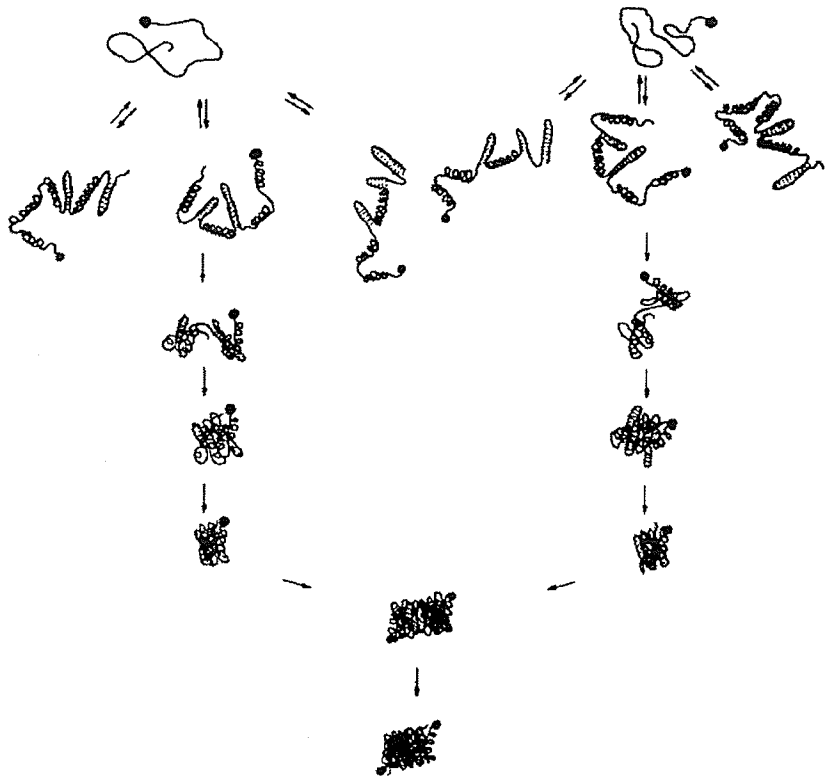

Figure 4: Schematic illustration of a dimeric protein folding pathway. The arrows show how the protein can fold through different folding pathways, sample different reversible secondary structures, interact with different domains to form a 'molten globule', refine the structure of the molten globule into the proper monomer conformation, and then in this specific case the monomers can interact to form the native dimer. Reprinted from [37] with permission.

1.3 Membrane Protein Insertion:

Membrane proteins are inserted into the membrane by two different methods. The first method is spontaneous insertion into the membrane, and the second method inserts membrane proteins through the translocon apparatus. The first method is found in nonconstitutive membrane proteins mellitin [40], colicins [41], diphtheria toxin [42], α-hemolysin [43], and several others and involves soluble proteins that interact with the membrane and insert into the membrane following refolding or assembly [10]. The second process for the endoplasmic reticulum (ER) begins with membrane protein mRNA binding with a ribosome to produce a signal-anchor sequence peptide that is 13 to 36 amino acids in length. This signal-anchor sequence recruits a particle (called a signal-recognition particle – SRP), which binds the ribosome and the signal sequence allowing the ribosome/signal-anchor peptide/SRP complex to bind the membrane-bound translocon and begin protein insertion into the membrane. Once polypeptide synthesis has concluded, the protein dissociates from the ribosome-translocon complex and protein insertion into the membrane has concluded [8, 44]. The translocon apparatus is a piece of cellular machinery in the membrane of the ER that receives elongating protein from the ribosome and directs the newly formed proteins either across or into the membrane bilayer. Because of the favourable free energy cost of about 40 kcal/mol from the hydrophobic effect for placing a transmembrane α-helix composed mainly of non-polar amino acids into a hydrophobic environment, and the unfavourable free energy cost of about 30 kcal/mol from the dehydration of the α-helical peptide backbone, there is a favourable free energy of about 10 kcal/mol for the insertion of a transmembrane α-helix into a biological membrane, assuming a typical 20 amino acid transmembrane helix [45].

1.4 Membrane Protein Folding:

The ultimate goal of membrane protein folding studies is to be able to determine the protein's folded form from the amino acid sequence. The major problem in membrane protein folding is in the insertion of the helix in the hydrophobic membrane. As stated in the previous section, there is a favourable free energy cost for the insertion of a membrane protein because of the non-polar residues that constitute the transmembrane amino acids. The non-polar amino acids that are typically found in these regions are Ala, Ile, Leu, Phe and Val. Because of the polarity of the peptide bonds in a protein, the peptide chain hydrogen bonding has to be exploited in such a way as to reduce the cost of their burial in the hydrophobic membrane. The two structural elements that have been found to fulfill this requirement are α-helices and β-barrels. Obviously there are many more elements that contribute to membrane protein folding such as post-translational modifications (e.g. glycosidic-linkages, phosphorylation, etc.), binding of cofactors (e.g. retinal in bacteriorhodopsin), and the formation of the quaternary structure.

Studies using model peptides have been particularly helpful in providing a framework for understanding membrane protein folding [46]. In one model, unfolded peptides partition from the aqueous solution (or the pore of the translocon) to the bilayer interface, the individual transmembrane α-helices fold at the interface, the helices insert into the membrane bilayer and finally, the α-helices come together within the bilayer forming the protein tertiary structure. It should be noted that very little is known about the formation of the quaternary structure in membrane proteins. It has been hypothesized

that the quaternary structure may form before the tertiary structure formation has completed [47, 48], or that well-folded monomers associate to become the final structure of the protein [49, 50]. Despite these hypotheses, very little is known for certain on the mechanisms of quaternary structure formation in membrane proteins, and in-depth studies investigating these mechanisms are very important for understanding membrane protein folding.

1.5 Osmolytes:

Osmolytes are small organic molecules that are used in the cells of many different water-stressed organisms to maintain cell volume and combat anhydrobiotic, thermal, and pressure stresses. There are many different categories of osmolytes including carbohydrates (e.g. mannitol and trehalose), free amino acids and derivates (e.g. glycine, proline, and ectoine), polyols and derivatives (e.g. glycerol and o-methyl-inositol), and methylamines (e.g. trimethylamine N-oxide and glycine betaine) [51]. Osmolytes are called "compatible solutes" because they do not have detrimental effects on macromolecules. They can be safely up-regulated or down-regulated without any harmful effects, most are neutral at physiological pH, and in many cases they can be used interchangeably even if they are from different chemical categories [52]. The protective qualities of osmolytes can be categorized as either protecting metabolic reactions, or counteracting destabilizing effects on macromolecules. The protection of metabolic processes is believed to be achieved through indirect actions rather than a direct interaction with a certain molecule. The metabolic protective qualities of osmolytes

contribute to antioxidation [53, 54], redox balancing [55], sulphate and sulphide detoxification and storage [56], energy reserve [52], predator repellent [57], and Ca^{2+} modulation [54]. Osmolytes counteract the destabilizing effects on macromolecules in a number of ways including urea inhibition [58], increasing thermostability [59], protection of the membrane from freezing [60], preservation in a dry state (anyhydrobiosis) [61], inorganic ion inhibition [58], and protection from hydrostatic pressure [62].

Trimethylamine N-oxide (TMAO) is a methylamine and it is most commonly found in the tissues of marine organisms [52, 58]. The stabilizing effects of methylamines are generally thought to be caused by the very strong interaction between the methylamine and water which results in osmolyte exclusion from the hydration layers of the peptide backbone, thus causing the unfolded state of the protein to be very unfavourable entropically [58, 63, 64]. The high levels of TMAO in polar fish are thought to decrease the point at which bodily fluids will freeze [65], and TMAO has been shown to counteract the detrimental effects of high hydrostatic pressure in deep-sea animals [66, 67]. TMAO has recently been shown to induce folding in an intrinsically disordered protein AF-1 [68]. Numerous studies of TMAO on urea and GdnHCl-denatured proteins have shown that TMAO counteracts the effects of these pertubants and refolds proteins [69, 70]. In a ratio of 2:1 urea:TMAO, several proteins have exhibited a well folded structure with proper protein activity. The counteracting effects of TMAO on urea denaturation are due to the preferential and very strong interaction between urea and TMAO, therefore reducing or eliminating the interaction between urea and the protein [71]. It has also been shown that the increase in protein stability caused

by TMAO is not due to an increase in the strength of the hydrophobic regions in the protein [71, 72].

1.6 Dynamic Light Scattering:

A molecule in solution will scatter light if it has a polarizability different from its surroundings. The oscillating dipole moment that is induced by the electric field of the incident light beam will radiate in all directions, and the scattered light intensity is related to the scattering angle, the direction of polarization of the incident light, and the solution parameters [73]. Dynamic light scattering (DLS), also known as photon correlation spectroscopy, is a biophysical method used to determine the hydrodynamic radius (R_h) of particles in a solution. DLS measures the instantaneous intensity fluctuation of scattered light caused by the illumination of particles in solution with a laser at a specific wavelength (in our case 633 nm) [74]. The intensity fluctuations are due to the Brownian motion of the molecules and can be related to the size of the particles in solution by the Stokes-Einstein-Sutherland equation: $D = \frac{k_B T}{6\pi\eta r}$ where D is the diffusion constant, k_B is the Boltzmann constant, T is the temperature (in K), η is the solvent viscosity (in $kg \cdot m^{-1} \cdot s^{-1}$), and r is the radius of the spherical particle. The Brownian motion of smaller particles is much faster than large particles, and it is this relationship that allows DLS to accurately determine the size of particles in solution using the Stokes-Einstein-Sutherland equation.

Backscatter detection is sometimes used in DLS measurements and involves collection of scattering data at an angle of 173° instead of at 90° which is also common in light scattering instruments. The 173° angle is relative to an angle of 180° when the detector and light source are in the same spot. There are several reasons for collecting the backscatter instead of 90° detection: by collecting backscatter data the incident beam does not have to travel through the entire sample, thus measurements can be made on higher concentrations of sample; because the beam has a shorter path length through the sample, this reduces the occurrence of multiple scattering (where the sample scatters light which then scatters off other particles in the solution); dust particles are usually much larger than the sample being tested and these particles mainly scatter light in the forward direction, therefore by measuring the backscatter the probability of measuring scattering from dust is greatly reduced; thus higher concentrations can be measured because of the detection of the signal at 173° [74].

1.8 Goals of the Research:

The goals of this research are to investigate the stability and the quaternary folding of the *E. coli* α-helical glycerol facilitator (GlpF) in several different detergents by means of SDS and thermal denaturations, and using SDS-PAGE and DLS to asses the folded state. Studies by DLS of the quaternary structure of a membrane protein dissolved in detergent have not previously been reported so the usefulness of DLS for this purpose will be examined. Investigations into the stability of GlpF in tetradecyl maltoside (TDM) and lysolauroylphosphatidylcholine (LLPC) have never been attempted, and therefore information will be gained on the effects of detergent headgroup and alkyl chain length

on the stability of GlpF. The effects of a protein osmolyte, TMAO, on the stability of GlpF will also be studied through SDS and thermal denaturations as monitored by SDS-PAGE and DLS. This is the first report on the effects of TMAO on the stability of a membrane protein and provides new insight into the factors affecting membrane protein stability.

Chapter II: Materials and Methods

2.1 Materials:

Dodecyl-β-D-maltoside (DDM) and sodium dodecyl sulphate (SDS) were purchased from Sigma-Aldrich (St. Louis, MO). n-tetradecyl-β-D maltoside (TDM) and n-hexadecyl-β-D maltoside (HDM) were purchased from Anatrace (Maumee, OH). Bis-Tris, SDS-PAGE molecular weight markers, Coomassie Brilliant Blue G-250, glycerol, and Tris, were from Fisher Scientific (Fairlawn, NJ). Imidazole was from Fluka (Switzerland). 1-myristoyl-2-hydroxy-sn-glycero-3-phosphocholine and 1-lauroyl-2-hydroxy-sn-glycero-3-phosphocholine was from Avanti Polar Lipids (Alabaster, AL). Nickel-nitrilotriacetic acid (NTA) resin was from Qiagen (Toronto, ON). Isopropyl-β-D-thiogalactopyranoside (IPTG) was purchased from Gold BioTechnology (St. Louis, MO). All other chemicals and materials were of the highest purity commercially available.

2.2 Methods:

2.2.1 Glycerol Facilitator Expression and Purification

E. coli glycerol facilitator was expressed in C43(DE3) cells [75] from a pET28b(+) plasmid (Novagen) encoding an N-terminal His_6 purification tag and N-terminal T7 epitope, as described previously [48, 75, 76]. The M_r of the GlpF including the N-terminal fusion tags is 33,505 kDa and was confirmed by mass spectrometry [77]; its calculated pI is 7.2 (MacVector, Oxford Molecular). Cells were grown to an optical density at 600 nm of 0.6, induced using 0.25 mM IPTG, and then grown overnight (14-16 hours). The cells were then centrifuged at 5000 rpm at 4°C for 15 minutes using a Sorvall RC-5B Refrigerated Superspeed centrifuge. The isolated cells were then resuspended in buffer (25 mM sodium phosphate, 250 mM NaCl, pH 7.5) and incubated with 5 mg of lysozyme for 45 minutes, then DNase (10 mg) and RNase (10 mg) were added and the incubation continued for another 15 minutes. The cells were then exposed to three freeze-thaw cycles, adjusting the pH to 7.5 in between each cycle, to ensure that all cells in the solution were lysed. Following this, 70% sucrose density gradient centrifugation at 100,000xg was performed at 4°C for 1 hour using a Beckman SW28 rotor and either a Beckman L8 70M or a Beckman-Coulter LE 80k centrifuge to isolate the membrane fraction of the lysed cells [78]. The membrane fraction was then suspended in a pH 7.5 phosphate buffer solution containing 25 mM sodium phosphate, 200 mM sodium chloride, 2 mM β-mercaptoethanol, and 30 mM detergent (either DDM, TDM, LLPC, or LMPC), overnight. The solution was then centrifuged at 10,000 rpm at 4°C for 1 hour using the Sorvall RC-5B, and the supernatant was then added to a Ni^{2+}-NTA immobilized metal chelate affinity column equilibrated in detergent-free phosphate

buffer. The non-specifically bound proteins were washed from the column using a pH 7.5 phosphate buffer solution containing 25 mM sodium phosphate, 200 mM sodium chloride, 30 mM imidazole, and 3 mM detergent (either DDM, TDM, LLPC, or LMPC) until the absorbance of the eluate at 280 nm was less than 0.01. Glycerol Facilitator was then isolated using the same buffer containing 250 mM imidazole to elute the protein from the resin. The protein concentration was calculated using the absorbance at 280 nm of the isolated protein solution in the Beer-Lambert equation $A = \varepsilon cl$ where A is the absorbance and 280 nm, ε is the extinction coefficient (in $M^{-1}cm^{-1}$), c is the concentration of the solution (in $mol \cdot L^{-1}$), and l is the cell path length in cm. The protein purity was assessed using SDS-PAGE experiments.

2.2.2 Electrophoresis:

The Hoefer® Mighty Small II SE 250 mini-vertical gel electrophoresis unit was used for all electrophoresis experiments. For SDS denaturations, aliquots of protein were added to concentrations of SDS varying from 0% to 98% of the total detergent in solution (0.33 mM, 0.75 mM, 1.29 mM, 2.0 mM, 3.0 mM, 4.5 mM, 7.0 mM, 12.0 mM, 27 mM, 97 mM, and 147 mM for 10%, 20%, 30%, 40%, 50%, 60%, 70%, 80%, 90%, 97%, and 98%, respectively) and the resulting solution was incubated at the desired temperature for 1 hour. SDS sample treatment buffer containing 50 mM Tris-HCl pH 6.8, 2% SDS, 0.1% Bromophenol blue, 10% glycerol, and 1% (V/V) β-mercaptoethanol was then added to the samples and 40 μL aliquots were loaded into the gel wells. Separation of protein was done by SDS-PAGE using a Laemmli discontinuous gel [79] composed of a 4%

acrylamide stacking gel and a 10% resolving gel. Proteins were then visualized by staining with Coomassie Brilliant Blue R250.

For temperature denaturations, the protein was incubated at the specified temperature for 10 minutes, then a 30 μL sample was taken from the solution and set aside for electrophoresis at room temperature, and the temperature was increased 10 degrees and the 10 minute incubation repeated at the new temperature. Samples were then electrophoresed as described above.

pH studies were performed by adjusting the pH of protein solutions prepared as described above using solutions of 12.1 M HCl and/or 4 M NaOH. pH was monitored using a Fisher Scientific Accumet pH Meter 915. Quaternary structure was observed using SDS-PAGE and electrophoresing protein samples at each pH.

TMAO concentration dependent effects were studied by preparing solutions with 0 M, 0.5 M, 1 M, 2 M and 4 M TMAO and containing SDS concentrations from 0% to 98% as described above. The samples were then incubated for 1 hour and then observed using SDS-PAGE.

TMAO kinetic studies were performed by incubating two samples of GlpF, one in the presence and the other in the absence of 4 M TMAO at room temperature, and another two samples prepared in the same way at 4°C. 30 μL samples were then taken after 1 day, 1 week, 3 weeks, and 6 weeks, and SDS-PAGE was used to monitor the quaternary structure.

2.2.3 Dynamic Light Scattering Studies:

All DLS studies were performed on a Malvern Instruments Zetasizer Nano Series (ZEN 160) spectrometer using a 3.0 mm path length DTS2145 Low Volume Glass Cuvette (Hellma). The wavelength of the laser was 532 nm and backscatter detection at an angle of 173° was collected. The 140 μL samples were spin filtered using Amicon Bioseparations Ultrafree-CL filters to remove any dust, prior to taking measurements. A thermal unfolding experiment was then performed in which measurements of the solution are taken in 10°C increments from 20°C to 90°C, with an equilibration time at each temperature of 4 minutes; measurements were taken at each temperature and averaged.

2.2.4 Gel Scanning and Curve Fitting

Photos were taken of the SDS gels, and the photos were then loaded into the Silk Scientific UN-SCAN-IT Gel 6.1 program. This program converts the photos to greyscale, digitizes the gel lanes (as defined by the user), and then the intensities of the protein bands are reported. The intensities of the GlpF tetramer bands were normalized by first dividing the intensity of the individual GlpF bands in question by the intensity of the 47 kDa M_r protein standard band. The ratios were then individually divided by the largest ratio in the SDS titration, giving a normalized distribution of tetramer dissociation.

The data were then fit to a two-state transition with the program Mathematica™. This program fits SDS-induced changes in SDS-PAGE band intensity to a two-state transition N→U, where N is the amount of native tetramer and U is the amount of

unfolded tetramer. The total amount of protein is $N + U = P_T$, and the fractional amount of each form is $f_N = N/P_T$ and $f_U = U/P_T$ where $f_N + f_U = P_T$. The equilibrium constant can then be written as $K_{eq} = f_U/f_N$, and then $f_U/K_{eq} + f_U - 1 = 0$. From this one can infer that $f_U = K_{eq}/(1 + K_{eq})$ and $f_N = 1/(1 + K_{eq})$. The equation $\Delta G = \Delta G_{H2O} - m[SDS]$ holds true if one assumes that the free energy change of the system is linearly proportional to the denaturant concentration, where ΔG_{H2O} is the energy required to unfold the protein in the absence of sodium dodecyl sulphate (SDS), and m is the calculated cooperativity index. Because $K_{eq} = \exp(-\Delta G/RT)$, this can be rewritten to become $K_{eq} = \exp(-(\Delta G_{H2O} - m[SDS]/RT)$. This equation can now become $f_N = 1/(1 + \exp-((\Delta G_{H2O} - m[SDS])/RT))$ and $f_U = (\exp-((\Delta G_{H2O} - m[SDS])/RT))/(1 + \exp-((\Delta G_{H2O} - m[SDS])/RT))$. This program then takes the normalized tetramer intensities produced by the UN-SCAN-IT 6.1 program as input with the concentrations of SDS corresponding to each tetramer value, and plots f_N as a function of [SDS]. The graph then yields the percentage of SDS in solution needed to unfold half of the tetramers (the SDS_{half}) in a given SDS denaturation experiment [80]. It should be noted that the SDS concentrations were adjusted according to the procedure outlined by Sehgal et al. [81], which converts the bulk mole fractions of SDS and DDM solutions to the micellar mole fraction of SDS that is actually incorporated into DDM micelles at varying concentrations.

2.2.5 Error Calculation

The Mathematica non-linear regression routine yields a standard error and a confidence interval for each of the parameters calculated (*e.g.* ΔG_o and m). The confidence interval is expressed as a minimum and maximum value for each of the fitted

parameters. In this thesis the confidence intervals were calculated by subtracting the minimum parameter value from the maximum value and dividing by two. This procedure gives very nearly the same result as multiplying the standard error by $t_{0.05}$ (Student's t-distribution at 95% confidence; see Statistical Methods by Snedecor and Cochran, 6th edition, 1979). The plot of [SDS] vs. f_N is directly proportional to ΔG_o, and it is this plot that is used to calculate the value of SDS_{half} because SDS_{half} is just the SDS concentration when $\Delta G_o = 0$. If the error of ΔG_o is then divided by the calculated best fit value of ΔG_o then a ratio of the percentage of error in the value is obtained. If this value is then multiplied to the SDS_{half} value, a margin of error is obtained for the value of SDS_{half}.

Chapter III: Results

3.1 GlpF in Dodecyl-β-D Maltoside

The detergent dodecyl-β-D-maltoside (DDM) was used to solubilize glycerol facilitator (GlpF) to study the effects of the osmolyte TMAO on membrane protein stability. Glycerol facilitator has been studied extensively in DDM and it was already known from previous work that GlpF is a stable tetramer in DDM [48]. Furthermore, the

yield of protein solubilized with DDM was the highest compared to all detergents used. In this work, the average yield in DDM was 8.0 ± 0.5 mg per litre of cell culture, compared to 4.5 ± 1 mg in TDM, and 6 ± 1 mg in LLPC, and LMPC. The high yields in DDM made it a good choice to test the chemical, thermal, and osmolyte-induced stability of GlpF using SDS-PAGE, DLS, and CD.

3.1.1 SDS Denaturations at Various Temperatures.

SDS denaturations of GlpF were performed at several different temperatures and concentrations of SDS to provide a baseline for comparison with added osmolyte. Varying amounts of SDS were added to samples of GlpF in DDM that did not alter the concentration of DDM, which were then incubated in a water bath at temperatures ranging from 22°C to 85°C. The goals were to find conditions at which there is a clear transition from tetramer to monomer, determine if this transition is reversible, and if so, obtain thermodynamic data on the quaternary folding of GlpF.

Figure 5 (Lane 1) shows that the vast majority of the protein dissolved in DDM electrophoreses on SDS-PAGE as a tetramer near the M_r standard protein of 118 kDa and a small amount of protein electrophoreses as a monomer near the M_r standard protein of 36 kDa. The figure also shows that over the range of SDS fractions from 0 - 50% there is no noticeable dissociation of the tetramer to monomer caused by SDS.

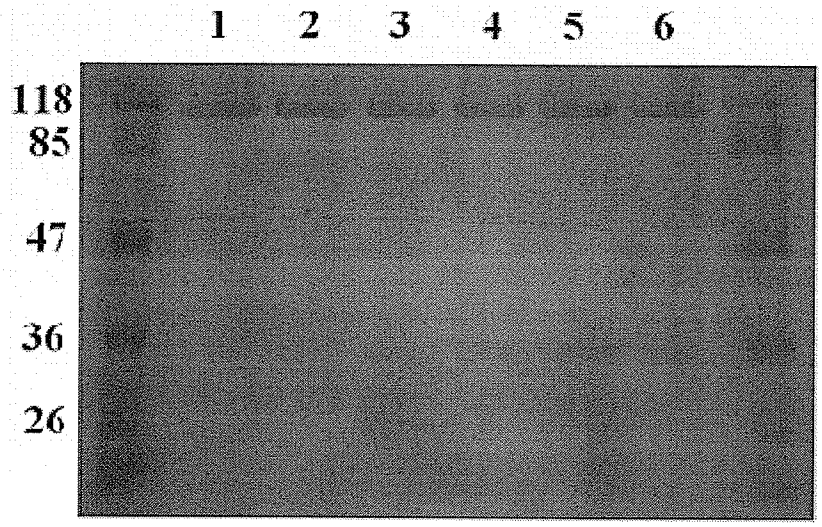

Figure 5: SDS-PAGE showing a 22°C SDS denaturation of GlpF in DDM. Lanes 1-6 correspond to the SDS percentages of 0%, 10%, 20%, 30%, 40%, and 50% of the total detergent in the solution used for the incubation period.

At higher concentrations of SDS, (Figure 6 lanes 1-6, 60-98% SDS) the tetramer band diminishes and the monomer band increases in intensity. There is still a small amount of tetramer at a SDS percentage of 98% (Lane 6) showing that at room temperature (22°C) the tetramer is very stable and complete dissociation by SDS is difficult. According to ideas put forward by Renthal [82], at high SDS concentrations (Lanes 4-6, 90-98% SDS), SDS preferentially intercalates between the hydrophobic transmembrane α-helices of the protein causing the inter- and intra-monomer interactions to decrease, dissociating the tetramer and denaturing GlpF.

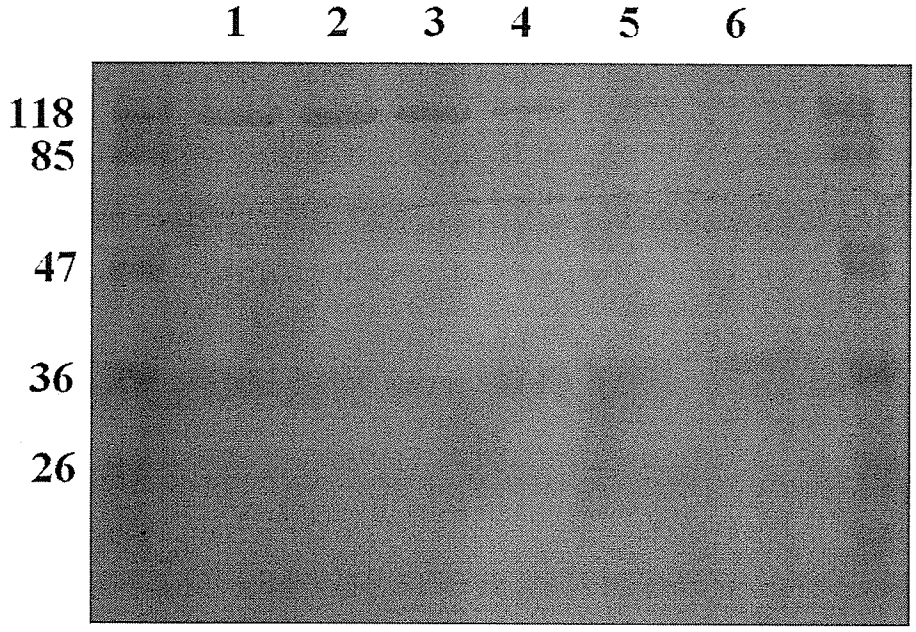

Figure 6: SDS-PAGE showing a 22°C SDS denaturation of GlpF in DDM. Lanes 1-6 correspond to SDS percentages of 60%, 70%, 80%, 90%, 97%, and 98% of the total detergent in the solution used for the incubation period, the other component being DDM.

The gel bands were quantified using the gel digitizing program UN-SCAN-IT Gel 6.1 and a Mathematica™ program described in Methods was used to fit the band intensities to a two-state transition (Figure 7). The curve fitting yields the percentage of SDS needed to dissociate half of the tetramers; the SDS_{half}. Figure 7 shows the band intensities from the gels in Figures 5 and 6, and the fit to a cooperative transition; the SDS_{half} at 22°C is 40 ± 23%.

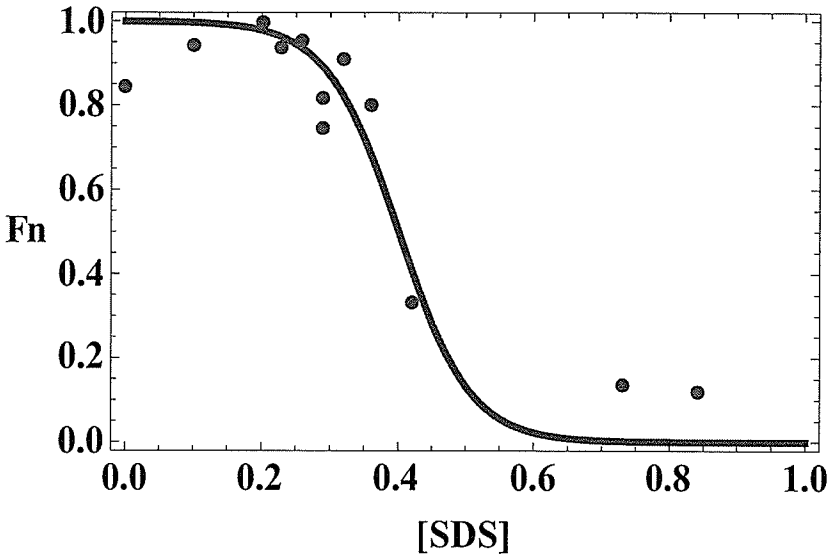

Figure 7: Mathematica graph showing the dissociation of tetramer to monomer at 22°C. The filled circles show the measured band intensities and the line through the points is the best fit to a two-state transition as described by the equation in Methods. The graph shows the normalized fraction of native tetramer (Fn) as a function of SDS concentration.

Figure 8 shows that in concentrations of SDS varying from 0 – 50% at 40°C there is no observable change in the amount of tetramer caused by the increasing SDS concentrations, although there does appear to be a small increase in monomer. The data at 40°C show that the tetramer is completely dissociated into monomer at higher SDS concentrations as can be seen in lanes 3 to 6 in Figure 9, corresponding to 80% to 98% SDS. At 40°C a very clear transition from tetramer to monomer is observed between lanes 3 and 4. In contrast to the experiment at 22°C where the tetramer is only partially denatured at higher concentrations of SDS (Figure 6 lanes 5 and 6), all the protein appears present in Figure 5 (40°C) as monomer at the highest SDS concentrations.

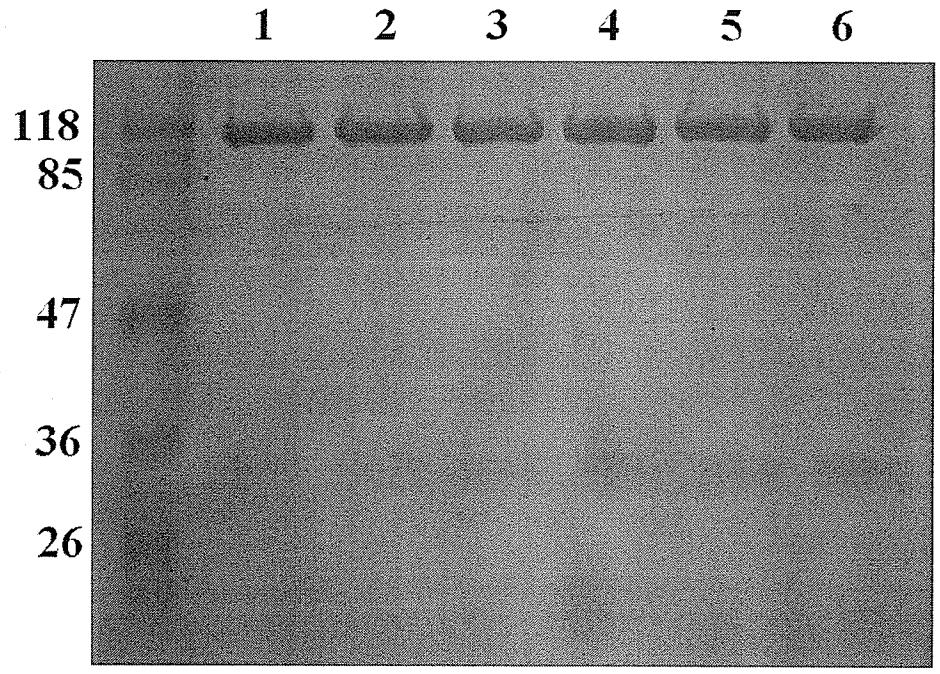

Figure 8: SDS-PAGE showing a 40°C SDS denaturation of GlpF in DDM. Lanes 1-6 correspond to SDS percentages of 0%, 10%, 20%, 30%, 40%, and 50% of the total detergent in the solution used for the incubation period, the other component being DDM.

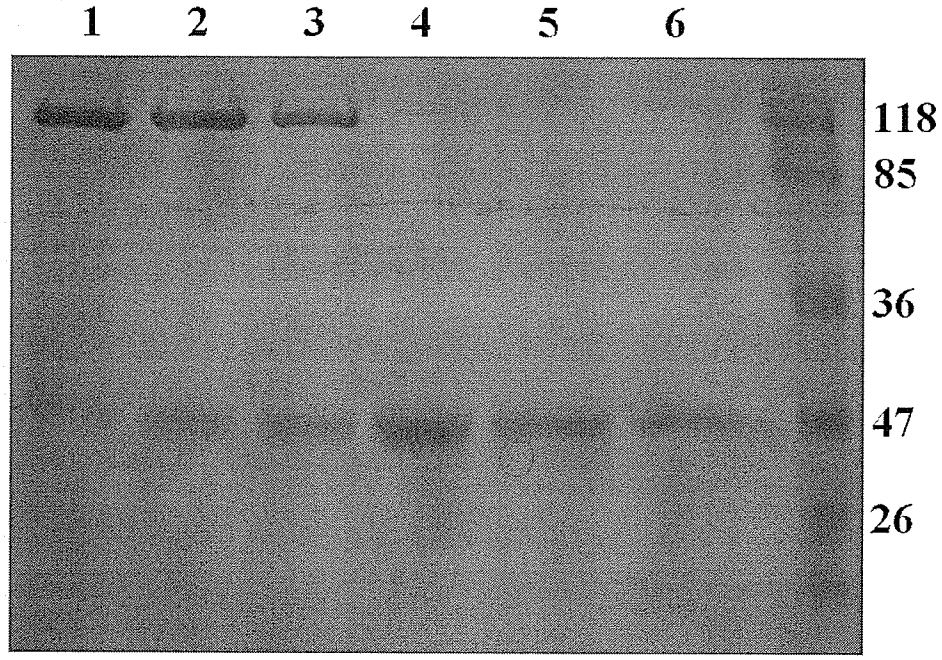

Figure 9: SDS-PAGE showing a 40°C SDS denaturation of GlpF in DDM. Lanes 1-6 correspond to SDS percentages of 60%, 70%, 80%, 90%, 97%, and 98% of the total detergent in the solution used for the incubation period, the other component being DDM.

The Mathematica fit of the data from Figures 8 and 9 is shown in Figure 10. The steepness of the curve shows that the transition from tetramer to monomer is very cooperative at 40°C. The SDS_{half} value achieved from Figures 8 and 9 is 32 ± 11%.

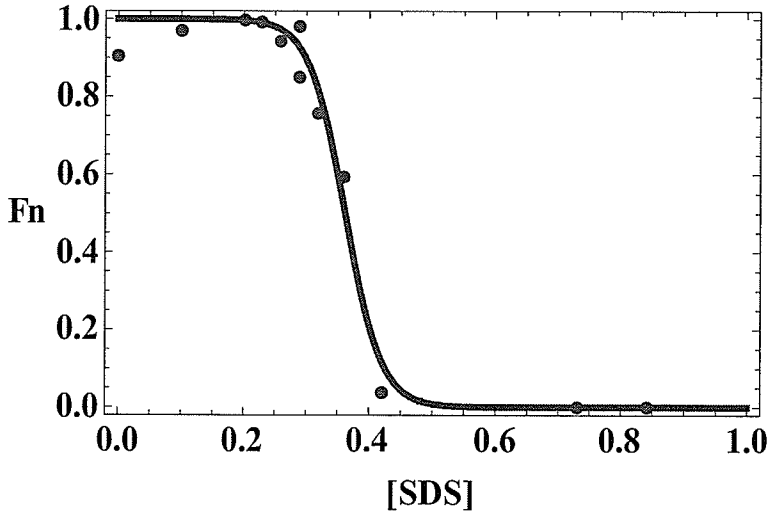

Figure 10: Mathematica graph showing the dissociation of tetramer to monomer at 40°C. The filled circles show the measured band intensities and the line through the points is the best fit to a two-state transition as described by the equation in Methods. The graph shows the amount of native tetramer (Fn) as a function of SDS mole fraction.

Similar experiments were performed at 35°C, 40°C, 45°C, 50°C, 55°C, 60°C, 65°C, 75°C, and 85°C. (Data are not shown for 35°C, 45°C, 50°C, 55°C, 60°C, 65°C, 75°C, and 85°C). The gels were analyzed as in Figure 7 yielding the SDS_{half} for all the corresponding temperatures and the values are listed in Table 1. At higher temperatures, the intensity of all the bands decreases making it more difficult to calculate an accurate SDS_{half}. Note that the 75°C and 85°C gels had such little band intensity, that they could not be confidently analyzed. In Table 1, it can be seen that as the temperature is increased, the amount of SDS that is needed to unfold half of the tetramers decreases. This shows that the resistance of GlpF to SDS denaturation is reduced as the temperature is increased.

Table 1: SDS_{half} values at given temperatures in DDM calculated from Mathematica

SDS_{half}	40 ± 23%	36 ± 17%	36 ± 11%	34 ± 10%	29 ± 15%	28 ± 15%	27 ± 11%	24 ± 17%	ND	ND
Temperature (°C)	22	35	40	45	50	55	60	65	75	85

3.1.2 GlpF Renaturation Experiments.

An experiment attempting to refold dissociated GlpF tetramer was performed. This was done by adding an appropriate amount of DDM to an SDS-denatured solution of GlpF, to reduce the fraction of SDS to one in which the protein is known to be a well folded tetramer, according to the earlier unfolding experiments. The percentage of SDS used to unfold the tetramer was 90%. In this environment, it had been found from earlier experiments that the tetramer was more than 95% dissociated into monomer or aggregate (Figure 9, lane 4) at 40°C. Enough DDM was then added to bring the percentage of SDS back to 50%, a level where it had been shown in previous experiments that GlpF is a stable tetramer (Figure 8, Lane 6). Two re-folding experiments were done; one at 35°C and one at 40°C. Unfortunately, these experiments did not show that the tetramer had been dissociated at the high fraction of SDS (90%) (Figure 11 lanes 1 and 2). One possible explanation is that the protein had not been left to incubate in SDS at the specified temperature for a time period long enough to dissociate the tetramer. At both temperatures the protein had been in high SDS concentrations for ten minutes, and then DDM was added and the sample incubated for another ten minutes. In contrast the high

temperature samples in Figures 7 and 9 have felt the cumulative effects of incubation at each temperature. Evidently, the incubation for 10 minutes in 90% SDS is not long enough for tetramer dissociation as indicated by the fact that the protein is still predominantly tetrameric as seen in Figure 11 lanes 1 and 3. Also noteworthy is that, judging from the intensities of the monomer and tetramer bands, the addition of DDM does not appear to restore any of the monomer to tetramer.

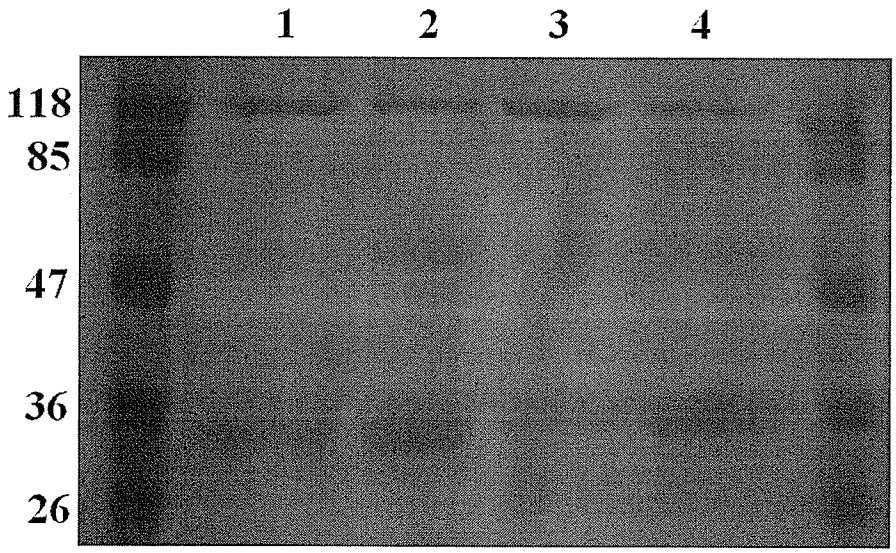

Figure 11: SDS-PAGE showing GlpF renaturation experiment in DDM. Lane 1 is 90% SDS at 35°C, Lane 2 is the same as Lane 1 but at 40°C, Lane 3 is 50% SDS after the addition of DDM at 35°C, and Lane 4 is the same as Lane 3 but at 40°C.

A second attempt at a renaturation experiment in DDM found similar results as the first, and are shown in Figure 12. It was established through this experiment that the tetramer is not dissociated more than 90% after a 30 minute incubation in 90% SDS at 35°C and 40°C (Lanes 4 and 8). Furthermore the dissociated monomer failed to re-fold to

tetramer after the addition of DDM. It was concluded that there is no reversibility in the SDS denaturation of GlpF.

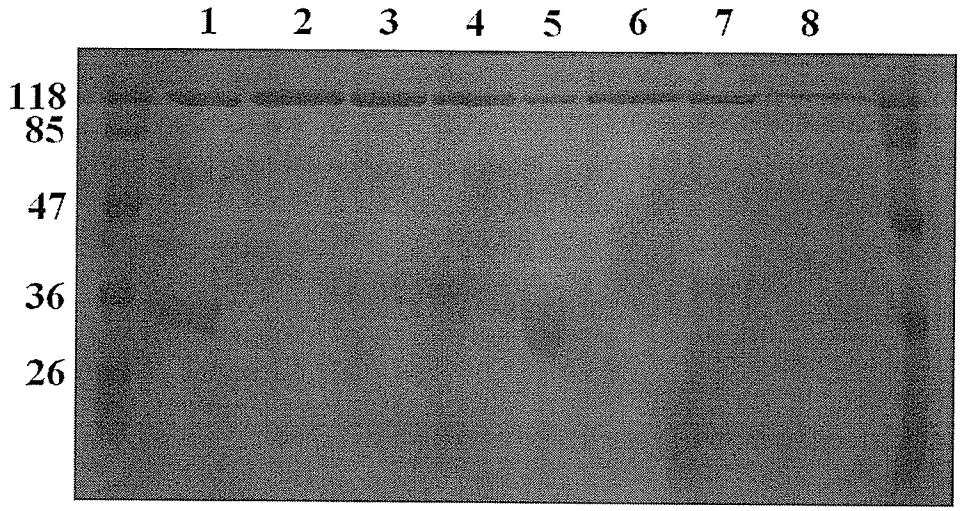

Figure 12: SDS-PAGE showing GlpF renaturation experiment in DDM. Lanes 1 through 4 are at 35°C, and Lanes 5 through 8 are at 40°C. Lanes 1 and 5 are the controls; they have been in 90% SDS for 1 hour at the corresponding temperatures. Lanes 2 and 6 correspond to 5 minutes in 90% SDS, then 55 minutes in 50% SDS. Lanes 3 and 7 correspond to 15 minutes in 90% SDS, then 45 minutes in 50% SDS. Finally, Lanes 4 and 8 correspond to 30 minutes in 90% SDS, then 30 minutes in 50% SDS.

3.1.3 SDS Denaturations at Various Temperatures in the Presence of a Protein Osmolyte.

Investigations of the effects of protein osmolytes on α-helical membrane proteins have never been previously reported. Osmolytes have been shown to stabilize protein structure against many different types of cellular stress in many different types of organisms [51, 83, 84]. Some of the stresses include high hydrostatic pressure, high salinity, desiccation, high and low temperatures, and high concentrations of denaturants such as urea. The counteracting effects of osmolytes against the detrimental effects of denaturants on proteins are thought to be due to the unfavourable transfer free energy of the peptide backbone from water to osmolyte, which preferentially destabilizes the unfolded states of the protein thereby increasing the free energy of unfolding [63, 64]. The natural osmolyte trimethylamine N-oxide (TMAO) was chosen for studies into the effects of osmolytes on membrane proteins.

The first experiments attempted were SDS denaturations at room temperature using 0.6 M TMAO. From the literature, it was found that 0.6 M TMAO had been used for similar protein stability studies [70], so experiments were initiated using this concentration. It was hypothesized that if TMAO was to confer stability to GlpF, the change in stability would be obvious by SDS-PAGE, and characterization of the effects of TMAO on GlpF could be achieved using this system. If Figure 14 is compared to Figure 6, a small increase in the stability of the tetramer in the presence of the 0.6 M TMAO is observable judging from the increased band intensity at the high SDS concentrations. This was confirmed by comparing the fact that a melting point could not

be obtained from Figures 13 and 14, by fitting to a two-state transition measured in the presence of TMAO, whereas an SDS_{half} of 40 ± 15% was obtained from Figures 5 to 7.

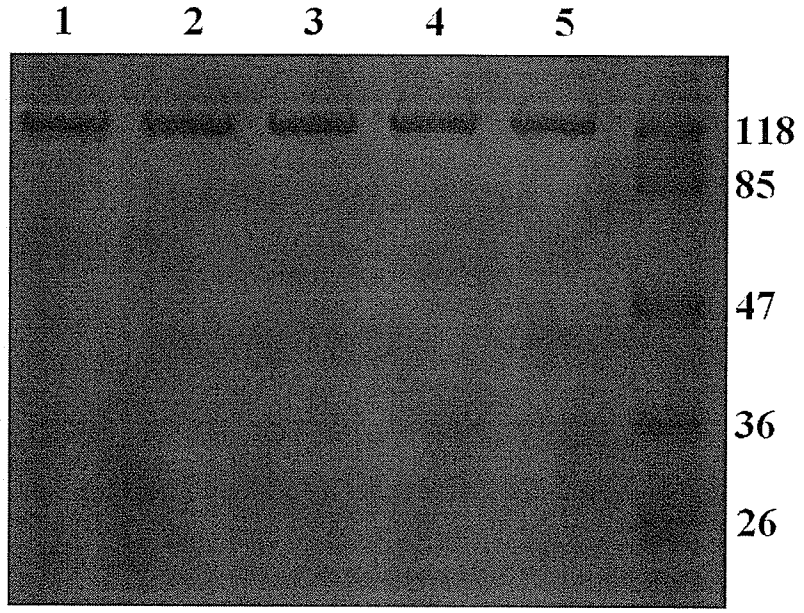

Figure 13: SDS-PAGE showing a 22°C SDS denaturation of GlpF in DDM in the presence of 0.6 M TMAO. Lanes 1-5 correspond to SDS percentages of 0%, 10%, 20%, 30%, and 40% of the total detergent in the solution used for the incubation period, the other component being DDM.

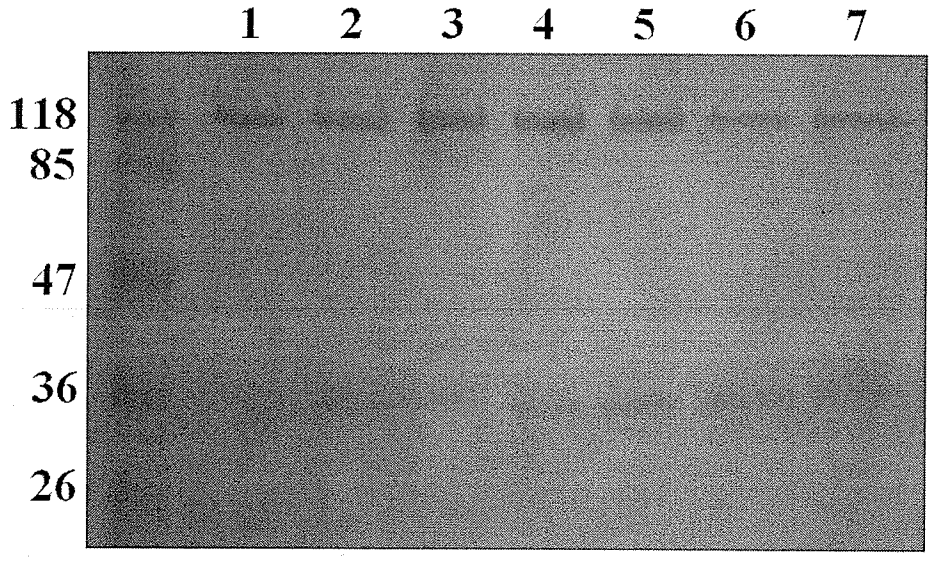

Figure 14: SDS-PAGE showing a 22°C SDS denaturation of GlpF in DDM in the presence of 0.6 M TMAO. Lanes 1-7 correspond to SDS percentages of 50%, 60%, 70%, 80%, 90%, 97%, and 98% of the total detergent in the solution used for the incubation period, the other component being DDM.

To measure the concentration dependence of TMAO stabilization on GlpF a range of TMAO concentrations from 0.5 M to 4 M were tested and the temperature increased to 40°C, a temperature at which full denaturation of the tetramer occurs in the absence of TMAO. TMAO concentration dependent effects have been previously reported in the literature [85]. Figures 15 and 16 show the effects of increasing SDS on DDM-solubilized GlpF in the presence of 4 M TMAO. In the absence of SDS (Figure 15, Lane 1) the protein in the presence of 4 M TMAO exists predominantly as an octamer. Between 0 and 50% SDS the protein is converted into a largely tetrameric form (see lane 6 of Figure 15 50% SDS). The results show that at high concentrations of TMAO, the octameric form of GlpF is preferred and protected from dissociation in DDM. At a concentration of 0.6 M TMAO (Figures 13 and 14), only the tetrameric form of GlpF is protected, and not to the extent of that which is found in 4 M TMAO. It is hypothesized that TMAO interacts strongly with the highly charged SDS molecules. This interaction thus prevents SDS from inserting into the DDM micelles causing denaturation. This effect has been found with TMAO and the denaturant urea [71].

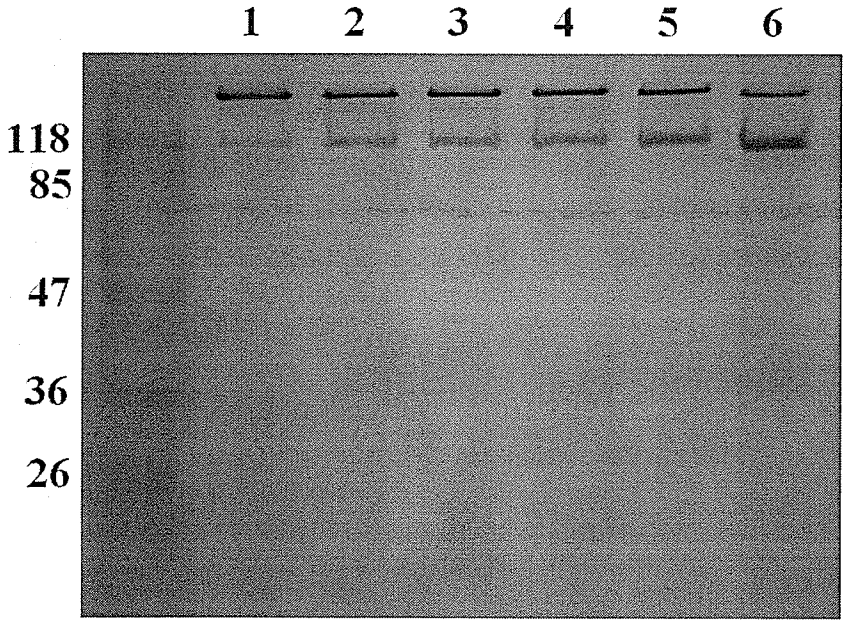

Figure 15: SDS-PAGE showing a 40°C SDS denaturation of GlpF in DDM in the presence of 4 M TMAO. Lanes 1-6 correspond to SDS percentages of 0%, 10%, 20%, 30%, 40%, and 50% of the total detergent in the solution used for the incubation period, the other component being DDM.

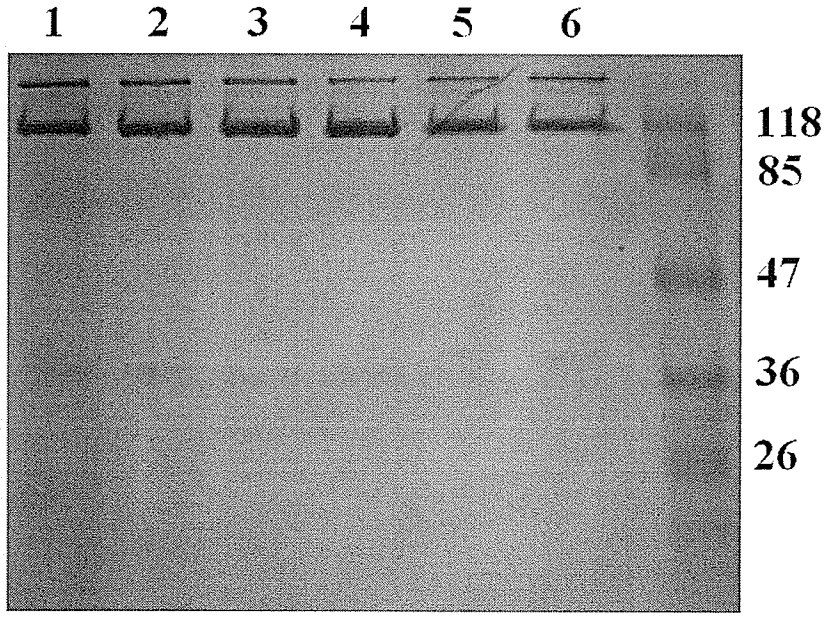

Figure 16: SDS-PAGE showing a 40°C SDS denaturation of GlpF in DDM in the presence of 4 M TMAO. Lanes 1-6 correspond to SDS percentages of 60%, 70%, 80%, 90%, 97%, and 98% of the total detergent in the solution used for the incubation period, the other component being DDM.

The concentration dependency of TMAO on GlpF in DDM was further examined by performing SDS denaturations in 0.5 M, 1 M, and 2 M TMAO at 40°C using SDS-PAGE. SDS_{half} values for the different TMAO concentrations were determined from fits of the band intensities to a two-state transition and were used to quantify the stability of the predominant quaternary form of the protein. From the fits in Figure 17 the SDS_{half} values in 0 M TMAO (36 ± 11%), 0.5 M TMAO (40 ± 16%), and 1 M TMAO (41 ± 17 %) were determined. When the concentration was increased to 2 M TMAO, full denaturation of the tetramer at 98% SDS does not occur, so an SDS_{half} value could not be determined. The most interesting result from the 2 M TMAO experiment is the fact that octamer is not seen. From this result we can conclude that the octameric quaternary form of the protein is only promoted at concentrations higher than at least 2 M TMAO in DDM, but the stability against denaturation by SDS is still conferred to the protein at 2 M TMAO.

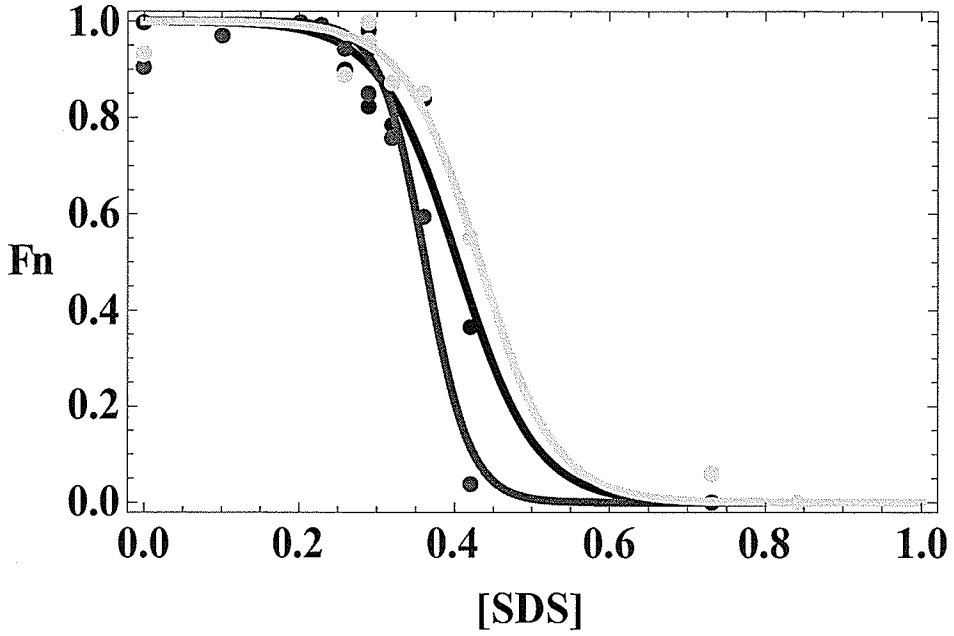

Figure 17: Mathematica graph showing the dissociation of tetramer to monomer. The graph shows the amount of native tetramer (Fn) as a function of SDS mole fraction. The TMAO concentrations shown are 0 M (purple), 0.5 M (black), and 1 M (green). The SDS_{half} for each of the curves from low to high are 36 ± 11%, 40 ± 16%, and 42 ± 17%.

The concentration dependency of TMAO supports the conclusion that TMAO is interacting with the SDS molecules to prevent denaturation by the fact that the stability of GlpF tetramer increases as the concentration of TMAO is increased. As more TMAO is added into the solution, then hypothetically, there are more molecules to interact with SDS causing an increase in the stability of GlpF. If there is an interaction between the SDS and TMAO, this is the result that would be expected. This interaction of TMAO with SDS, coupled with the known effect of destabilization of the unfolded states by the

high energy price for transfer of the peptide backbone from water to osmolyte (caused by TMAO), stabilizes the protein even further.

3.1.4 Thermal Denaturations in the Presence and Absence of TMAO.

Thermal characterization of GlpF tetramer with and without 0.6 M and 4 M TMAO was performed. As can be seen from Figure 18, at 75°C (Lane 6) in the absence of TMAO, only a very small fraction of the protein is present in a tetramer. There are elevated levels of higher molecular weight species shown in Lane 5 (65°C) that correspond to large, irreversibly denatured GlpF. The dark band at the bottom of the loading well, the distinct band just beneath the stacking gel, and the "smear" between the two are indicative of large, unfolded oligomers. This result demonstrates that GlpF in DDM is thermally stable until temperatures above 65°C, and that the thermal "melting" of the quaternary and tertiary structure has a transition temperature in between 65°C and 75°C.

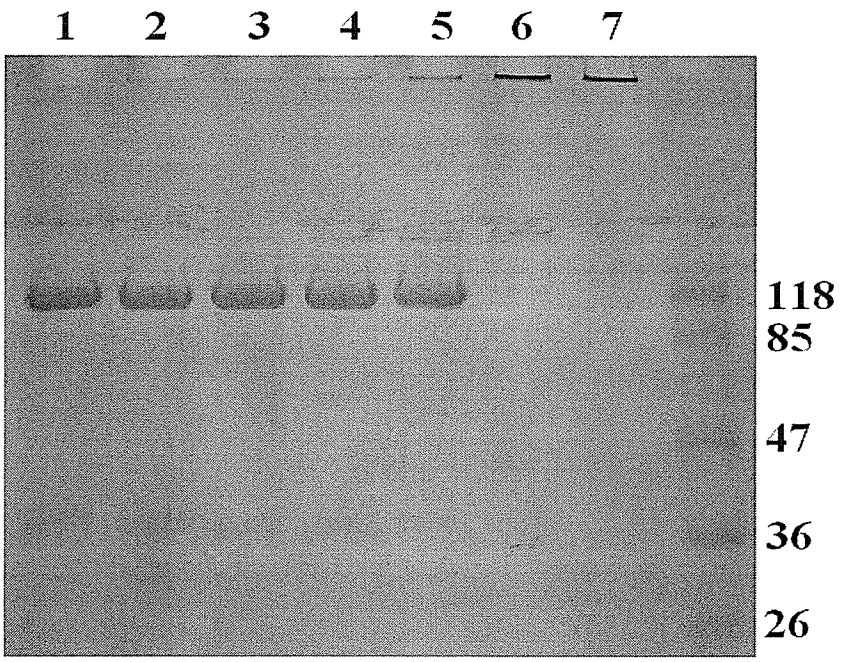

Figure 18: SDS-PAGE showing a temperature denaturation of GlpF in DDM. Lanes 1-7 correspond to the temperatures 22°C, 35°C, 45°C, 55°C, 65°C, 75°C, and 85°C. The dark band at the bottom of the loading well, the distinct band just beneath the stacking gel, and the smear between the two in lanes 6 and 7 correspond to aggregated GlpF.

In the presence of 0.6 M TMAO (Figure 19), there is a noticeable increase in the stability of the tetramer. Much more tetramer is observed at 75°C (Lane 6) in the presence of TMAO than in its absence (Figure 18, Lane 6). There is a comparable amount of high molecular weight species in lanes 5, 6, and 7 of Figures 18 and 19. A small amount of stable octamer is also seen on this gel in Figure 19, showing that low levels of TMAO promote small amounts of the octameric form of GlpF.

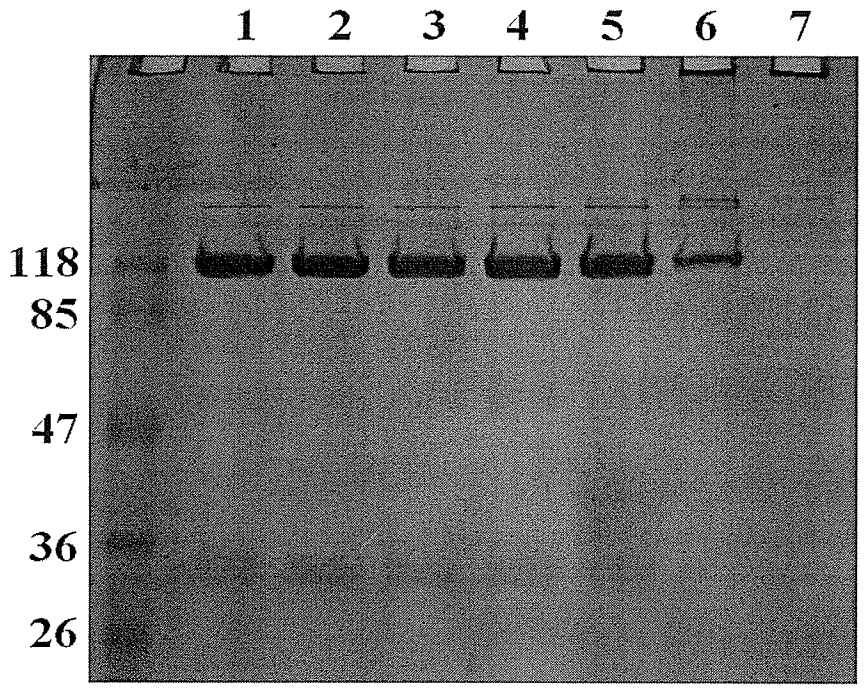

Figure 19: SDS-PAGE showing a temperature denaturation of GlpF in DDM in the presence of 0.6 M TMAO. Lanes 1-7 correspond to the temperatures 22°C, 35°C, 45°C, 55°C, 65°C, 75°C, and 85°C.

The effects of 4 M TMAO on the thermal stability of the protein were then tested. Figure 20 shows that in 4 M TMAO the predominant form of the protein is the octamer and that the octamer is stable at 75°C (Lane 6 – Figure 20); it is only at 85°C (Lane 7 – Figure 20) that it is denatured into high molecular weight aggregate. There is a small amount of aggregate at the bottom of the well in Lane 6 (75°C), even though the amount of octamer in the lane appears identical to previous lanes. This result shows that although a very small quantity of aggregate is found at this temperature (75°C, Lane 6), the amount of aggregated protein is drastically reduced as compared to experiments with 0.6 M TMAO or no TMAO (Figures 18 and 19), illustrating the stabilizing effect of 4 M TMAO.

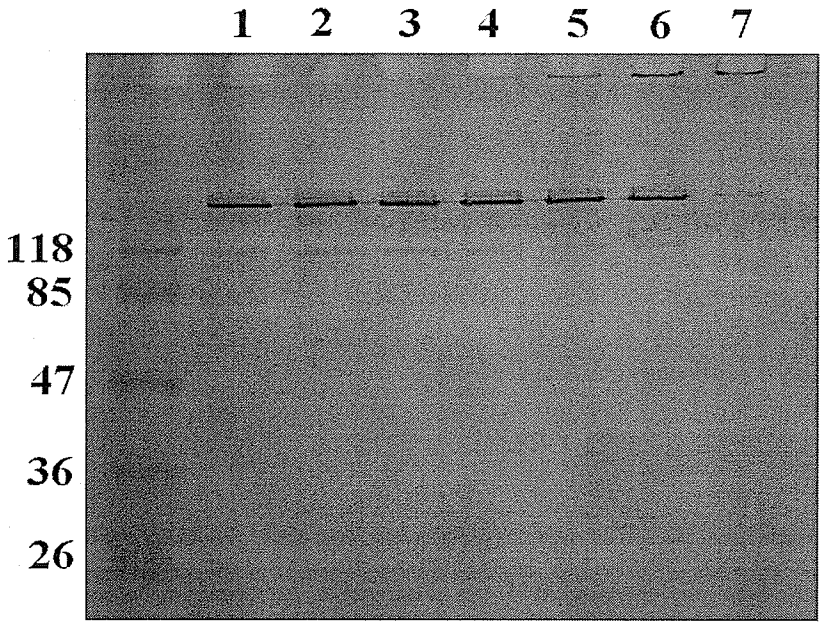

Figure 20: SDS-PAGE showing a temperature denaturation of GlpF in DDM in the presence of 4 M TMAO. Lanes 1-7 correspond to the temperatures 22°C, 35°C, 45°C, 55°C, 65°C, 75°C, and 85°C.

Thermal melting point (T_m) values from were determined from the fits of the band intensities in the presence and absence of 4 M TMAO to a two-state thermal transition. The T_m values were used to analyse the thermal stability of the tetrameric form of GlpF. From the fits in Figure 21 the T_m values in 0 M TMAO (69 ± 5°C) and 4 M TMAO (80 ± 1°C) were calculated. This result shows that 4 M TMAO gives the GlpF tetramer another 9°C of thermal stability in DDM.

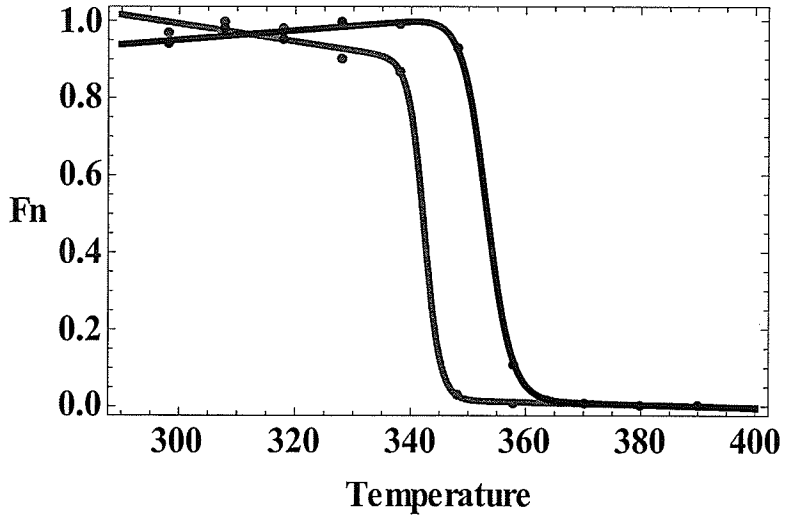

Figure 21: Mathematica graph showing the thermal dissociation of tetramer to monomer. The graph shows the fraction of native tetramer (Fn) as a function of temperature. The TMAO concentrations shown are 0 M (purple), and 4 M (black). The T_m for both curves from low to high are 69 ± 5°C and 80 ± 1°C.

3.1.5 Kinetic Studies at Various Temperatures.

Earlier work on GlpF showed that incubation of the protein in DDM and LMPC at 4°C over the period of 3 weeks results in small amounts of protein unfolding [47, 48](Figure 7). To explore the possible stabilization of the protein by TMAO a kinetic study was initiated as described in Methods. Figure 22 shows the effects of 0.6 M TMAO on GlpF in DDM after 48 hours at two different temperatures. It is noticed that in the presence of 0.6 M TMAO (Lanes 1 and 3), a small amount of GlpF adopts an octameric quaternary form, but there is also a smaller quantity of octamer promoted in the lanes without TMAO (Lanes 2 and 4). At both temperatures inspection by eye suggests that in the presence of TMAO (Lanes 1 and 3) the samples contain slightly more

octamer and less monomer than in the absence of TMAO (Lanes 2 and 4), though the effect is more noticeable at room temperature.

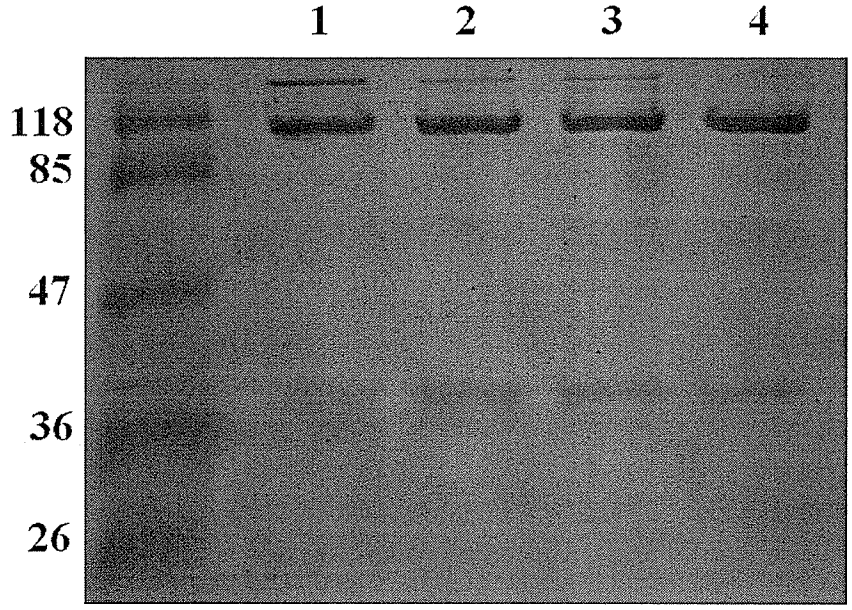

Figure 22: SDS-PAGE showing a kinetic stability experiment of GlpF in DDM in the presence and absence of 0.6 M TMAO after 48 hours. Lanes 1 and 2 correspond to GlpF kept at room temperature (22°C), with and without TMAO, respectively. Lanes 3 and 4 correspond to GlpF kept in the refrigerator (4°C), with and without TMAO, respectively.

After 96 hours under the same conditions (results not shown) the room temperature samples seemed to be slightly more stable and have a higher percentage of octamer than those left at 4°C, but the difference between the two was still not very pronounced.

In Figure 23 the same samples have been electrophoresed after incubation for 26 days. Similar to the previous results, incubation in 0.6 M TMAO increases the relative amount of octameric protein (Lanes 1 and 3). It is interesting to note also that there is

significantly less monomer in all the lanes in Figure 23 compared to Figure 22 and that the total amount of protein in each of the lanes appears to be lower than in Figure 22. Of course the length of time the gels are stained and destained, and the differences in the quality of the gel images make comparisons between the gels problematic. However, to test the idea that protein is being lost over the period of the incubation, a sample of freshly-prepared protein with about the same total concentration as the incubating samples was electrophoresed alongside the samples in the next point in the kinetic assay (Figure 24). In Lanes 1-4 in Figure 24, the protein has been incubating in its respective environments for 55 days. Lane 5 shows GlpF from a fresh preparation with a similar protein concentration, and it is obvious that even though the octamer levels have slightly increased compared to Figure 22, the amount of tetramer left is significantly less than in a fresh protein preparation. This suggests that while some of the tetramer is promoted to octamer, significant amounts are being denatured over the course of the experiment. The small differences between the amounts of protein in the presence and absence of TMAO show that at 0.6 M it is having little effect on the kinetic stability of the protein. The results do suggest that the protein is slightly more stable at room temperature than at 4°C.

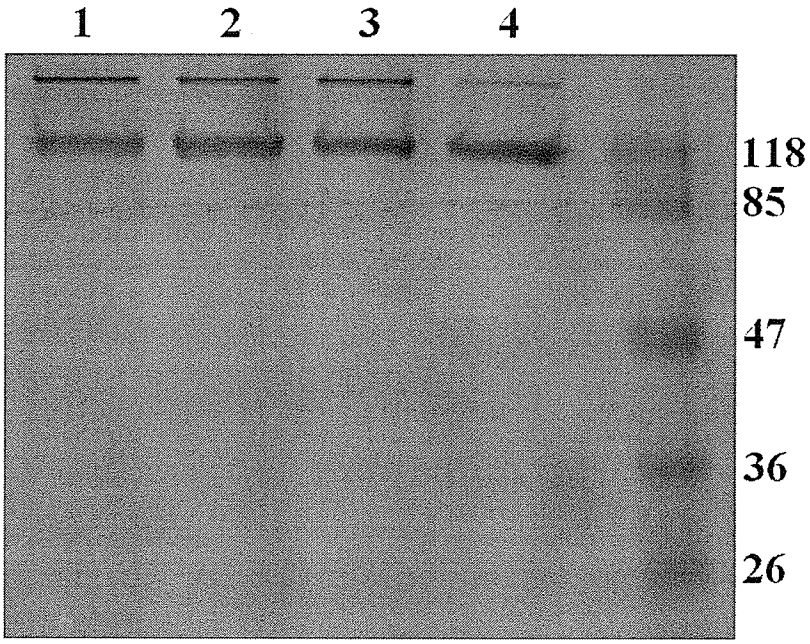

Figure 23: SDS-PAGE showing a kinetic stability experiment of GlpF in DDM in the presence and absence of 0.6 M TMAO after 26 days. Lanes 1 and 2 correspond to GlpF kept at room temperature (22°C), with and without TMAO, respectively. Lanes 3 and 4 correspond to GlpF kept in the refrigerator (4°C), with and without TMAO, respectively.

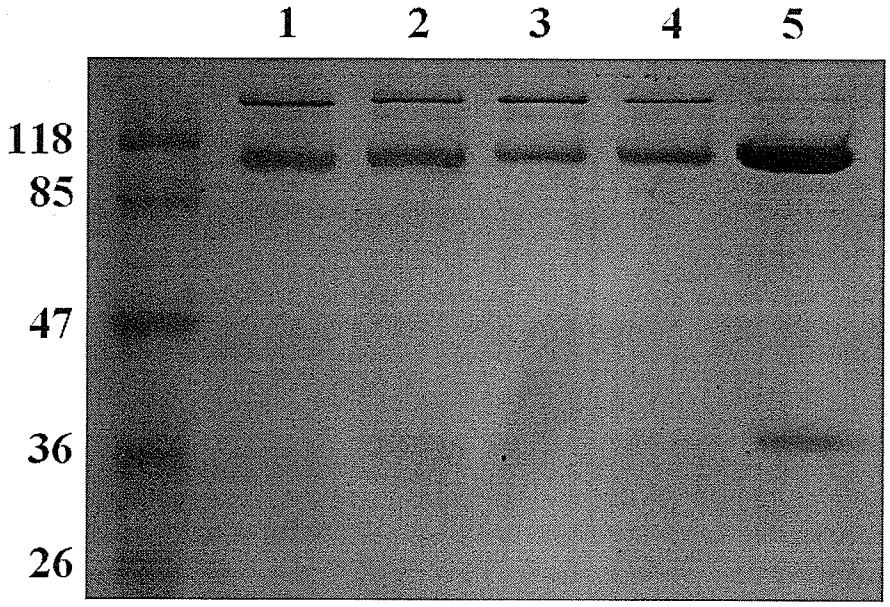

Figure 24: SDS-PAGE showing a kinetic stability experiment of GlpF in DDM in the presence and absence of 0.6 M TMAO after 55 days. Lanes 1 and 2 correspond to GlpF kept at room temperature (22°C), with and without TMAO, respectively. Lanes 3 and 4 correspond to GF kept in the refrigerator (4°C), with and without TMAO, respectively. Lane 5 is "fresh" GlpF in DDM.

3.1.6 Dynamic Light Scattering Heat Denaturations of GlpF in Absence and Presence of TMAO.

Thermal denaturations of GlpF in DDM were performed in the presence and absence of TMAO to determine the usefulness of Dynamic Light Scattering (DLS) to monitor the quaternary structure of a membrane protein. Dynamic Light Scattering

(DLS) is a technique that measures the scattering of light by small particles undergoing Brownian dynamics to determine the hydrodynamic radius of particles in solution. It must be noted that although comparisons are made in this thesis between DLS data and SDS-PAGE experiments, the environment of a protein in an SDS-PAGE experiment is dramatically different than in a DLS experiment. So, as the average diameter of the particles in solution is reported, it must also be taken into account that the particles are not spherical in shape, or composed of one type of molecule. The intensity profiles that are shown in the following graphs demonstrate the evolution of different particles in solution as a function of temperature. The intensities of the peaks are indicative of the relative populations of the different species in solution, and not their actual concentrations. All data above 80°C is unreliable and was not included in the DLS spectra because of the large amounts of aggregated protein causing problems with the light scattering signal, such as multiple scattering.

Figure 26 is a DLS graph showing the effect of heating DDM in the absence of GlpF. This is effectively a blank to see the effect that temperature has on the detergent DDM, so comparisons can be made between this graph, and a graph with GlpF in the solution. The average size of the particles at 22°C is 8.1 nm (orange curve) which is in good agreement with the diameter of DDM measured by Heerklotz et al., [86]. As the temperature is increased the micelles decrease in diameter until they reach the size of 2.7 nm (brown curve) at 80°C. At 50°C (black curve), the formation of a second peak corresponding to very large particles with a diameter of 275 nm is observed. This peak continues to grow in intensity as the temperature increases, shifting to a slightly smaller diameter of 220 nm by 80°C.

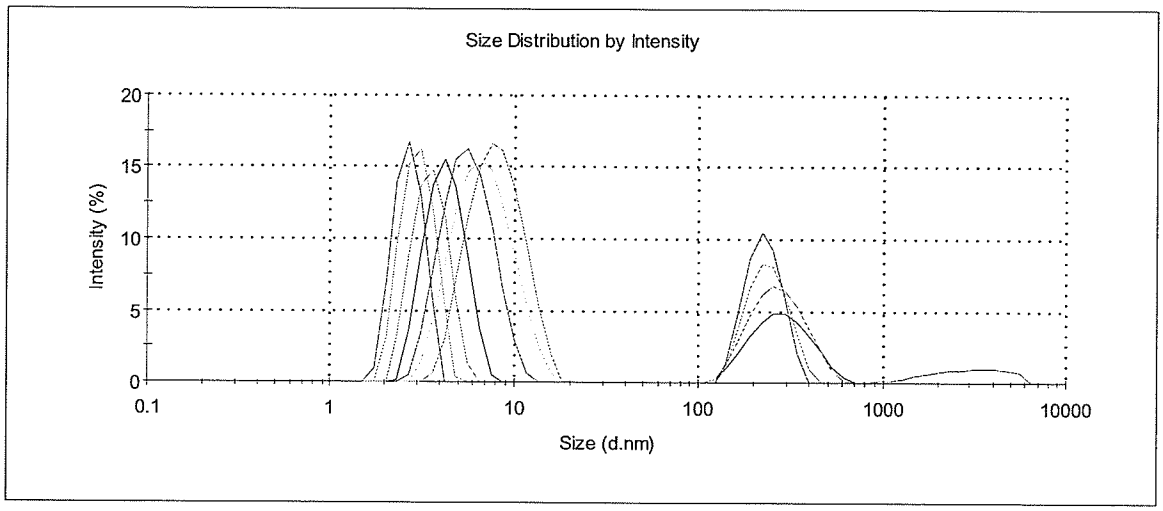

Figure 26: DLS of DDM at several temperatures (from right to left). The temperatures shown here are 20°C (orange), 30°C (green), 40°C (blue), 50°C (black), 60°C (red), 70°C (purple), and 80°C (brown).

Figure 27 shows a DLS spectrum of GlpF solubilized in DDM. At 20°C a single peak is observed indicating a particle diameter of 10.1 nm (orange curve). As the temperature is raised the peak diminishes in intensity and moves to a lower diameter. At 40°C the particle diameter is 7.5 nm (blue). At 50°C a new peak with a diameter of about 171 nm appears in the spectrum. Further increases in temperature continue to decrease the intensity of the small diameter peak and move it to lower values, but cause only minor changes in the large diameter peak. At 70°C a new intermediate diameter peak appears at about 13.5 nm and this increases to about 15.7 nm at 80°C. The effect of GlpF being included in the DDM micelles is evident in Tables 2-4 which list the diameters of the detergent micelles in the presence and absence of GlpF and the difference between them. The previously empty detergent micelles now have GlpF solubilized in them, and the diameter of the particles has shifted to a larger size. The diameter of the 20°C (Figure

26, orange curve) from the "empty" micelles is 8.1 nm, whereas the protein containing micelles are 11.6 nm (Figure 27, orange curve) in diameter yielding a difference of 3.5 nm. According to X-ray diffraction the diameter of the GlpF tetramer is approximately 4.5 nm (Fu et al., [21]), so the measured difference in micelle diameter is a little smaller than would be expected if one GlpF tetramer was added to an empty micelle. Of course this is unlikely as GlpF likely displaces some of the detergent from the micelle so that the size of the solubilized protein is a little smaller than the sum of the empty micelles and the protein.

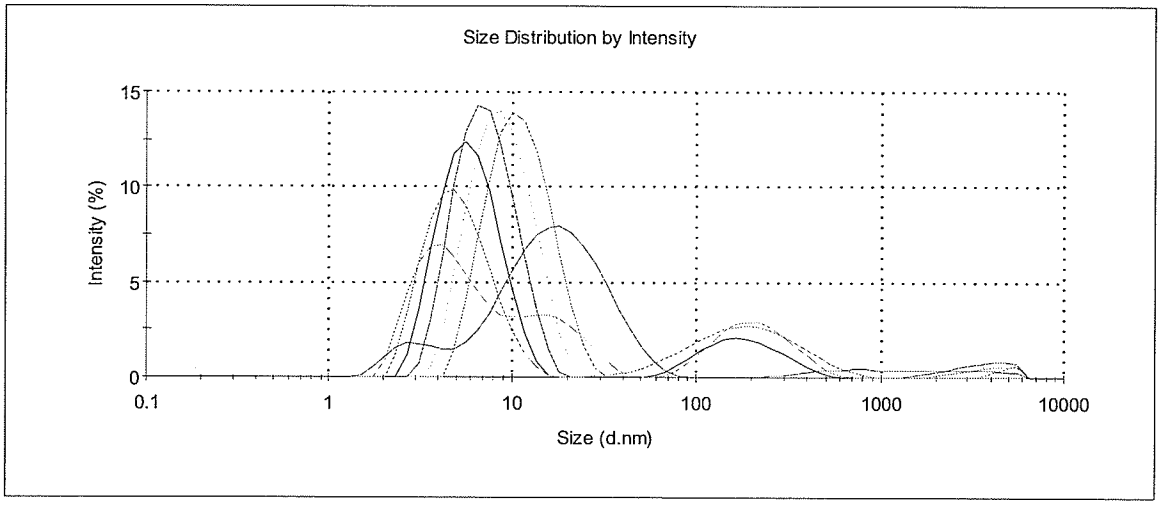

Figure 27: DLS in the presence of GlpF in DDM at several temperatures. The temperatures shown here are 20°C (orange), 30°C (green), 40°C (blue), 50°C (black), 60°C (red), 70°C (purple), and 80°C (brown). The GlpF concentration is 5 μM.

Table 2 shows that as the temperature increases, this difference in size between the micelles in the presence and absence of protein gets smaller. This observation may reflect the reversible dissociation of the protein into dimers and monomers at the higher

temperatures; however, note that this is not observed in the SDS-PAGE experiments where the protein tetramer appears stable up to its melting point.

In both sets of data the large particle peaks appear at 50°C and higher. Interestingly the larger particles are bigger in the absence of protein than in their presence (see Table 3). However, the differences in size are small compared to the sizes of the particles and furthermore the peaks in the presence of protein (Figure 27) are broader than in the case of pure micelles (Figure 26). The nature of these peaks is uncertain. Perhaps of greater significance is the appearance of the peaks of intermediate sized particles only when protein is present at 70°C and higher (Figure 27 and Table 3). This observation agrees with the tetramer dissociation and aggregation observed in SDS-PAGE above 65°C in Figure 19. It suggests that the intermediate diameter peaks represent irreversibly-unfolded GlpF in DDM micelles.

Table 2: DDM Small Particle Diameters at Different Temperatures

Temperature (°C)	**20**	**30**	**40**	**50**	**60**	**70**	**80**
Detergent diameter (nm)	8.1	7.1	5.8	4.3	3.6	3.0	2.7
Diameter of detergent and GlpF (nm)	11.6	9.2	7.5	6.2	5.4	5.0	2.9
Difference caused by presence of GlpF (nm)	3.5	2.1	1.7	1.9	1.8	2.0	0.2

Table 3: DDM Large Particle Diameters at Different Temperatures

Temperature (°C)	**50**	**60**	**70**	**80**
Detergent diameter (nm)	255	255	220	220

Diameter of detergent and GlpF (nm)	164	190	190	ND
Difference caused by presence of GlpF (nm)	-91	-65	-30	ND

Table 4: DDM Intermediate Particle Diameter at Different Temperatures

Temperature (°C)	**70**	**80**
Diameter of detergent and GlpF (nm)	13.5	15.7

When TMAO is added to a solution of DDM (Figure 28), the DLS spectrum is dramatically different from that measured in the absence of TMAO (Figure 26). At 20°C two peaks are observed in the presence of TMAO (Figure 28, orange curve); one indicates small particles about 26 nm in diameter and the other reports very large particles about 1800 nm in diameter. As pointed out by Heerklotz et al., [86], even the 26 nm particles are likely to be rod-shaped as the small size of the DDM monomer makes a 26 nm spherical micelle impossible to form. The smaller particle is nearly 18 nm larger than those observed in the absence of TMAO (Table 5). Similar to its behaviour in the absence of TMAO, as the temperature is raised the intensity of the small diameter peak decreases as it moves to smaller diameters (Figure 28). Between 20°C and 50°C, the peak corresponding to very large particles increases in intensity slightly and moves to smaller diameters. Between 50°C and 80°C larger increases in intensity are observed along with small shifts in particle size (Figure 28) and this behaviour is similar to but not identical with the behaviour of the large diameter peaks in the absence of TMAO (Figure 26). The specific interaction between TMAO and DDM that is causing this change in the spectrum is unknown.

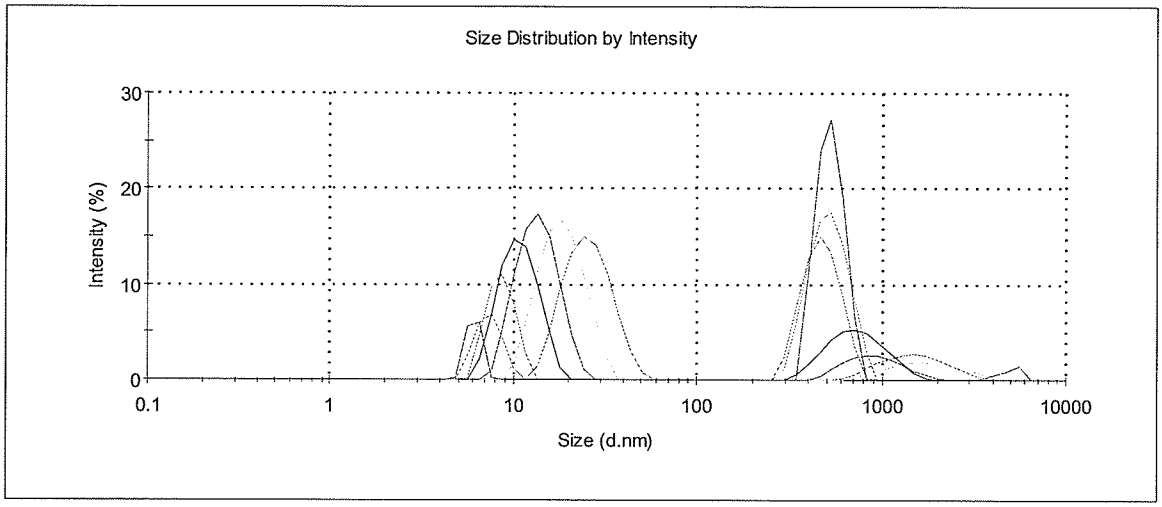

Figure 28: DLS of 4 M TMAO in DDM at several temperatures. The temperatures shown here are 20°C (orange), 30°C (green), 40°C (blue), 50°C (black), 60°C (red), 70°C (purple), and 80°C (brown). The GlpF concentration is 5 μM.

Table 5: Small Particle Diameters at Different Temperatures in DDM with 4 M TMAO

Temperature (°C)	**20**	**30**	**40**	**50**	**60**	**70**	**80**
Diameter of detergent (nm)	8.1	7.1	5.8	4.3	3.6	3.0	2.7
Diameter of detergent in TMAO (nm)	26.5	18.9	13.9	10.9	8.6	7.4	6.1
Difference caused by presence of TMAO (nm)	18.4	11.8	8.1	6.6	5.0	4.4	3.4

Table 6: Large Particle Diameters at Different Temperatures in DDM with 4 M TMAO

Temperature (°C)	**20**	**30**	**40**	**50**	**60**	**70**	**80**

Diameter of detergent (nm)	ND	ND	ND	255	255	220	220
Diameter of detergent in TMAO (nm)	1484	1990	825	712	531	531	531
Difference caused by presence of TMAO (nm)	ND	ND	ND	457	276	311	311

In the presence of GlpF and 4 M TMAO at 20°C a major broad peak is observed in the DLS spectrum at 44 nm (Figure 29, orange curve). This peak suggests particles that are 17 nm larger than in the TMAO-containing detergent spectrum (Figure 28, Table 7) and nearly 34 nm larger than the particles present in the solution containing GlpF in DDM (Figure 27 and Table 2). In the absence of TMAO, GlpF tetramers increase the micelle size by 3.5 nm so an increase in size by 17 nm suggests particles containing about 5 protein tetramers or 2.5 octamers, or perhaps 1 hexadecamer. Recall that octamers were observed in SDS-PAGE analysis of the effects of 4 M TMAO on GlpF (Figure 20). Possible explanations for the slight discrepancy between the SDS-PAGE and DLS results are that SDS dissociates oligomers that are observable by DLS, and a change in the aggregation state of the detergent caused by TMAO that can only be observed in DLS.

At 20°C a minor peak suggesting particles distributed about 400 nm in diameter is observed in the solution containing GlpF solubilized in DDM and 4 M TMAO (Figure 29, orange curve). Increasing the temperature of the solution to 30°C eliminates the 600 nm peak and a new peak appears at about 120 nm (Figure 29, green). This peak may arise from a shift of the 400 nm peak or it could also arise from a separation of the broad peak at 44 nm (Figure 29, orange curve) into two peaks at 28 nm and 120 nm (green

curve). Regardless of the origin of the larger peak it moves to lower diameters and increased intensity as the temperature of the solution is elevated to 80°C. Over the same range of temperatures, the lower diameter peak diminishes in intensity and moves to lower particle diameters (Figure 29). The behaviour of the two peaks is highly similar to that observed in the TMAO-detergent solution (Figure 28) except that in the presence of protein the peaks are broader. Note also that no new peaks appear nor is there any significant change in the behaviour of any of the peaks at elevated temperatures suggesting that most of the changes observed arise from rearrangements of the detergent rather than unfolding of the protein. This agrees closely with the results obtained by SDS-PAGE in which no octamer dissociation was observed until temperatures reached 85°C (Figure 20). These results also confirm the observations from SDS-PAGE that TMAO promotes higher order oligomers of GlpF and stabilizes the protein against thermal unfolding.

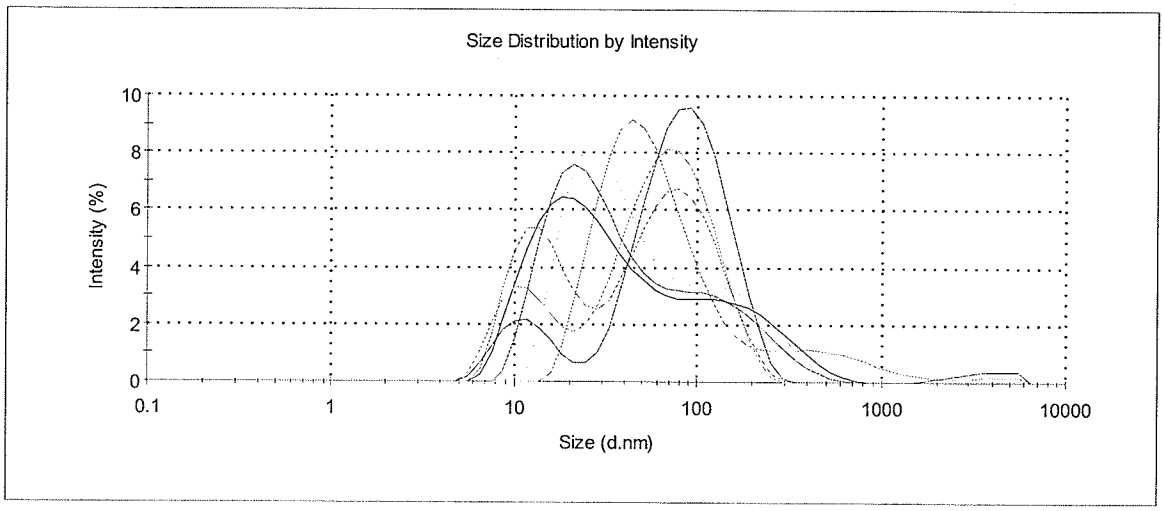

Figure 29: DLS of GlpF in 4 M TMAO and DDM at several temperatures. The temperatures shown here are 20°C (orange), 30°C (green), 40°C (blue), 50°C

(black), 60°C (red), 70°C (purple), and 80°C (brown). The GlpF concentration is 5 μM.

Table 7: Small Particle Diameters at Different Temperatures in DDM with 4 M TMAO

Temperature (°C)	**20**	**30**	**40**	**50**	**60**	**70**	**80**
Diameter in absence of GlpF (nm)	26.5	18.9	13.9	10.9	8.6	7.4	6.1
Diameter in presence of GlpF (nm)	43.8	28.2	21.0	15.7	13.5	10.1	11.7
Difference caused by presence of GlpF (nm)	17.3	9.3	7.1	4.8	4.9	2.7	5.6

Table 8: Large Particle Diameters at Different Temperatures in DDM with 4 M TMAO

Temperature (°C)	**20**	**30**	**40**	**50**	**60**	**70**	**80**
Diameter in absence of GlpF (nm)	1484	1990	825	712	531	531	531
Diameter in presence of GlpF (nm)	396	122	106	91.3	78.8	78.8	91.3
Difference caused by presence of GlpF (nm)	1088	1868	719	621	452	452	440

In order to determine if thermally-unfolded GlpF could be refolded, the protein was heated to different temperatures and then returned to 20°C and DLS was used to monitor the quaternary structure of the protein. Figure 30 shows a DLS spectrum of DDM-solubilized GlpF at 20°C (red curve) revealing a single population of molecules with a mean diameter of 11.7 nm (Figure 30) in agreement with the results shown in Figure 27. At 65°C the solution of GlpF in DDM shows two populations with diameters of about 5 nm and 80 nm (Figure 30, green curve). Missing is the peak at 20 nm that is diagnostic of unfolded aggregated protein observed at high temperatures in Figure 26 suggesting that little protein has unfolded at this temperature. Restoration of the temperature to 20°C (Figure 30, blue curve) results in a DLS spectrum that is slightly broader and has a mean diameter (13.5 nm) that is slightly greater than the initial spectrum obtained at 20°C (12.4 nm). This suggests a minor amount of unfolding and aggregation may have occurred during the course of the thermal cycling of the sample, and that a large fraction of the tetramers have returned to their native form.

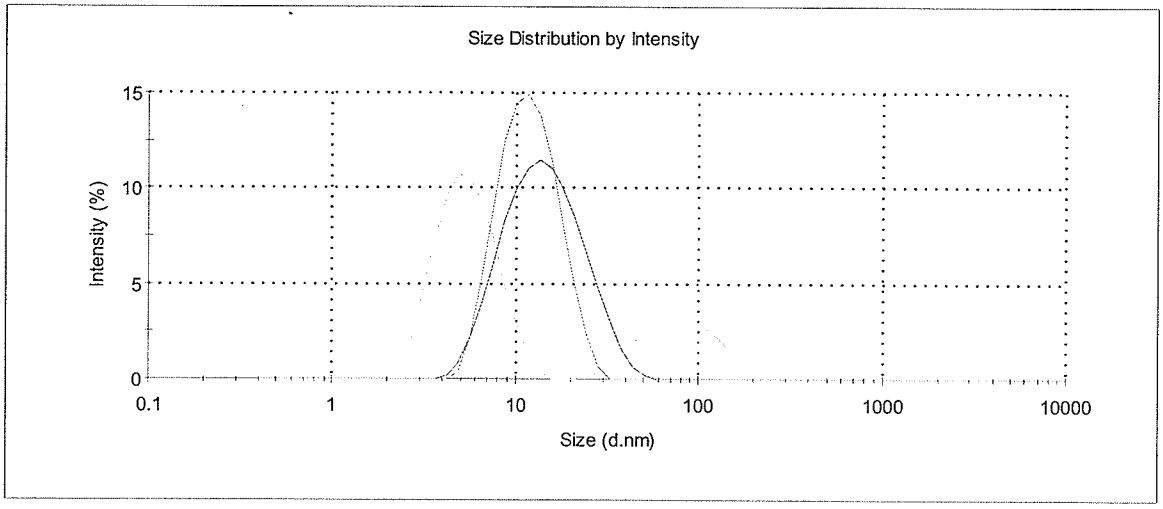

Figure 30: DLS thermal renaturation in the presence of GlpF in DDM. The temperatures shown here are 20°C (orange), 65°C (green), and 20°C (blue). The GlpF concentration is 5 μM.

Similar thermal unfolding experiments to that shown in Figure 30 were done except that the temperature was raised to 67, 68, 69, and 70°C and the results are summarized in Table 9. Figure 31 shows the DLS spectra for the sample that was heated to 70°C. The peak at 70°C has a maximum at 7.5 nm and a long broad tail at higher wavelengths suggesting the presence of higher molecular weight aggregates. The spectrum of the sample restored to 20°C has a peak at 21 nm suggesting that thermal cycling of the sample has resulted in complete unfolding and aggregation. These results show little evidence for any reversibility in the thermal unfolding transition.

Table 9: Particle Diameters at Different Temperatures in First Peak in DDM with 4 M TMAO

T_1 (°C)	D_1 (nm)	T_2 (°C)	D_2 (nm)	T_3 (°C)	D_3 (nm)	T_4 (°C)	D_4 (nm)	T_5 (°C)	D_5 (nm)
20	11.7	**20**	11.7	**20**	11.7	**20**	11.7	**20**	11.7
65	4.8	**67**	5.6	**68**	5.6	**69**	5.6	**70**	7.5
20	13.5	**20**	13.5	**20**	15.7	**20**	21.0	**20**	21.0

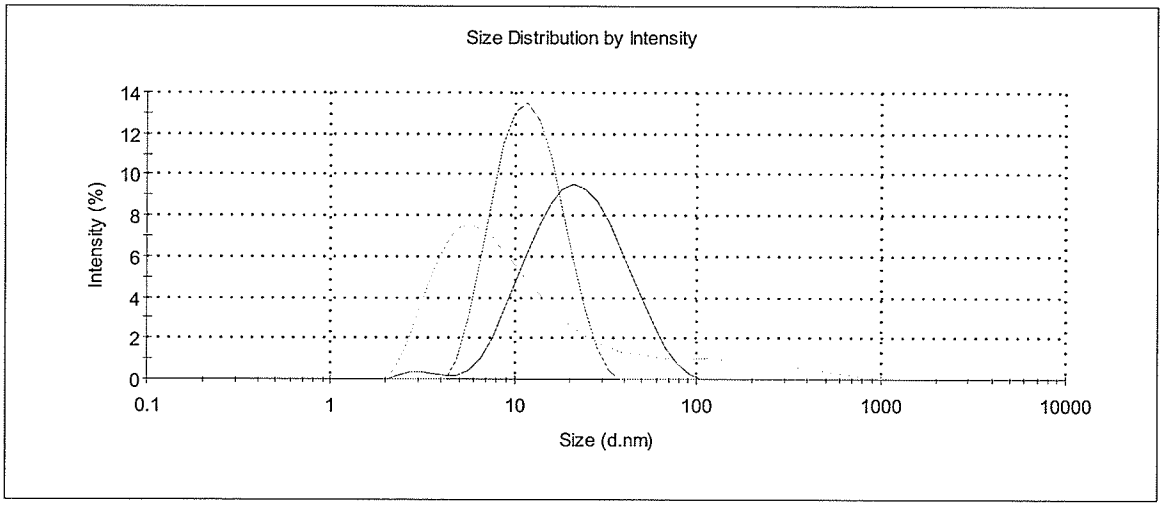

Figure 31: DLS thermal renaturation in the presence of GlpF in DDM. The temperatures shown here are 20°C (orange), 70°C (green), and 20°C (blue). The GlpF concentration is 5 μM.

Refolding experiments were then performed in the presence of 4 M TMAO (Figure 32). The temperature in the sample was increased to 75°C. The spectrum at 20°C (orange curve) is similar to that shown in Figure 29 (orange curve); however the small diameter peak is at a significantly smaller diameter (28 nm) than its counterpart in Figure 29 (43 nm) resulting in better separation between the large and small diameter peaks. A similar observation applies to the peaks in the DLS spectra at 75°C (Figure 32). In the former spectrum (Figure 29) the small diameter peak has a maximum at about 10 nm (purple curve) whereas in Figure 32 the maximum is at about 8 nm (green curve) and the result is a better separation of the peaks in Figure 32. The spectrum of the protein after restoration to 20°C (Figure 32, blue curve) is similar though not identical to the initial experiment obtained at 20°C (red curve). The small diameter peak has decreased in intensity but the peak maximum has increased only to 32.7 nm from 28.2 nm. The large

diameter peak is increased in intensity and has moved from 459 nm to 342 nm. As discussed above, the DLS spectra in Figure 29 show little evidence of protein unfolding and the observed changes in the spectra can be rationalized by reorganization of the detergent as the sample is heated making reference to the data in Figure 28. The spectra in Figure 32 also lack any features diagnostic of protein unfolding at the elevated temperatures although it might be argued that the fact that the preheating and post-heating 20°C spectra are not identical is evidence that some irreversible changes have occurred in the protein as a result of the thermal cycling. It can be seen that although the original and re-natured 20°C spectra are not the exact same as each other, their two peaks indicate nearly identical diameters. It seems that after the renaturation there is still a significant amount of folded octamer, but the ratio between octamer and aggregate has shifted to more aggregate. The smaller diameter peak in the orange curve is 28.2 nm and the larger is 459 nm, where the blue curve has peaks of diameter 32.7 nm and 342 nm.

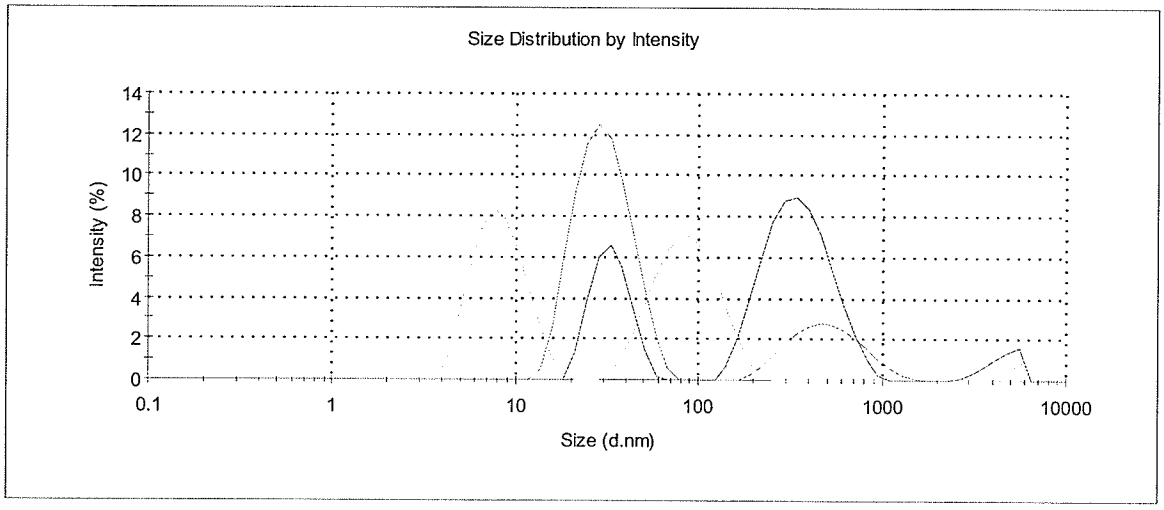

Figure 32: DLS thermal renaturation in the presence of GlpF and 4 M TMAO in DDM. The temperatures shown here are 20°C (orange), 75°C (green), and 20°C (blue). The GlpF concentration is 5 μM.

From the refolding DLS data presented here, it appears that some thermal reversibility can be seen in the absence of TMAO. There is a point between 67°C and 70°C at which there is a dramatic increase in the size of the particles in solution after return to the original temperature. This suggests that in a two-state unfolding mechanism, the protein unfolds and then immediately aggregates and cannot be refolded to its native form. At a temperature between 67°C and 70°C there seems to be a "tipping-point" where the majority of the protein is being unfolded, and therefore cannot be refolded. This temperature range of unfolding is very similar to that found previously where a cooperative unfolding transition at 65.5 ± 0.7°C was reported [48], suggesting that the approximation of the unfolding temperature using this system was reasonable. In TMAO, there is partial reversibility as well. It would be preferable to have a temperature denaturation of GlpF in solution without detergent, to compare against our data, but unfortunately this experiment is not possible.

3.2 GlpF in n-Tetradecyl-β-D Maltoside

To further characterize the stability of GlpF, the effects of SDS and thermal denaturations on GlpF were studied in the detergent n-tetradecyl-β-D maltoside (TDM), in the presence and absence of TMAO. Because TDM has a hydrocarbon tail that is 2 carbons longer than that of DDM, but shares the same maltoside headgroup as DDM, it was hypothesized that the two carbon increase in chain length may have a substantial

effect on the stability of GlpF through a better match between the detergent chain length, and the length of the membrane span of the protein [21, 87]. The experimental conditions were kept exactly the same as for DDM, so as to have a comparison between the stabilities caused only by the difference in the tail-length of the detergent.

It was found that the protein yields in TDM were about half those in DDM. As reported earlier, the average protein yield in TDM is 4.5 ± 1 mg per litre of cell culture, whereas the yields are 8 ± 1 mg in DDM per litre of cell culture. After purification of GlpF in TDM, precipitated material was observed in the samples within one day of storage in the refrigerator, and after three days of storage at room temperature. The material did not go back in to solution after precipitation in either case. This observation contributed to the conclusion that the stability of GlpF in TDM is lower than in DDM.

3.2.1 SDS Denaturations at 40°C in the Presence and Absence of 4 M TMAO.

SDS denaturation experiments of GlpF solubilized in the detergent TDM were done at 40°C to enable direct comparison to the results in Section 3.1.1 describing the SDS denaturation of GlpF in DDM.

Figure 34 shows an SDS electrophoregram of GlpF dissolved in TDM and tested with varying concentrations of SDS. There is an apparent decrease in the stability of the tetramer compared to what was observed for the protein in DDM (Figure 9, lanes 3 and 4), shown by the absence of a band at 90% SDS (Lane 7) and a decrease in intensity of the band at 80% SDS (Lane 6).

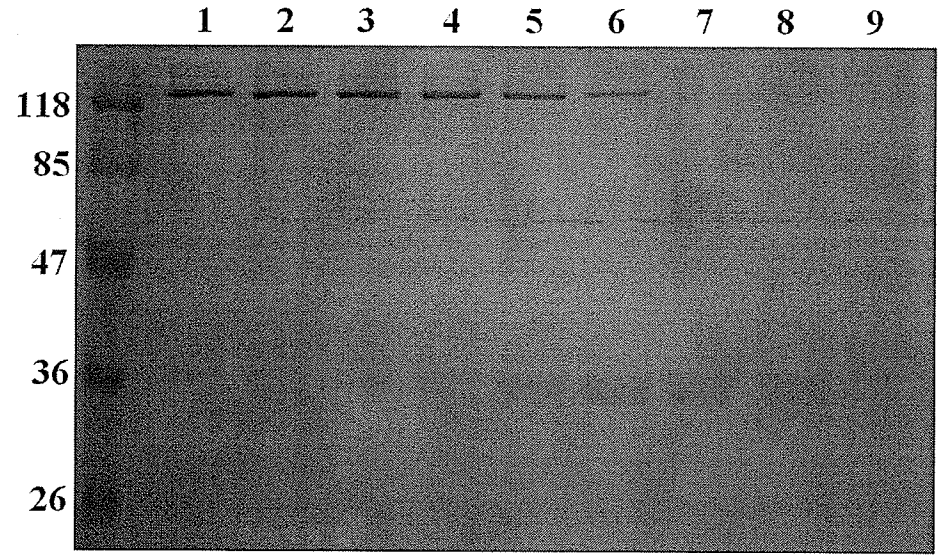

Figure 34: SDS-PAGE showing a 40°C SDS denaturation of GlpF in TDM. Lanes 1-9 correspond to SDS percentages of 0%, 40%, 50%, 60%, 70%, 80%, 90%, 97%, and 98% of the total detergent in the solution used for the incubation period, the other component being TDM.

The least-squares fit of the band intensities in Figure 34 to a two-state unfolding transition is shown in Figure 35. From the fit the SDS_{half} in TDM at 40°C is 34 ± 11% which is only slightly less than the value measured for GlpF in DDM (36 ± 11%).

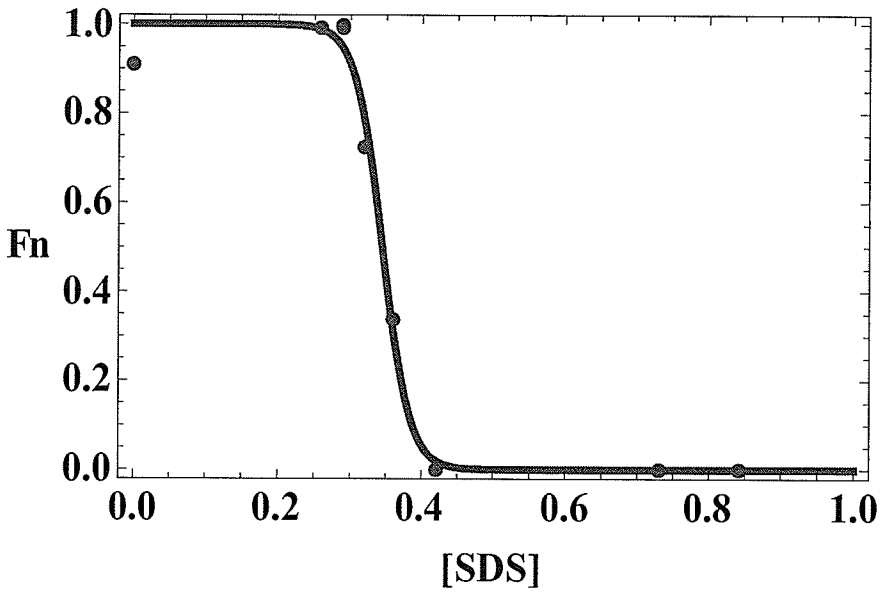

Figure 35: Mathematica™ graph showing the dissociation of tetramer to monomer in TDM at 40°C. The filled circles show the measured band intensities and the line through the points is the best fit to a two-state transition as described by the equation in Methods. The graph shows the normalized fraction of native tetramer (Fn) as a function of SDS mole fraction.

If 4 M TMAO is present in the TDM solution, the GlpF tetramer is significantly stabilized to unfolding by SDS; even at 98% SDS (Lane 9, Figure 36) the tetramer band is similar in intensity to that in the absence of SDS (Lane 1) and very little monomer, dimer, and trimer are observable on the gel. This result is similar, though not identical to the measurements made in DDM (Figure 11). In DDM, the protein is predominantly an octamer at 0% SDS and the octamer unfolds to form tetramer as the SDS fraction increases. Very small amounts of octamer were observed in one replicate of this experiment, but were never observed again in any further experiments in TDM. Thus, it was concluded that the octamer was an artefact of the protein preparation and not induced

by the detergent. In contrast, in DDM the octameric form of GlpF was reproducible in 4 M TMAO for all thermal and chemical denaturation experiments conducted under these conditions (2 different experiments that were each repeated several times).

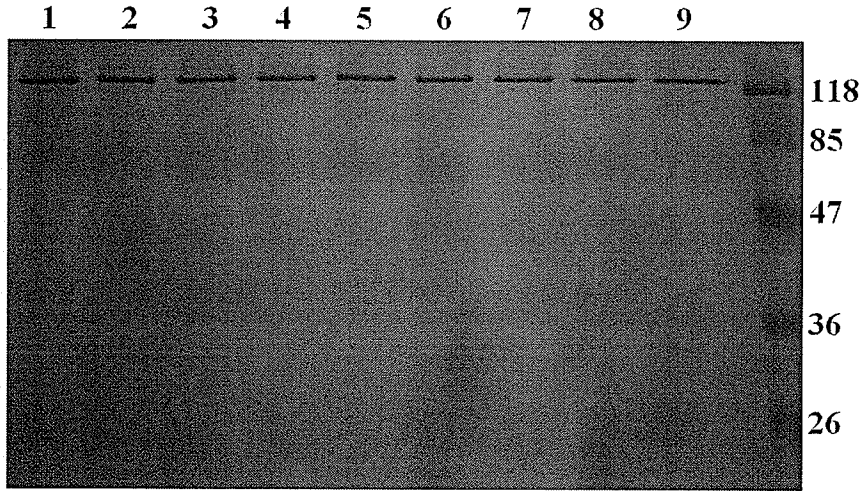

Figure 36: SDS-PAGE showing a SDS denaturation of GlpF dissolved in TDM in the presence of 4 M TMAO at 40°C. Lanes 1-9 correspond to SDS percentages of 0%, 40°C, 50%, 60%, 70%, 80%, 90%, 97%, and 98% of the total detergent in the solution used for the incubation period, the other component being TDM.

3.2.2 Concentration Dependence of TMAO on GlpF.

The concentration dependent effects of TMAO were tested in TDM. SDS denaturation experiments were performed in 0.5 M, 1 M, and 2 M TMAO concentrations. The purpose of these experiments was to see if the concentration dependence of TMAO on GlpF is different in TDM as compared to DDM.

The effects of 0.5 M TMAO on GlpF were studied and it is noticed that the tetramer is completely dissociated by 97% SDS (Figure 37, Lane 8). Comparing this stability to lane 7 in Figure 34 (90% SDS, no TMAO) where there is no tetramer present, suggests that 0.5 M TMAO increases the stability of the tetramer as shown by the fact that there is a faint tetramer band in Figure 37 at a SDS concentration of 90% (Lane 7).

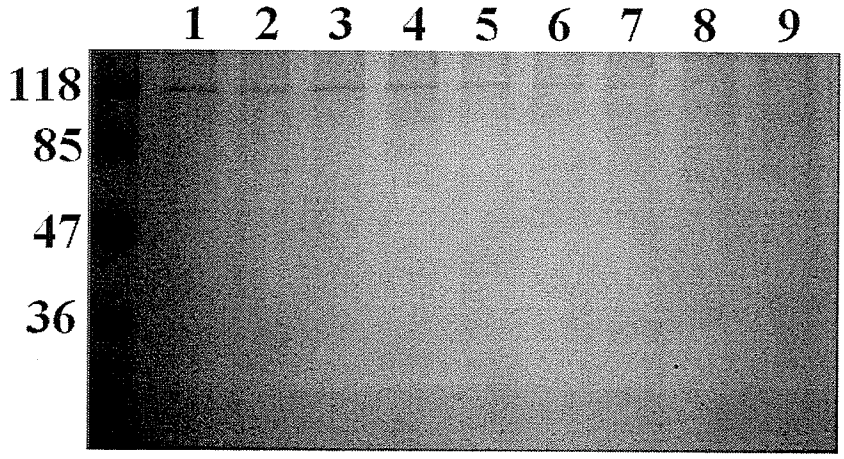

Figure 37: SDS-PAGE showing a 40°C SDS denaturation of GlpF in TDM in the presence of 0.5 M TMAO. Lanes 1-9 correspond to SDS percentages of 0, 40, 50, 60, 70, 80, 90, 97, and 98% of the total detergent in the solution used for the incubation period, the other component being TDM.

When the concentration of TMAO is increased to 1 M (Figure 38), a faint tetramer band at 97% SDS (Lane 8) is observed showing that the stability of the tetramer has been increased, compared to the solution containing 0.5 M TMAO (Figure 37, lane 8).

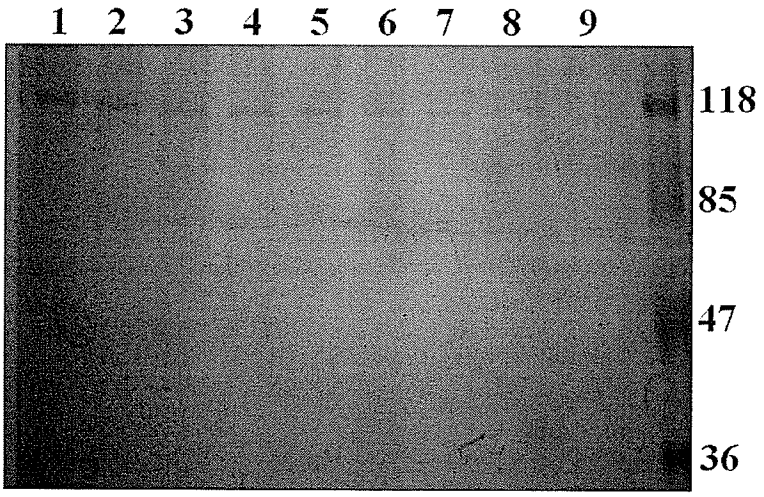

Figure 38: SDS-PAGE showing a 40°C SDS denaturation of GlpF in TDM in the presence of 1 M TMAO. Lanes 1-9 correspond to SDS percentages of 0, 40, 50, 60, 70, 80, 90, 97, and 98% of the total detergent in the solution used for the incubation period, the other component being TDM.

In the experiment shown in Figure 39 the concentration of TMAO has been further increased to 2 M. The tetramer does not completely dissociate at high levels of SDS, but when the gel photo is scanned and analyzed the less intense tetramer bands at 90%, 97%, and 98% (Lanes 7, 8, and 9, respectively) dissociated to an intensity level that was low enough for a SDS_{half} value of 55 ± 19% to be calculated (see Figure 40).

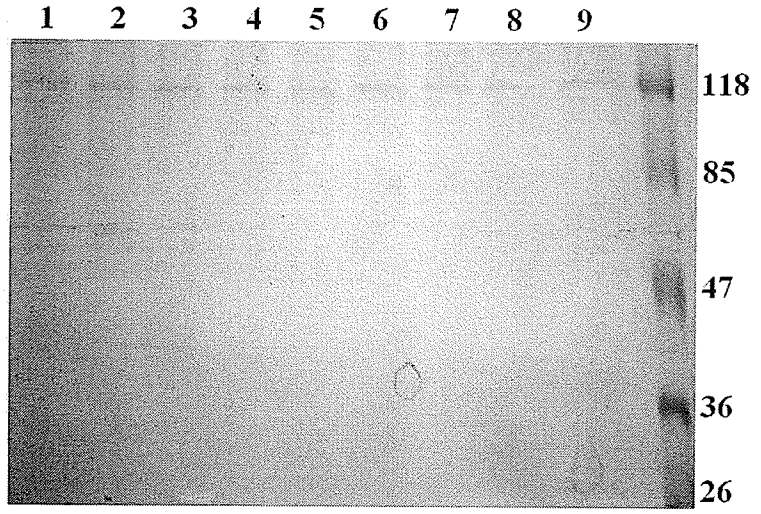

Figure 39: SDS-PAGE showing a 40°C SDS denaturation of GlpF in TDM in the presence of 2 M TMAO. Lanes 1-9 correspond to SDS percentages of 0, 40, 50, 60, 70, 80, 90, 97, and 98% of the total detergent in the solution used for the incubation period, the other component being TDM.

In Figure 40, the fits of the band intensities to a two-state transition obtained from the SDS denaturations of GlpF in TDM and 0 M, 0.5 M, 1 M, and 2 M TMAO are presented. SDS_{half} values were determined from the fits in Figure 40 and the values are 35 ± 11% (0 M TMAO), 37 ± 22% (0.5 M TMAO), 41 ± 18% (1 M TMAO), and 55 ± 19% (2 M TMAO). The fact that a SDS_{half} value could be determined at 2 M TMAO shows that the tetramer is less stable in TDM as compared to DDM where the amount of tetramer dissociation was small enough that an SDS_{half} could not be measured.

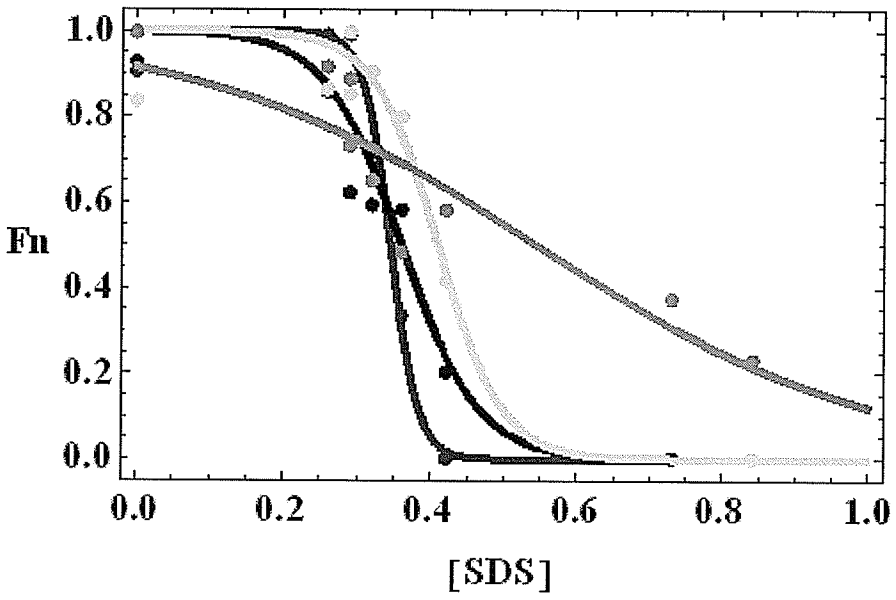

Figure 40: Mathematica graph showing the dissociation of tetramer to monomer in TDM. The graph shows the fraction of native tetramer (Fn) as a function of SDS mole fraction. The TMAO concentrations shown are 0 M (purple), 0.5 M (black), 1 M (green), and 2 M (red). The SDS_{half} for each of the curves from low to high are 35 ± 11%, 37 ± 22%, 41 ± 18%, and 55 ± 19%.

3.2.3 Thermal Denaturations in the Presence and Absence of TMAO.

The thermal stability of GlpF in TDM was tested by performing thermal denaturations on GlpF in the presence and absence of 4 M TMAO. In Figure 41 the tetramer appears very stable until temperatures above 60°C, and above this temperature aggregates are visible (Lanes 6, 7, and 8). At 80°C (Lane 7) the tetramer is no longer

visible and only very large aggregates are observed at the top of the running gel and at the bottom of the loading wells in Lanes 7 and 8. This result shows that the temperature at which the unfolding transition occurs at in TDM is between 70°C and 80°C.

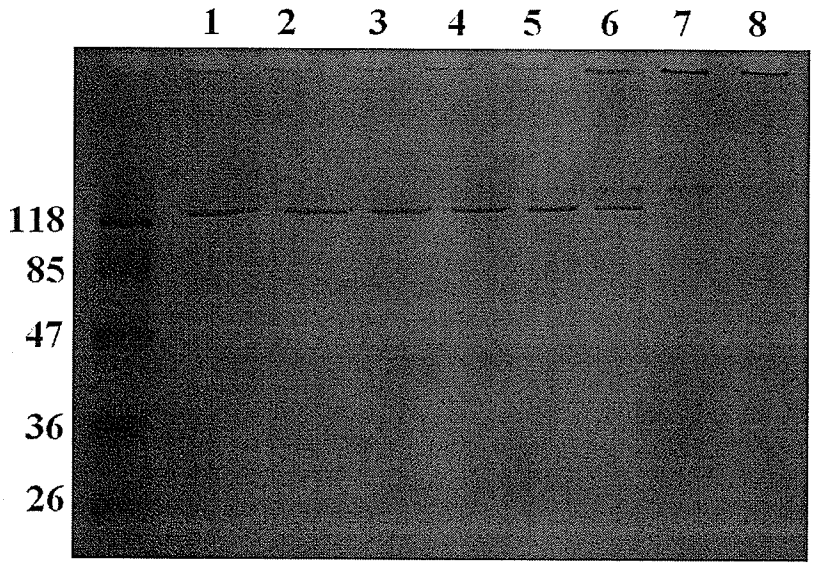

Figure 41: SDS-PAGE showing a temperature denaturation of GlpF in TDM. Lanes 1-8 correspond to the temperatures 22°C, 30°C, 40°C, 50°C, 60°C, 70°C, 80°C, and 85°C.

In 4 M TMAO (Figure 42), the tetramer is provided another 10°C of thermal stability from the TMAO as observed by the considerable amount of tetramer present at 80°C (Lane 7). Aggregate is visible at 70°C (Lane 6) shown by the small amount of higher molecular weight species above the tetramer. By 85°C (Lane 8) there is no tetramer present illustrating that the temperature in which GlpF dissolved in TDM is unfolded at in 4 M TMAO is between 80°C and 85°C.

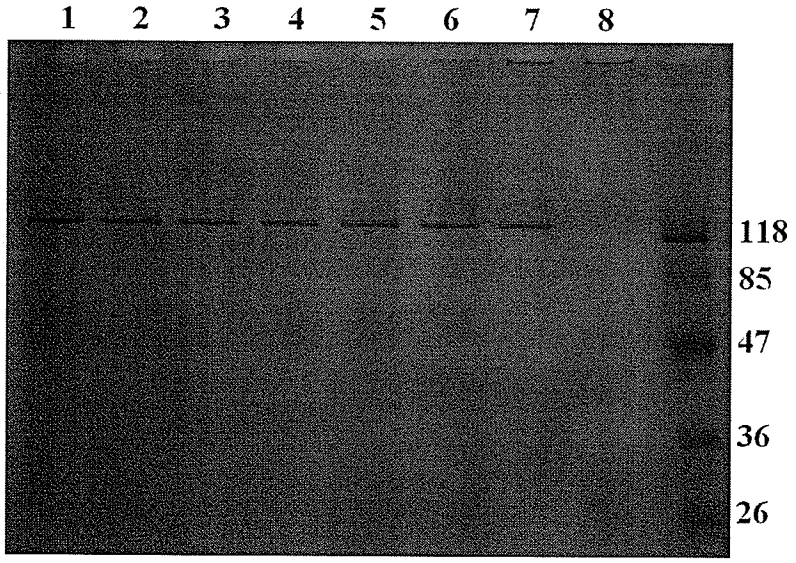

Figure 42: SDS-PAGE showing a temperature denaturation of GlpF in TDM in the presence of 4 M TMAO. Lanes 1-8 correspond to the temperatures 22°C, 30°C, 40°C, 50°C, 60°C, 70°C, 80°C, and 85°C.

Although the transition temperatures are very clear in the previous examples, it must be kept in mind that the actual temperature in which the tetramer is completely unfolded at is slightly higher than what is reported because of the inherent high amounts of SDS present in the gel, running buffers, and sample treatment buffers in SDS-PAGE experiments. This is not expected to be a significant problem though, and the difference between the SDS-PAGE determined transition value and the actual value is anticipated to be small (less than 5°C).

T_m values from were calculated from the fits of the band intensities in the presence and absence of 4 M TMAO to a two-state thermal transition. The determined values are 70 ± 1°C in 0 M TMAO and 81 ± 2°C in 4 M TMAO, showing that 4 M TMAO enhances the thermal stability of GlpF in TDM by eleven degrees.

3.2.4 Dynamic Light Scattering Analysis of Heat Denaturations on GlpF in Presence and Absence of TMAO.

DLS thermal experiments were performed on TDM in the presence and absence of GlpF, and then on GlpF in the presence and absence of 4 M TMAO. These experiments are directly comparable to the DLS thermal studies in DDM, and give a snapshot of the sizes of the particles in solution at the varied temperatures, which can be related to protein and detergent aggregation, thus indicating the effects of detergent and TMAO on the stability of GlpF.

Figure 43 shows the effects of increasing heat on TDM micelles in the absence of GlpF. At 20°C the average micelle diameter is 11.3 nm which compares to a value of about 8 nm measured by Ericsson et al., [88], using DLS. The difference in size of the measured micelles may be due to the fact that the lowest concentration of TDM used in the study by Ericsson et al., [88], was 5 g/L which is more than three times the concentration that is used in our study. The peak at 20°C (orange curve) indicates that the micelles increase in diameter and decrease slightly in intensity as the temperature increases until 40 and 50°C (blue and black curves, respectively) where it reaches a maximum of 18.5 nm. Further increases in temperature cause the micelles to decrease in diameter and the peaks increase slightly in intensity. The peaks in the DLS spectra in TDM are considerably broader than those measured in DDM (Figure 26). Furthermore, the thermal behaviour of the peaks contrasts sharply with what was observed in DDM

(Figure 26) and suggests that heating has only a minor effect on the structure of the TDM micelle.

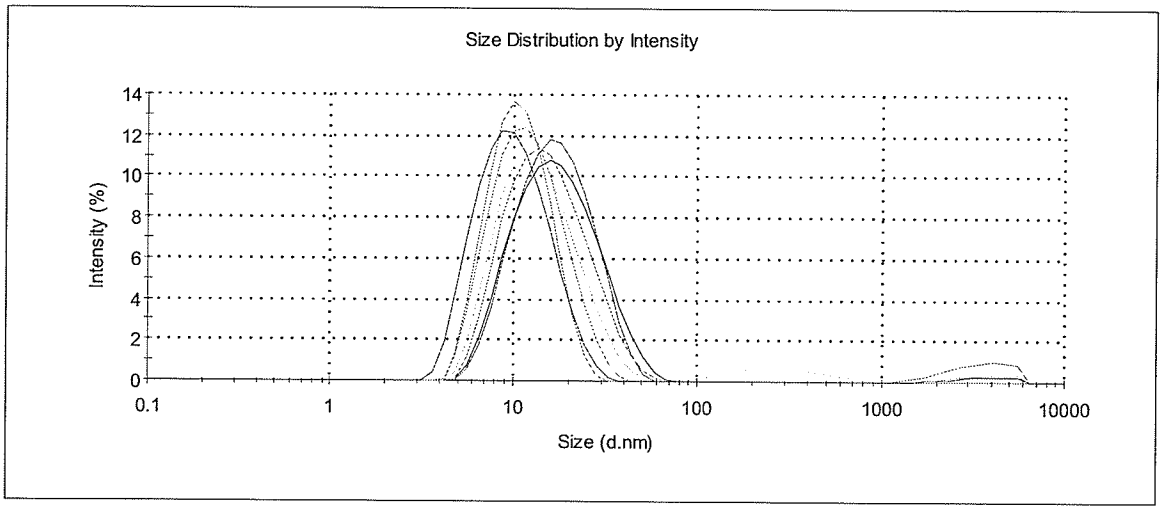

Figure 43: DLS of TDM at several temperatures. The temperatures shown here are 20°C (orange), 30°C (green), 40°C (blue), 50°C (black), 60°C (red), 70°C (purple), and 80°C (brown).

In Figure 44, DLS spectra of GlpF solubilized in TDM are shown. At 20°C a single peak is observed and the diameter is 12.1 nm (orange curve). As the temperature is increased to 30°C, the peak does not change intensity and indicates a smaller diameter of 11.7 nm (green curve). At 40°C the peak has decreased in intensity and moved to a diameter of 14.1 nm (blue curve). When the temperature is increased to 50°C, a new peak emerges with a diameter of about 220 nm (black curve), it grows in intensity and moves to smaller micelle diameters as the temperature is increased to 80°C. This large peak may be indicative of increasing amounts of large protein aggregates because a large diameter peak is not found in the absence of GlpF (Figure 43). The size of the large aggregates in TDM (Figure 44, ~220 nm) is much larger than those found in DDM (~15

nm, Figure 27 and Table 4) and this may signify a change in the aggregation state of the detergent caused by the presence of the protein. The large increase in intensity in the large diameter peaks and the large decrease in intensity in the small diameter peaks from 60°C to 70°C (Figure 44) is evidence for the denaturation and aggregation of GlpF which was found to occur from SDS-PAGE (Figure 34) at about 65°C. The fact that an intermediate peak between the large and small diameter peaks is observed in DDM (Figure 27) but not in TDM (Figure 44) may be explained by the larger peak widths observed in TDM and the fact that heat does not appear to reduce the size of the small diameter detergent peaks in TDM (Figure 43) as it does in DDM (Figure 26). Alternatively, the protein-detergent aggregates in TDM may be significantly larger than those formed in DDM.

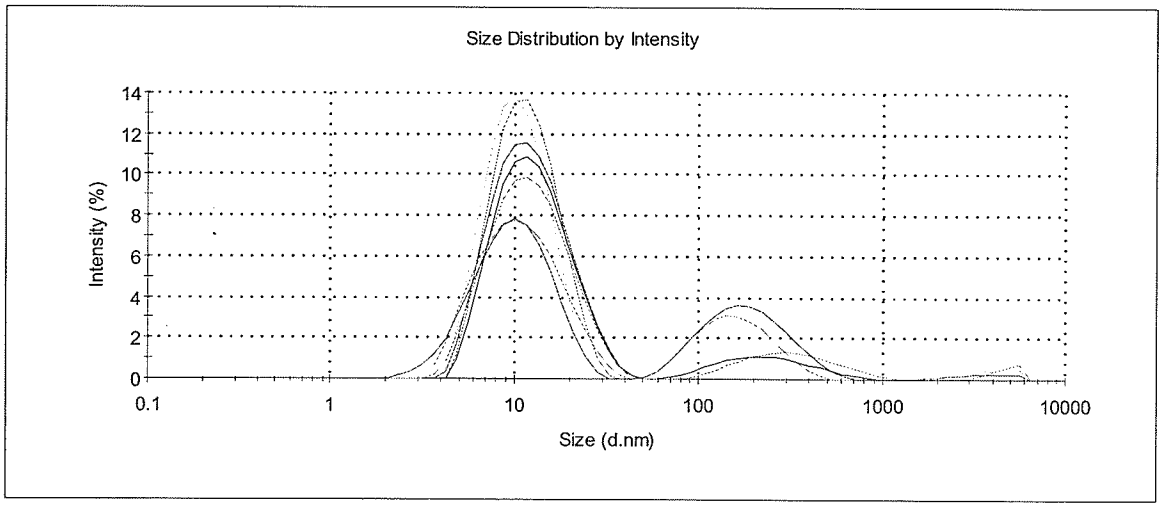

Figure 44: DLS of GlpF in TDM at several temperatures. The temperatures shown here are 20°C (orange), 30°C (green), 40°C (blue), 50°C (black), 60°C (red), 70°C (purple), and 80°C (brown). The GlpF concentration is 5 μM.

The effect of temperature on TDM in the presence and absence of GlpF is apparent in Tables 10 and 11 where the diameters of the peaks and the differences between them are listed. The interpretation of the differences between the peaks is difficult as, for e.g., the difference between the small peaks at 20°C is 0.85 nm, which is much smaller than the 4.5 nm size of the tetramer previously reported in the literature [21]. This suggests that the protein-detergent mixed micelle is about the same size as the empty detergent micelle. Changes in the diameters of the empty and mixed micelles as a function of temperature are also not easily interpreted, but for the small diameter peaks the differences are on the order of or less than the size of a protein tetramer. As mentioned above it is conceivable that the large diameter peaks, first observed at 50°C and not observed in the detergent in the absence of protein, represent unfolded protein aggregates solubilized in detergent.

Table 10: TDM Small Particle Diameters at Different Temperatures

Temperature (°C)	**20**	**30**	**40**	**50**	**60**	**70**	**80**
Detergent diameter (nm)	11.3	15.9	18.2	18.5	16.6	13.0	10.9
Diameter of detergent and GlpF (nm)	12.1	11.7	14.1	14.7	13.7	11.3	11.0
Difference caused by presence of GlpF (nm)	0.8	-4.2	-4.1	-3.8	-2.9	-1.7	0.1

Table 11: TDM Large Particle Diameters at Different Temperatures

Temperature (°C)	**50**	**60**	**70**	**80**
Detergent diameter (nm)	ND	ND	ND	ND
Diameter of detergent and GlpF (nm)	220	295	141	164
Difference caused by presence of GlpF (nm)	ND	ND	ND	ND

In 4 M TMAO there is a very significant change in the DLS spectra. When TMAO is added to a solution of TDM in the absence of GlpF (Figure 45), the spectra are much different than TDM in the absence of TMAO (Figure 43). At 20°C there is only one peak found in the presence of TMAO at about 142 nm (Figure 45, orange peak), and as the temperature increases the micelle steadily gets smaller in diameter. There is a slight increase in intensity from 20°C to 40°C (blue curve), but at temperatures above 40°C there is a steady decline in the intensity. At 70°C a second peak is found with a diameter of almost 400 nm, and at 80°C this large diameter peak has increased in intensity and diameter to about 530 nm (brown curve, Figure 45, Table 13)

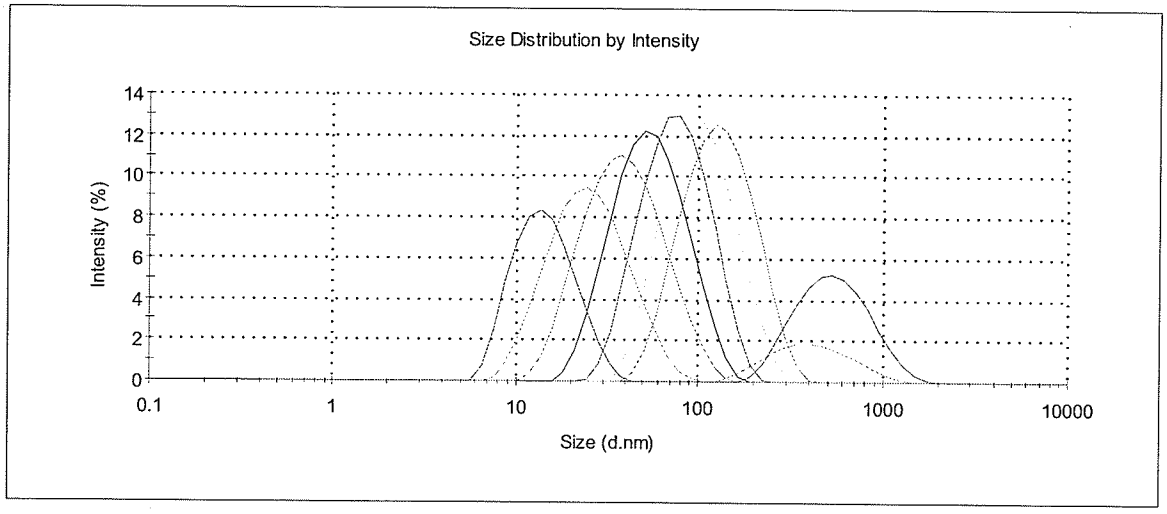

Figure 45: DLS of TDM in the presence of 4 M TMAO at several temperatures. The temperatures shown here are 20°C (orange), 30°C (green), 40°C (blue), 50°C (black), 60°C (red), 70°C (purple), and 80°C (brown). The GlpF concentration is 5 μM.

Figure 46 is a thermal denaturation curve of GlpF in TDM in the presence of 4 M TMAO. The figure shows a major peak at 20°C (orange curve) with a diameter of 127 nm which decreases in intensity and diameter as the temperature increases. The 20°C peak is almost 115 nm bigger than the particles observed in the absence of 4 M TMAO (Figure 44, Table 10), and about 15 nm smaller than those found in the absence GlpF (Figure 45, Table 12). This result demonstrates that in the presence of TMAO, GlpF is influencing the aggregation state of the detergent, causing smaller micelles to be the preferred state of the protein and detergent particle. At 40°C (blue curve, Figure 46) the peak has significantly broadened suggesting that it is comprised of two or more populations of small and large diameter particles. Indeed, at 50°C (black curve, Figure 46) the appearance of a second larger diameter peak is observed at about 190 nm. This large peak increases in diameter and intensity as the temperature is increased until it reaches a diameter of about 712 nm by 80°C (brown curve).

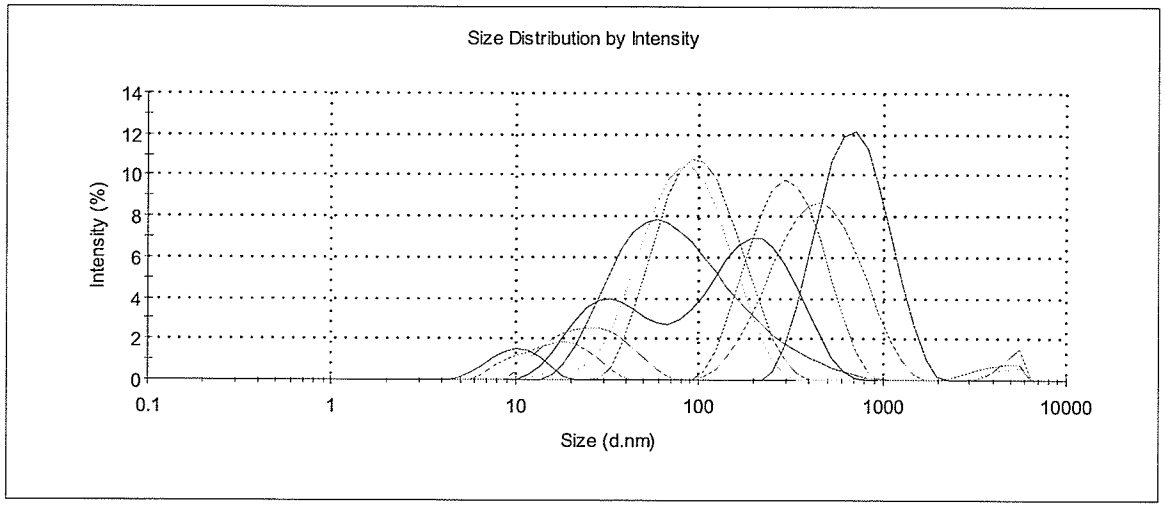

Figure 46: DLS thermal denaturation in the presence of GlpF and 4 M TMAO in TDM at several temperatures. The temperatures shown here are 20°C (orange), 30°C (green), 40°C (blue), 50°C (black), 60°C (red), 70°C (purple), and 80°C (brown). The GlpF concentration is 5 μM.

Table 12 shows that the small detergent particles are smaller in the presence of GlpF and TMAO than in the presence of TMAO alone suggesting that they contain no protein. In contrast, the large particles that appear at higher temperatures are larger in the presence of protein than in its absence (Table 12) suggesting that they contain protein. The DLS data in Figure 46 and Table 12 are dramatically different to what was observed by SDS-PAGE (Figure 42) which shows very little change in the quaternary structure of GlpF up to 70°C. However, most of the changes in particle size observed in Figure 46 are likely attributable to the changes in detergent induced by heating and observed in Figure 45. The particles observed in Figure 46 at 80°C likely represent detergent-solubilized protein aggregates, but the only indication of this is that the particles are much larger in the presence of protein than in its absence.

Table 12: Small Particle Diameters at Different Temperatures in TDM with 4 M TMAO

Temperature (°C)	**20**	**30**	**40**	**50**	**60**	**70**	**80**
Diameter in absence of GlpF (nm)	141.7	106.8	80.4	59.8	44.1	27.6	14.6
Diameter in presence of GlpF (nm)	127.0	96.6	92.6	37.1	23.9	17.2	9.5
Difference caused by presence of GlpF (nm)	-14.7	-10.2	-12.2	-22.8	-20.2	-10.4	-5.1

Table 13: Large Particle Diameters at Different Temperatures in TDM with 4 M TMAO

Temperature (°C)	**50**	**60**	**70**	**80**
Diameter in absence of GlpF (nm)	ND	ND	514	480
Diameter in presence of GlpF (nm)	190	295	458	712
Difference caused by presence of GlpF (nm)	ND	ND	-62.6	-181

3.3 GlpF in 1-Lauroyl-2-Hydroxy-sn-Glycero-3-Phosphocholine

Experiments were performed on GlpF solubilized in 1-Lauroyl-2-Hydroxy-sn-Glycero-3-Phosphocholine (LLPC) which is a detergent that has the same alkyl tail length as DDM (12 carbons), but with a phosphatidylcholine head group. By changing the head group, but keeping the length of the detergent tail the same as in DDM, information is gained on the effect of the detergent head group on the stability of GlpF. Protein yields of GlpF in LLPC were approximately 6 ± 1 mg per litre of cell culture. The protein was found to be very stable in LLPC, and did not come out of solution in the refrigerator or at room temperature.

3.3.1 SDS Denaturations at 40°C in the Presence and Absence of 4 M TMAO.

SDS denaturations of GlpF in LLPC were performed at 40°C in the presence and absence of 4 M TMAO. Figure 47, shows that there is little change in the tetramer band intensity up to 80% SDS (Lane 6) whereas at 90% SDS (Lane 7) the tetramer is greatly diminished. By 97% SDS (Lane 8, Figure 47) the tetramer has been completely denatured as shown by the increase in monomer and the absence of tetramer. This result is very similar to the result obtained in DDM where the tetramer band is very intense up to 80% SDS and is greatly diminished by 90% SDS (Figure 9). The low level of monomer that is found in Lane 1 (0% SDS) is due to the inherent and unavoidable presence of SDS in the gel and sample treatment buffer. It causes a small amount of the

monomer to dissociate, but has no significant effect on the quaternary structure of the majority of the sample.

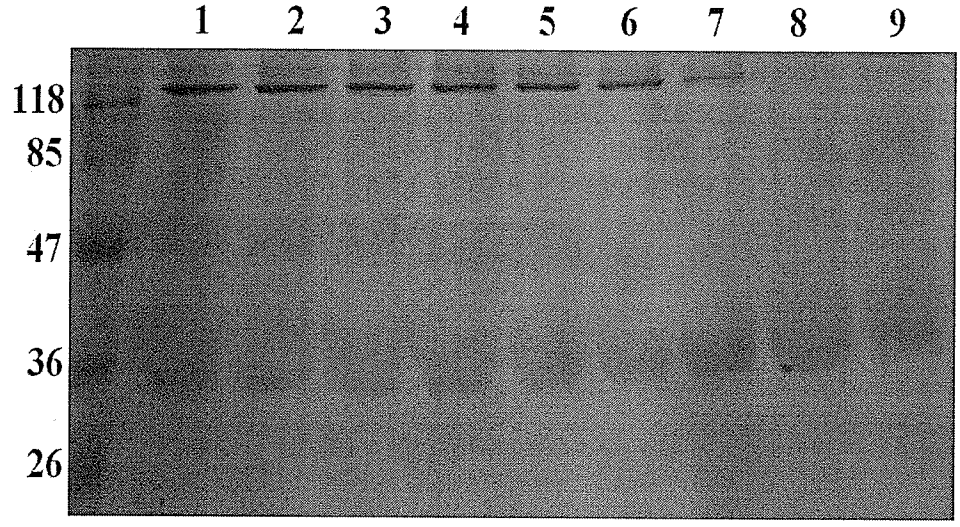

Figure 47: SDS-PAGE showing a 40°C SDS denaturation of GlpF in LLPC. Lanes 1-9 correspond to SDS percentages of 0, 40, 50, 60, 70, 80, 90, 97, and 98% of the total detergent in the solution used for the incubation period, the other component being LLPC.

The least-squares fit of the band intensities in Figure 47 to a two-state unfolding transition is shown in Figure 48. From the fit the 40°C SDS_{half} in LLPC is 39 ± 14%.

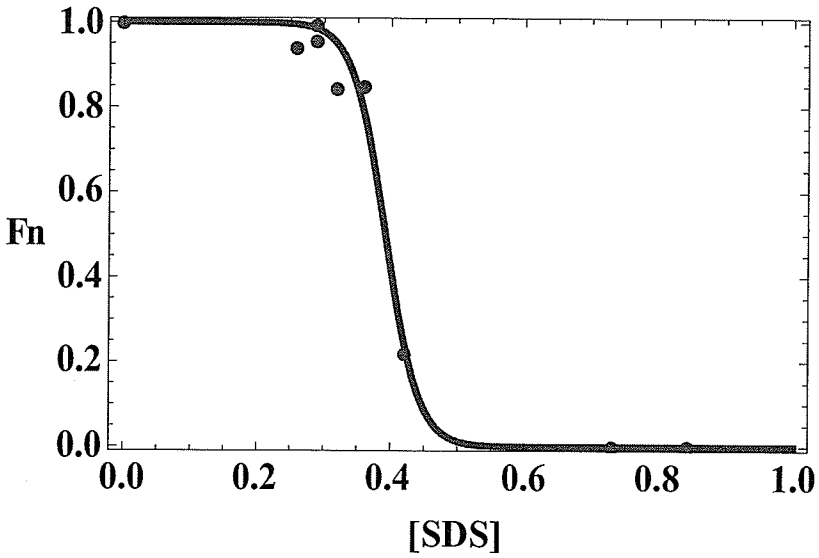

Figure 48: Mathematica graph showing the dissociation of tetramer to monomer in LLPC at 40°C. The filled circles show the measured band intensities and the line through the points is the best fit to a two-state transition as described by the equation in Methods. The graph shows the normalized fraction of native tetramer (Fn) as a function of SDS mole fraction.

Figure 49 shows an SDS denaturation of GlpF dissolved in LLPC in the presence of 4 M TMAO. Similar to what was observed in DDM (Figures 11 and 12) and TDM (Figure 36), 4 M TMAO completely prevents the dissociation of GlpF tetramer at all concentrations of SDS. Unlike the situation in DDM (Figures 15 and 16), no octamer is observed in LLPC at high TMAO concentrations.

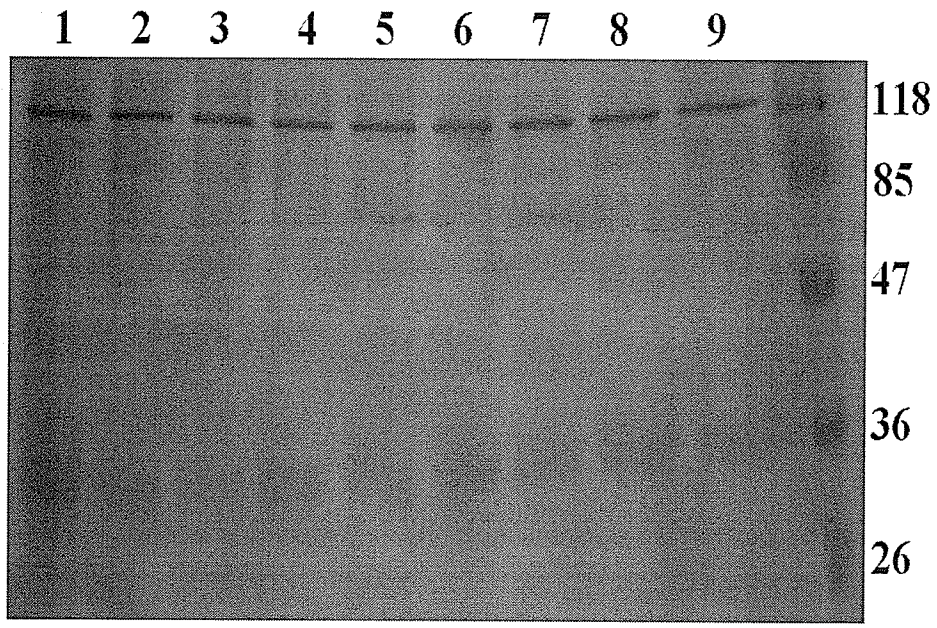

Figure 49: SDS-PAGE showing a 40°C SDS denaturation of GlpF in LLPC in the presence of 4 M TMAO. Lanes 1-9 correspond to SDS percentages of 0, 40, 50, 60, 70, 80, 90, 97, and 98% of the total detergent in the solution used for the incubation period, the other component being LLPC.

3.3.2 Concentration Dependence of TMAO.

The concentration dependence of TMAO was determined for GlpF solubilized in LLPC at 40°C. Figures 50 to 53 show the effects of 0.5 M, 1 M, and 2 M TMAO on the denaturation by SDS of GlpF in LLPC at 40°C. The faint background of dimer bands present throughout the titrations in Figures 50 and 51 is an artefact of the protein preparation that was used for these two experiments and was not found in any other preparations. The rare occurrence of small amounts of dimer present has been previously reported in GlpF preparations [47], and suggests an increased level of denatured protein in the preparations. In Figure 50 (0.5 M TMAO) a very faint amount of tetramer can be

observed at 97% SDS (Lane 8), but at 98% SDS the tetramer has been dissociated. TMAO significantly stabilizes GlpF in LLPC in comparison to DDM and TDM. This is shown by the increased amounts of tetramer at high percentages of SDS observed in Lane 7 compared to that observed at 90% in DDM (figure not shown) and TDM (Figure 37, Lane 7) in the presence of 0.5 M TMAO.

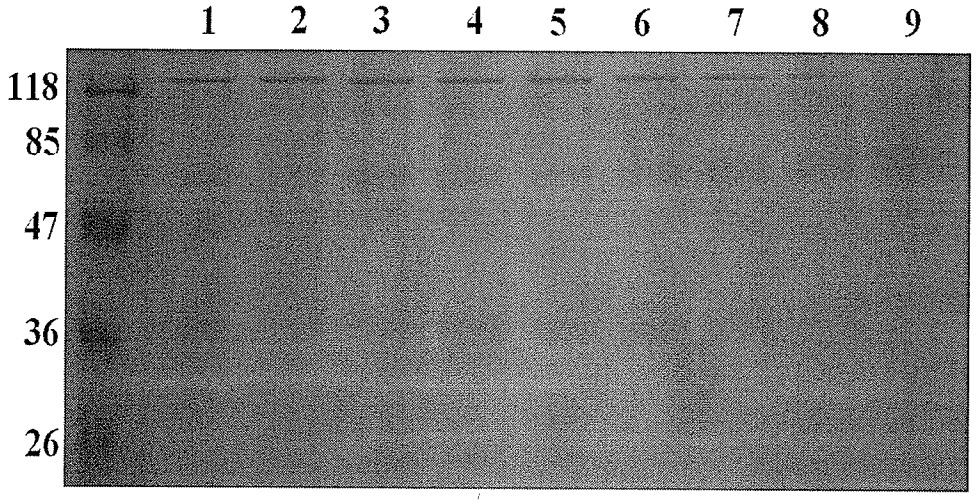

Figure 50: SDS-PAGE showing a 40°C SDS denaturation of GlpF in LLPC in the presence of 0.5 M TMAO. Lanes 1-9 correspond to SDS percentages of 0, 40, 50, 60, 70, 80, 90, 97, and 98% of the total detergent in the solution used for the incubation period, the other component being LLPC.

At 1 M TMAO concentration (Figure 51), there is still a small amount of tetramer present at 98% SDS (Lane 9). LLPC is the only detergent tested in which 1 M TMAO stabilized GlpF to a level in which complete denaturation of the tetramer by SDS is not found.

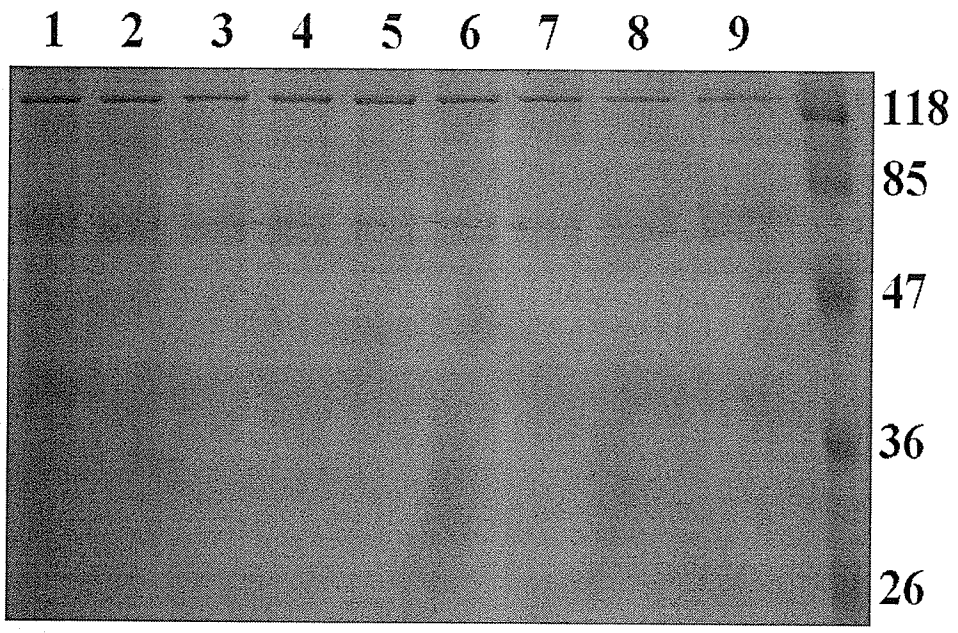

Figure 51: SDS-PAGE showing a 40°C SDS denaturation of GlpF in LLPC in the presence of 1 M TMAO. Lanes 1-9 correspond to SDS percentages of 0, 40, 50, 60, 70, 80, 90, 97, and 98% of the total detergent in the solution used for the incubation period, the other component being LLPC.

Figure 52 shows the effect of 2 M TMAO on GlpF, where the tetramer is not dissociated by SDS. The tetramer band is present in Lanes 8 and 9. This indicates that the tetramer is very stable at high concentrations of SDS, and that significant stability is conferred to the protein by 2 M TMAO.

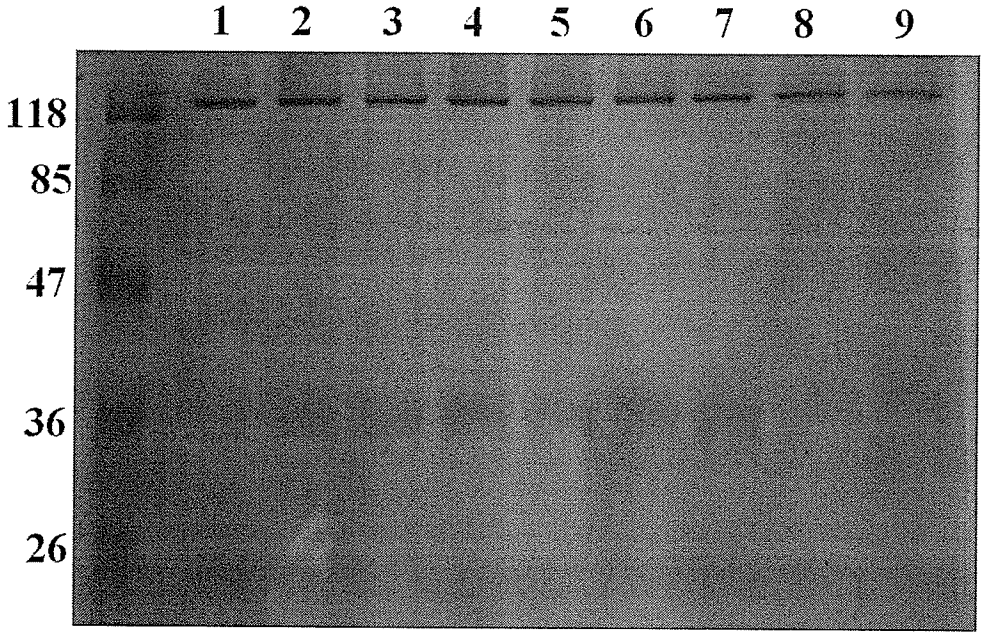

Figure 52: SDS-PAGE showing a 40°C SDS denaturation of GlpF in LLPC in the presence of 2 M TMAO. Lanes 1-9 correspond to SDS percentages of 0, 40, 50, 60, 70, 80, 90, 97, and 98% of the total detergent in the solution used for the incubation period, the other component being LLPC.

A graph of the fits of the band intensities to two-state transitions of GlpF in the increasing TMAO concentrations is shown in Figure 53. TMAO significantly stabilizes GlpF in LLPC in comparison to DDM and TDM indicated by a large increase in the SDS_{half} value to 66 ± 19% for GlpF in LLPC that is caused by the addition of 0.5 M TMAO. This large increase is not observed in DDM (Figure 17, 40 ± 16%) or TDM (Figure 40, 37 ± 22%) in the presence of 0.5 M TMAO. The fact that the data measured in 2 M TMAO could not be fit to a two-state transition because the protein did not dissociate sufficiently supports the observation that TMAO greatly stabilizes GlpF in LLPC in comparison to DDM and TDM. Interestingly, GlpF in LLPC has the highest

SDS_{half} in the absence of TMAO showing that the protein has its highest stability in that detergent.

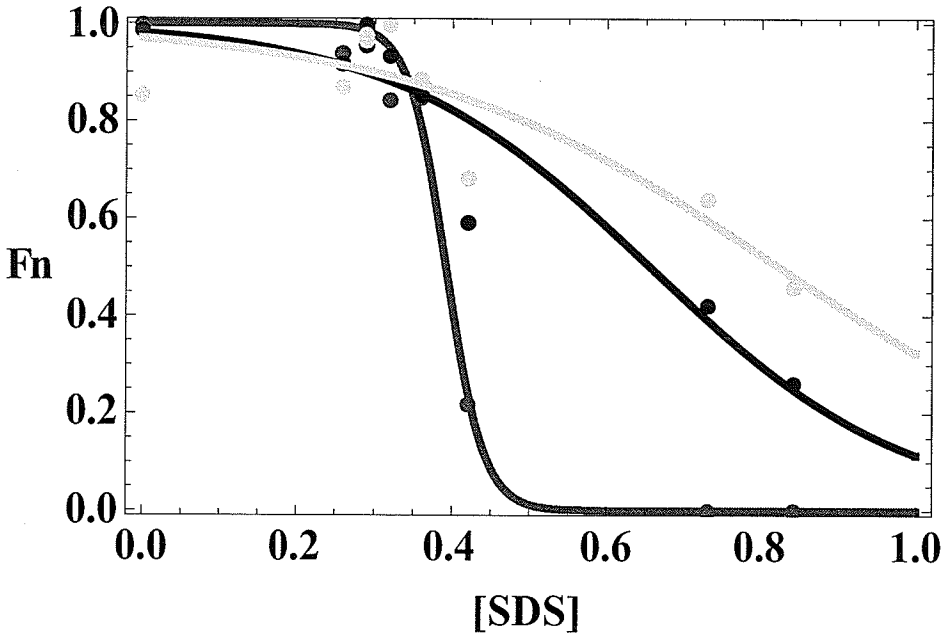

Figure 53: Mathematica graph showing the dissociation of GlpF tetramer to monomer in LLPC. The graph shows the fraction of native tetramer (Fn) as a function of SDS mole fraction. The TMAO concentrations shown are 0 M (purple), 0.5 M (black), and 1 M (green). The SDS_{half} for each of the curves from low to high are 39 ± 14%, 66 ± 19%, and 82 ± 25%.

3.3.3 Thermal Denaturations in the Presence and Absence of TMAO.

Investigations into the thermal stability of GlpF in LLPC were performed in the presence and absence of 4 M TMAO. Figure 54 illustrates that in the absence of TMAO there is still a significant amount of tetramer present at 80°C (Lane 7); the rest of the protein has been denatured into higher molecular weight aggregates as deduced from the band in the loading well, the band at the interface of the running and stacking gels, and from the smear of large aggregated proteins above the tetramer band. By 85°C (Lane 8), all of the tetramer has been denatured. Aggregated GlpF is found in lanes 5 and 6 (60°C and 70°C), but the tetramer band does not seem to decrease in intensity until lane 6. This demonstrates the slightly higher thermal stability of GlpF in LLPC as compared to that in DDM, where the tetramer is completely absent at 75°C (Lane 6, Figure 18) and in TDM, where the tetramer has been completely eliminated by 80°C (Lane 7, Figure 41). The low level of monomer that is observed at 22°C in Figure 54 is due to the inherent high levels of SDS present in the gel and sample treatment buffer, which cause a very small amount of tetramer to be dissociated into monomer.

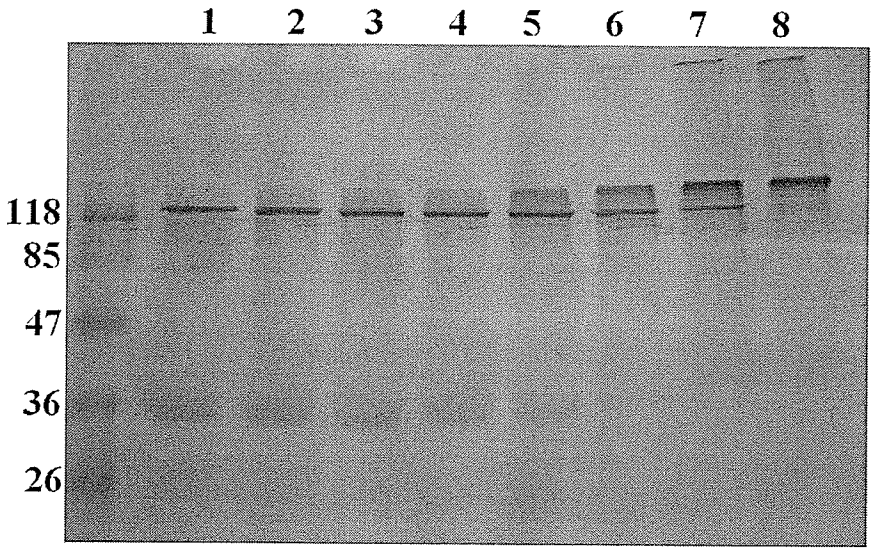

Figure 54: SDS-PAGE showing a temperature denaturation of GlpF in LLPC. Lanes 1-8 correspond to the temperatures 22°C, 30°C, 40°C, 50°C, 60°C, 70°C, 80°C, and 85°C.

In Figure 55 it is observed that 4 M TMAO gives an increase in the thermal stability of GlpF from the fact that there is a significant tetramer band at 85°C (Lane 8), and although there is a lot of aggregate in lane 7 (80°C), the tetramer band is nearly as intense as previous lanes.

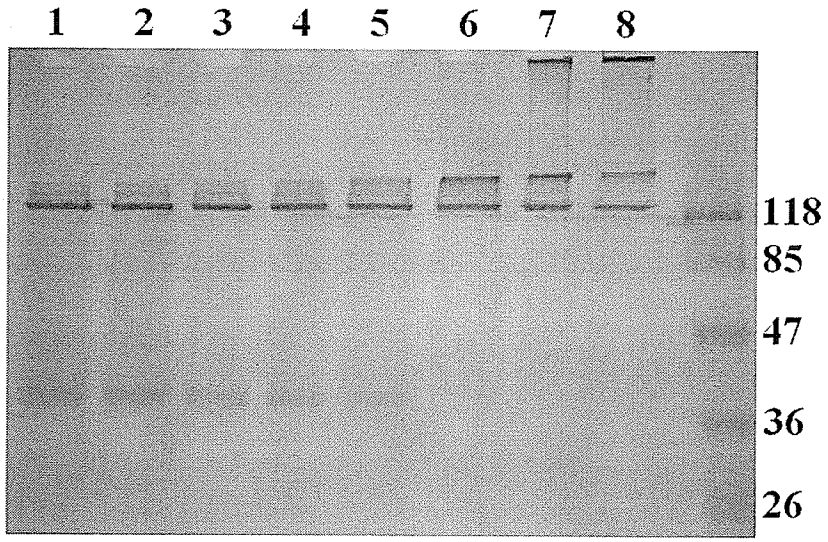

Figure 55: SDS-PAGE showing a temperature denaturation of GlpF in LLPC in the presence of 4 M TMAO. Lanes 1-8 correspond to the temperatures 22°C, 30°C, 40°C, 50°C, 60°C, 70°C, 80°C, and 85°C.

T_m values from were calculated from the fits of the band intensities in the presence and absence of 4 M TMAO to a two-state thermal transition. The determined values are 82 ± 4°C in 0 M TMAO and 91 ± 2°C in 4 M TMAO, showing that 4 M TMAO enhances the thermal stability of GlpF in LLPC by nine degrees. These values also show the increased thermal stability of GlpF solubilized in LLPC as compared to the protein solubilized in DDM and TDM. The stability of the GlpF tetramer in LLPC in the absence of TMAO is comparable in stability to GlpF in DDM and TDM in the presence of 4 M TMAO (80 ± 1°C in DDM, 81 ± 2°K in TDM).

3.3.4 Dynamic Light Scattering Heat Denaturations on GlpF in Presence and Absence of TMAO.

Figure 56 is a DLS graph of the effect of temperature on LLPC particle diameter in the absence of GlpF. The average size of the particles at 20°C is 7.7 nm (orange curve). It should be noted that there is no literature on the diameter of LLPC micelles, therefore no diameter comparisons can be made to the current literature. As the temperature is increased the average particle diameter decreases as does the intensity of the peak until a size of 2.2 nm (brown curve) at 80°C is observed. There is a second peak at 20°C that corresponds to particles 585 nm in diameter. This peak disappears as 30°C, but re-emerges at 40°C with a particle diameter of 196 nm and continues to grow in intensity as the temperature increases, shifting to a slightly larger diameter of 210 nm by 80°C.

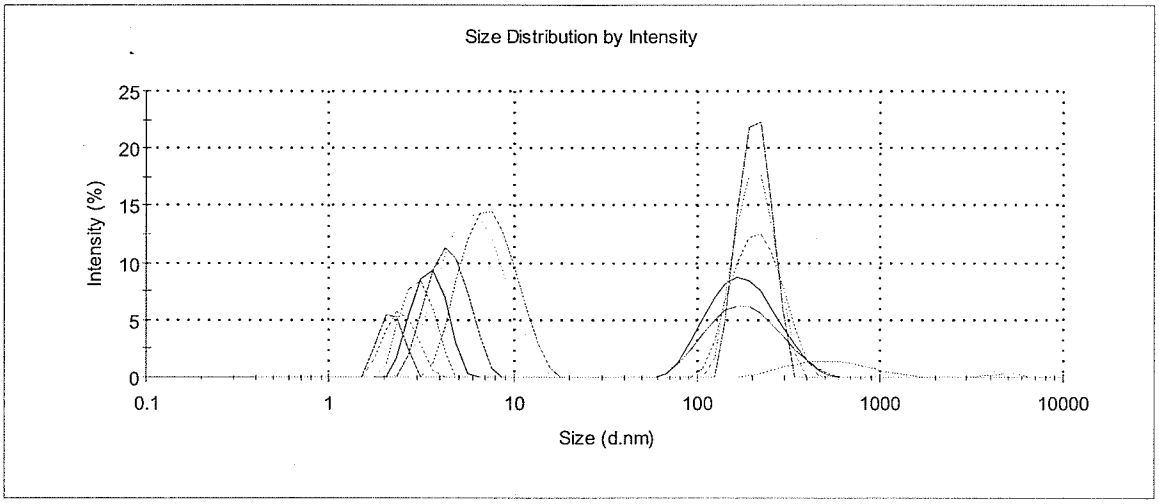

Figure 56: DLS of LLPC at several temperatures. The temperatures shown here are 20°C (orange), 30°C (green), 40°C (blue), 50°C (black), 60°C (red), 70°C (purple), and 80°C (brown).

Figure 57 shows a DLS spectrum of GlpF solubilized in LLPC. At 20°C two peaks are observed indicating particle diameters of 11.7 nm and 254 nm (orange curve). As the temperature is raised the small diameter peak diminishes in intensity and moves to a lower diameter until it reaches a size of 4.3 nm at 80°C. The large diameter peak increases in intensity and decreases in particle size until at 40°C it has a diameter of 138 nm. Further increases to the temperature cause the peak to increase in intensity and particle size, and at 80°C the particles are 228 nm in diameter.

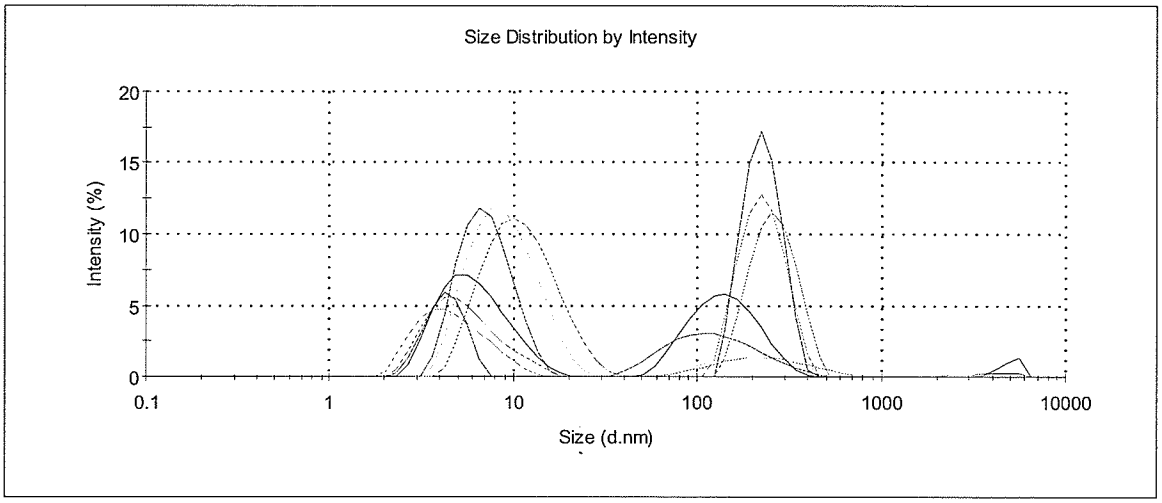

Figure 57: DLS of GlpF in LLPC at several temperatures. The temperatures shown here are 20°C (orange), 30°C (green), 40°C (blue), 50°C (black), 60°C (red), 70°C (purple), and 80°C (brown). The GlpF concentration is 5 μM.

The effect of GlpF being included in the LMPC micelles is evident in Tables 13-14 which list the diameters of the detergent micelles in the presence and absence of GlpF and the differences between them. The difference in the diameter of the 20°C curves in the presence and absence of GlpF (Figures 56 and 57, orange curve) is 4.1 nm.

According to X-ray diffraction the diameter of the GlpF tetramer is approximately 4.5 nm (Fu et al., [21]), so the measured difference in micelle diameter is very similar to the protein structure. Table 13 also shows that as the temperature increases, this difference in size between the micelles in the presence and absence of protein decreases to about 2 nm. The peak also broadens suggesting a heterogeneous mixture of particles perhaps containing various protein aggregates.

In both sets of data the large particle peaks are present at all temperatures (with the exception of 30°C in the absence of GlpF). Interestingly the larger particles are bigger in the absence of protein than in their presence (see Table 14), until the temperature reaches 60°C where the particles in the presence of GlpF become larger. This may indicate the onset of denaturation as protein aggregates begin to reorganize the detergent. Recall that SDS-PAGE indicated small amounts of aggregate forming at 60°C (Figure 54, Lane 6).

Table 13: LLPC Small Particle Diameters at Different Temperatures

Temperature (°C)	**20**	**30**	**40**	**50**	**60**	**70**	**80**
Detergent diameter (nm)	7.6	6.3	4.5	3.5	3.0	2.5	2.2
Diameter of detergent and GlpF (nm)	11.7	9.3	7.3	6.5	5.8	5.0	4.3
Difference caused by presence of GlpF (nm)	4.1	3.0	2.8	3.0	2.8	2.5	2.1

Table 14: LLPC Large Particle Diameters at Different Temperatures

Temperature (°C)	**20**	**30**	**40**	**50**	**60**	**70**	**80**
Detergent diameter (nm)	585	ND	196	190	220	212	210
Diameter of detergent and GlpF (nm)	255	223	139	149	266	231	229
Difference caused by presence of GlpF (nm)	-330	ND	-57.0	-41.0	46.0	19.0	19.0

Figure 58 shows the effects of 4 M TMAO on the particle sizes in LLPC at various temperatures. At 20°C (orange curve) three families of particles are observed including a particle 1.3 nm in diameter, a particle 24 nm in diameter, and large family with an average diameter of 1818 nm. The very small particle disappears from the spectrum when the temperature is increased to 30°C. This is the first time a peak has been observed of this size in any of the temperature studies performed. Disregarding the very small particles, the effect of TMAO is to increase the size of the small detergent particles by about 16 nm and the size of the large particles by about 1200 nm. As the temperature is further increased to 60°C the small particle peaks decrease in size and intensity until this peak is no longer visible in the spectrum above 60°C. Between 20°C and 40°C the peak representing large diameter particles decreases in particle size and increases in intensity particularly between 30°C and 40°C. At higher temperatures the peak continues to increase in intensity and minor fluctuations in particle diameter are observed. At 80°C the differences between the large diameter particles in the presence and absence of

TMAO has been reduced to about 110 nm (Tables 14 and 16). Overall then, TMAO induces an increase in the aggregation number of LLPC micelles.

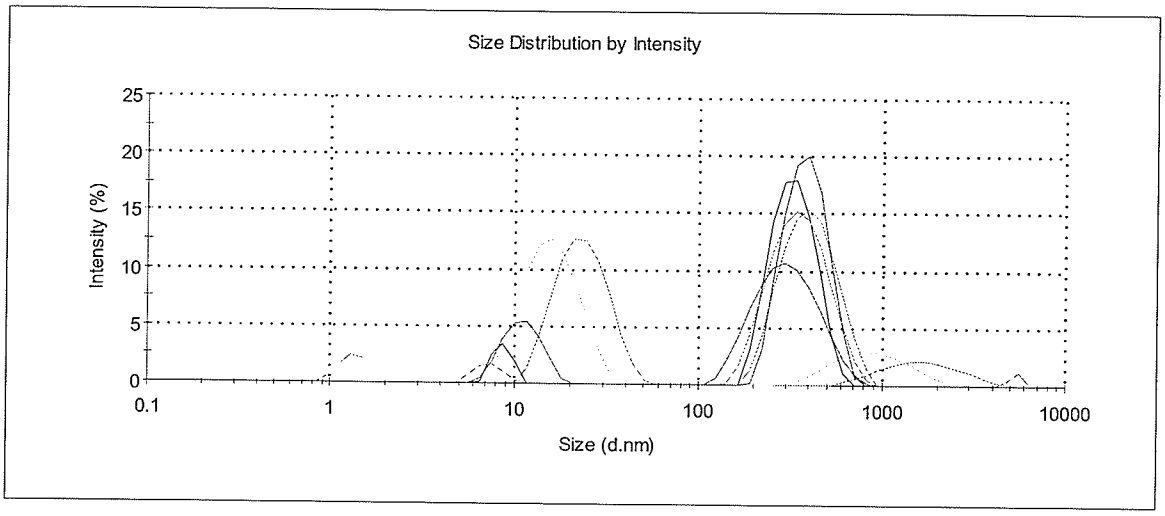

Figure 58: DLS of LLPC in 4 M TMAO at several temperatures. The temperatures shown here are 20°C (orange), 30°C (green), 40°C (blue), 50°C (black), 60°C (red), 70°C (purple), and 80°C (brown).

In the presence of GlpF and 4 M TMAO at 20°C two major peaks are observed in the DLS spectrum at 36nm and 419 nm (Figure 59, orange curve). The large particle peak is actually higher in intensity than the smaller peak, and this was not observed in any of the other detergents. The small diameter peak in Figure 59 is 12 nm larger than the peak found in Figure 58 (LLPC with TMAO), suggesting that about three tetramers are associating in the solution. Recall however that SDS-PAGE detected only tetramers in LLPC with 4 M TMAO (Figure 49, Lane 1). As the temperature is increased, the small particle peak decreases in size and intensity until it disappears at temperatures above 60°C, analogous to the observation in the absence of GlpF (Figure 58). The

differences in the particle diameters in the presence and absence of GlpF decrease only slightly up to 60°C (Table 15). The large diameter peak increases in intensity and decreases in size until 40°C, where it begins to increase in size and intensity as the temperature is raised until at 80°C where it is about 950 nm in diameter. Curiously, the large diameter peaks are significantly smaller in the presence of GlpF (Figure 59) than in its absence (Figure 58 and Table 16) over the temperature range from 20-50°C. At 60°C and higher the large diameter peaks move to increasingly larger diameters resulting in peaks that are at considerably larger diameters than the peaks in the absence of GlpF. The biggest change in the large diameter peaks in the DLS spectrum is between 50°C and 60°C (Figure 59) whereas in SDS-PAGE only minor changes are observed over those temperatures (Figure 55). It should also be noted that no new peaks appear nor is there any significant change in the behaviour of any of the peaks at elevated temperatures suggesting that most of the changes observed arise from rearrangements of the detergent rather than unfolding of the protein.

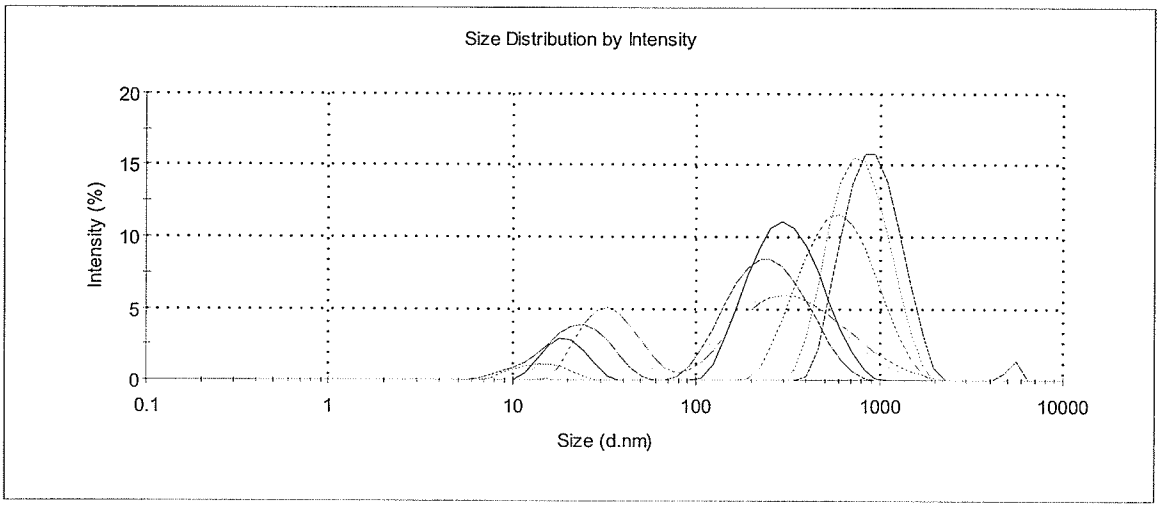

Figure 59: DLS of GlpF in LLPC and 4 M TMAO at several temperatures. The temperatures shown here are 20°C (orange), 30°C (green), 40°C (blue), 50°C

(black), 60°C (red), 70°C (purple), and 80°C (brown). The GlpF concentration is 5 μM.

Table 15: Small Particle Diameters at Different Temperatures in LLPC with 4 M TMAO

Temperature (°C)	**20**	**30**	**40**	**50**	**60**
Diameter in absence of GlpF (nm)	23.9	16.3	11.2	8.6	7.4
Diameter in presence of GlpF (nm)	36.2	29.0	23.2	19.6	14.8
Difference caused by presence of GlpF (nm)	12.3	12.7	12.0	11.0	7.4

Table 16: Large Particle Diameters at Different Temperatures in LLPC with 4 M TMAO

Temperature (°C)	**20**	**30**	**40**	**50**	**60**	**70**	**80**
Diameter in absence of GlpF (nm)	1818	953	320	336	414	368	390
Diameter in presence of GlpF (nm)	419	370	270	332	646	813	954
Difference caused by presence of GlpF (nm)	-1398	-583	-50.0	-4.0	232	445	564

3.4 GlpF in 1-Myristoyl-2-Hydroxy-sn-Glycero-3-Phosphocholine

Experiments in 1-Myristoyl-2-Hydroxy-sn-Glycero-3-Phosphocholine (LMPC) were performed so as to have a direct comparison of the contribution of chain length and headgroup to the stability of GlpF. Comparison of the effects of LMPC and TDM which have 14 carbon chain lengths will reveal the importance of detergent headgroup on protein stability. Comparison of the stability of GlpF in LMPC (14 carbons) with that in LLPC (12 carbons) will yield the importance of detergent chain length. It is found from all the following experiments that the stability of GlpF in LMPC is very similar to the stability in LLPC, but the protein is more stable than in DDM and TDM. It is again concluded that the contribution of the detergent head group is more important to the stability of the protein than alkyl chain length. The average yield of protein from a preparation in LMPC is 6 ± 1 mg per litre of cell culture.

3.4.1 SDS Denaturations at 40°C in the Presence and Absence of 4 M TMAO.

SDS denaturations of GlpF in LMPC were performed at 40°C to investigate the stability of GlpF in the absence (Figure 60) and presence (Figure 61) of 4 M TMAO. In lane 1 of both electrophoregrams there is a small amount of monomer present which is due to the SDS that is inherent to an SDS-PAGE experiment causing a small amount of tetramer to dissociate into monomer. Figure 60 shows that, in the absence of TMAO, there is a low level of the tetramer band at 90% SDS (Lane 7), but the intensity of the band in 80% SDS is very significant. Thus, the stability of the tetramer in LMPC appears

visually to be slightly higher as compared to solutions in DDM (Figures 5 and 6) and TDM (Figure 34), but is about the same as that measured in LLPC (Figure 47). The band intensities in Figure 60 were fit to a two-state transition using Mathematica resulting in an SDS_{half} determination of 38 ± 14% (see Figure 65). Although the fitted values are not statistically significantly different, the mean values do confirm the conclusions based on visual inspection of the electrophoregrams. The SDS_{half} values in all detergents are 38 ± 14%, 39 ± 14%, 35 ± 11%, and 36 ± 11% in LMPC, LLPC, TDM, and DDM, respectively.

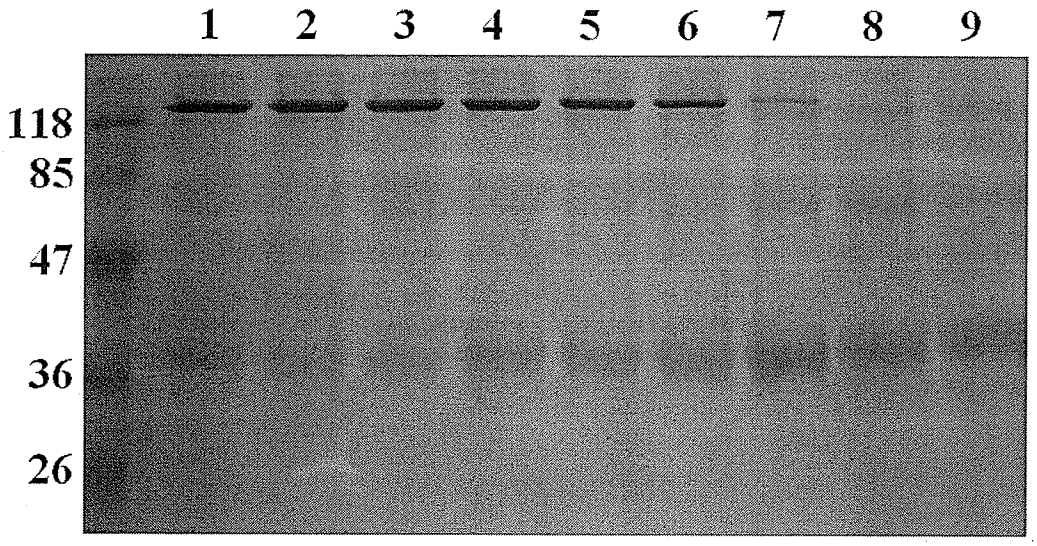

Figure 60: SDS-PAGE showing a 40°C SDS denaturation of GlpF in LMPC. Lanes 1-9 correspond to SDS percentages of 30%, 40%, 50%, 60%, 70%, 80%, 90%, 97%, and 98% of the total detergent in the solution used for the incubation period, the other component being LMPC.

In the presence of 4 M TMAO (Figure 61), GlpF dissolved in LMPC is stable in all concentrations of SDS; no dissociation of the tetramer is observed even at the highest concentrations of SDS used (Figure 61, Lane 9, 98% SDS). It is also clear that in

contrast to what was observed in DDM (Figures 15 and 16) the octamer is not promoted by TMAO. Because the tetramer does not dissociate in 4 M TMAO in LMPC no SDS_{half} could be determined.

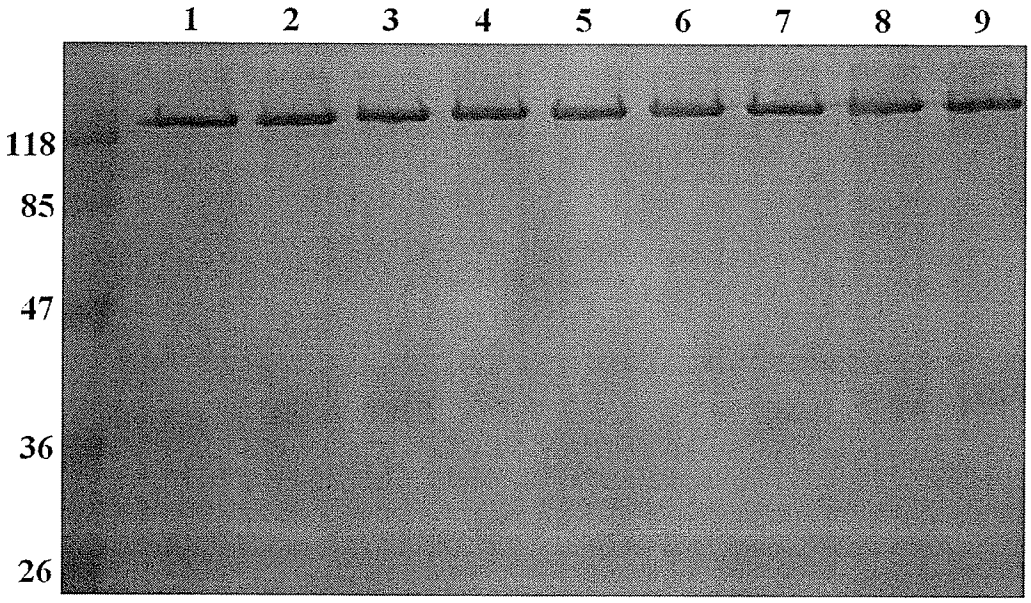

Figure 61: SDS-PAGE showing a 40°C SDS denaturation of GlpF in LMPC in the presence of 4 M TMAO. Lanes 1-9 correspond to SDS percentages of 0%, 40%, 50%, 60%, 70%, 80%, 90%, 97%, and 98% of the total detergent in the solution used for the incubation period, the other component being LMPC.

3.4.2 Concentration Dependence of TMAO.

Experiments were performed to investigate the effects of increasing TMAO concentration on GlpF in LMPC, which could then be directly compared to the results from LLPC, DDM, and TDM. Figures 62, 63, and 64 show the effects of 0.5 M, 1 M, and 2 M TMAO, respectively on the unfolding of the tetramer by SDS. Fits of the band

intensities to two-state transitions using Mathematica are shown in Figure 65. Similar to what is observed in Figure 60 in the absence of TMAO the largest change in tetramer band intensity is observed between 80% and 90% SDS (Lanes 5 and 6) in 0.5 M TMAO. Figure 65 shows that 0.5 M TMAO in LMPC raises the SDS_{half} to 41 ± 14%. By 98% SDS (Lane 8, Figure 62) the tetramer visually appears to be more than 95% dissociated into monomer and aggregate.

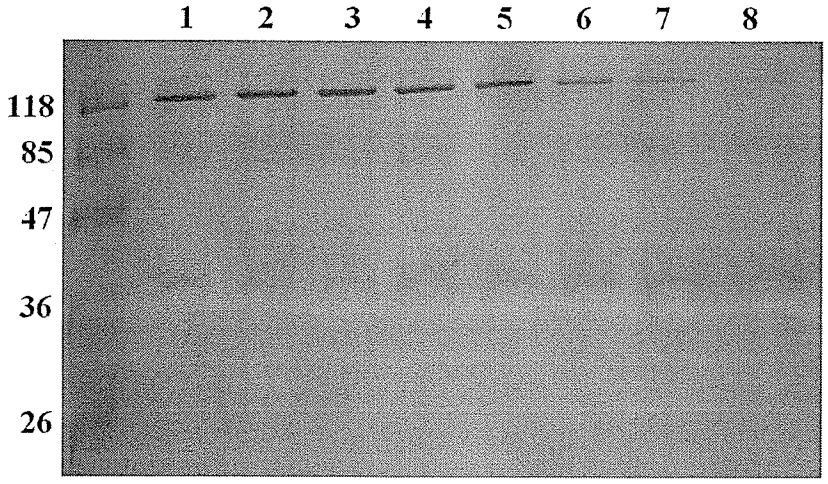

Figure 62: SDS-PAGE showing a 40°C SDS denaturation of GlpF in LMPC in the presence of 0.5 M TMAO. Lanes 1-9 correspond to SDS percentages of 0%, 50%, 60%, 70%, 80%, 90%, 97%, and 98% of the total detergent in the solution used for the incubation period, the other component being LMPC.

When the concentration of TMAO is increased to 1 M (Figure 63), the SDS_{half} increases to 69 ± 21%, and the tetramer cannot be completely dissociated in 98% SDS (Lane 8).

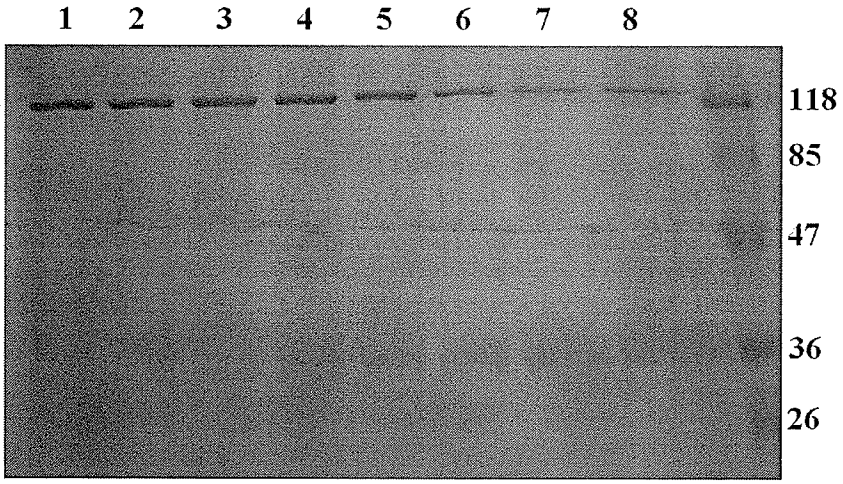

Figure 63: SDS-PAGE showing a 40°C SDS denaturation of GlpF in LMPC in the presence of 1 M TMAO. Lanes 1-9 correspond to SDS percentages of 0%, 50%, 60%, 70%, 80%, 90%, 97%, and 98% of the total detergent in the solution used for the incubation period, the other component being LMPC.

At 2 M TMAO (Figure 64), the tetramer does not dissociate to a large degree in 97% and 98% SDS (Lanes 7 and 8), and the amount of dissociation appears visually to be just slightly more than in 50% SDS (Lane 1). Even though the tetramer does not completely dissociate at 2 M TMAO, the bands in Lanes 8 and 9 are not as intense as those found in previous lanes and in 4 M TMAO (Figure 60), and therefore an SDS_{half} value of 95 ± 19% is obtained for this concentration of TMAO.

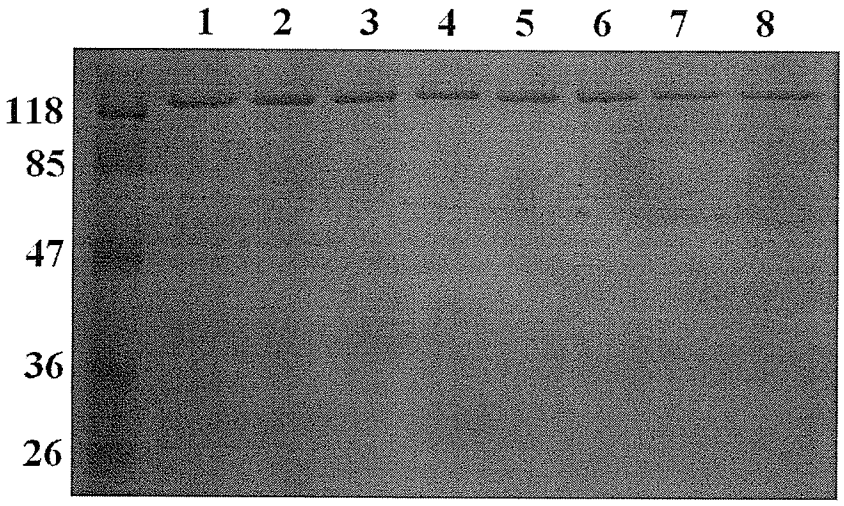

Figure 64: SDS-PAGE showing a 40°C SDS denaturation of GlpF in LMPC in the presence of 2 M TMAO. Lanes 1-9 correspond to SDS percentages of 0%, 50%, 60%, 70%, 80%, 90%, 97%, and 98% of the total detergent in the solution used for the incubation period, the other component being LMPC.

Figure 65 shows the fits of the electrophoregram band intensities in Figures 60 and 62-64 to two-state transitions. It is evident that there is not much change in stability from 0 M to 0.5 M TMAO as is found in LLPC (Figure 50), but a large increase in the stability is observed when the TMAO concentration is increased from 0.5 M to 1 M. By 2 M TMAO the denaturation curve barely reaches an Fn value of 0.5, giving the SDS_{half} value of 95 ± 19%, giving a value if the curve is "completed".

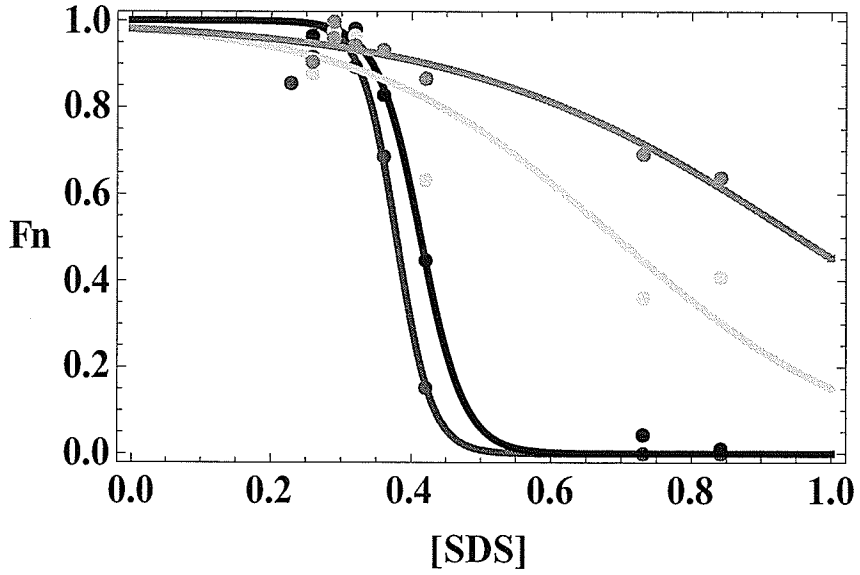

Figure 65: Mathematica graph showing the SDS-induced dissociation of GlpF tetramer in LMPC at 40°C. The graph shows the fraction of native tetramer (Fn) as a function of SDS mole fraction. The SDS_{half} for each of the curves are 38 ± 14% (0 M TMAO, purple), 41 ± 14% (0.5 M TMAO, black), 69 ± 21% (1 M TMAO, green), and 95 ± 19% (2 M TMAO, red), respectively.

Table 17 shows the SDS_{half} values from all the detergents tested. It is observed that the stabilities of GlpF of all detergents in the absence of TMAO are very similar. Addition of 0.5 M TMAO has the largest effect on the protein in LLPC whereas in the other three detergents stability is only marginally increased. At 1 M TMAO the stability of GlpF is significantly enhanced in both LLPC and LMPC with the stability being greatest in the latter detergent. At 2 M TMAO a significant increase in GlpF stability is observed in all detergents with the lowest stability observed in TDM. These results suggest that the protein is marginally more stable in detergents with phosphatidyl choline head groups and that lower concentrations of TMAO can stabilize the protein when it is

dissolved with the use of detergents with phosphatidyl choline head groups rather than maltoside head groups.

Table 17: SDS_{half} Values for GlpF Tetramer Dissociation all Detergents at Specific TMAO Concentrations

Detergent	**0 M TMAO Solution**	**0.5 M TMAO Solution**	**1 M TMAO Solution**	**2 M TMAO Solution**
DDM	36 ± 11%	40 ± 16%	42 ± 17%	ND
TDM	35 ± 11%	37 ± 22%	41 ± 18%	55 ± 19%
LLPC	39 ± 14%	66 ± 19%	82 ± 25%	ND
LMPC	38 ± 14%	41 ± 14%	69 ± 21%	95 ± 19%

3.4.3 Thermal Denaturations in the Presence and Absence of TMAO.

The thermal stability of GlpF in LMPC was investigated by performing temperature denaturations in the presence and absence of 4 M TMAO and the results are presented in Figure 66. It had been found previously that GlpF is slightly more heat stable in LMPC as compared to DDM [47, 48], so it was tested to see if TMAO confers any more thermal stability to the tetramer. In results very similar to those found in Figure 54 for LLPC, there is a small amount of tetramer present at 80°C (Lane 7, Figure 66), but the majority of the protein is in higher molecular weight aggregates. By 85°C (Lane 8), there is no tetramer left and all the protein is aggregated. In lane 1 there is a small

amount of monomer which is due to the SDS that is inherent in an SDS-PAGE experiment that causes a small amount of tetramer to dissociate into monomer.

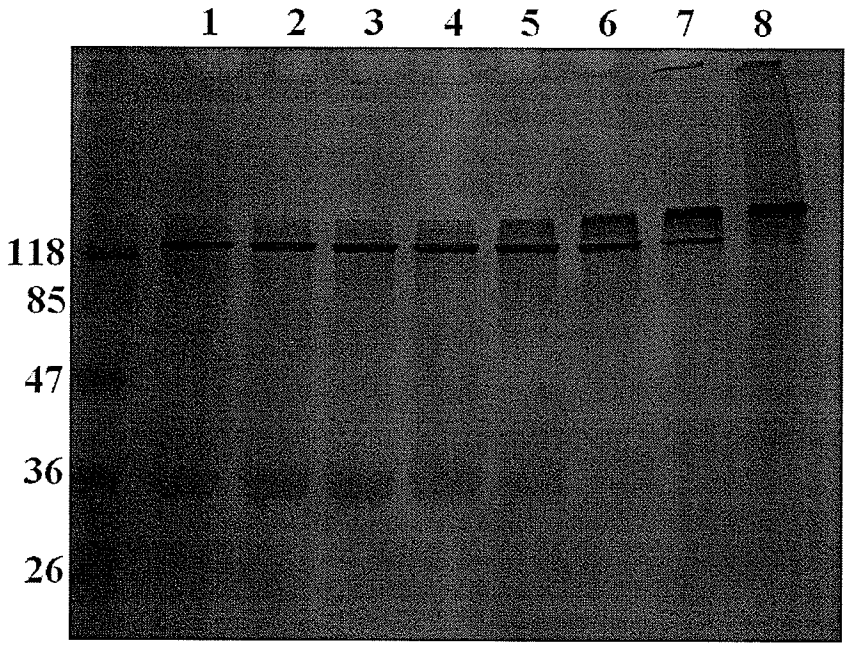

Figure 66: SDS-PAGE showing a temperature denaturation of GlpF in LMPC. Lanes 1-8 correspond to the temperatures 22°C, 30°C, 40°C, 50°C, 60°C, 70°C, 80°C and 85°C.

Figure 67 shows a thermal denaturation of GlpF in LMPC in the presence of 4 M TMAO. The intense tetramer bands still present in lanes 7 and 8 (80°C and 85°C) indicate that the GlpF tetramer is more thermal stable in the presence of 4 M TMAO compared to its absence (Figure 66). Some denaturation does occur at the higher temperatures as indicated by the high molecular weight aggregates found in lanes 6, 7, and 8 (70°C, 80°C, and 85°C, respectively) and by the disappearance of the bands corresponding to monomer and dimer.

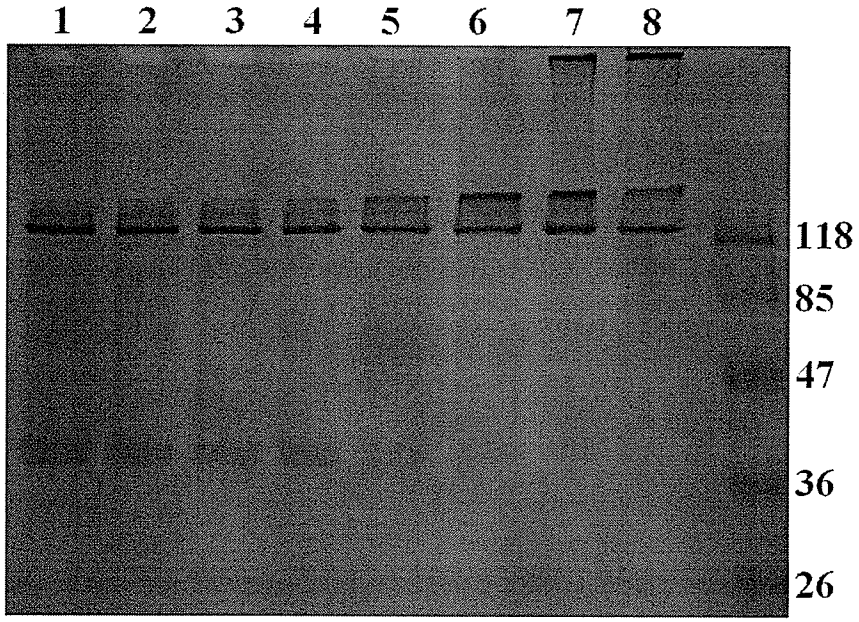

Figure 67: SDS-PAGE showing a thermal denaturation of GlpF in LMPC in the presence of 4 M TMAO. Lanes 1-8 correspond to the temperatures 22°C, 30°C, 40°C, 50°C, 60°C, 70°C, 80°C, and 85°C.

If visual comparisons are made between the electrophoregrams of the thermal denaturations in the absence of TMAO in DDM (Figure 18), TDM (Figure 41), LLPC (Figure 54) and LMPC (Figures 66), it is noticed that GlpF in LMPC and LLPC is about 10°C more stable than in TDM and DDM. For the thermal melts in TMAO (Figures 20, 43, 55, and 67), it is found that the stabilities are very similar among the four detergents, except for the presence octamer that is protected in DDM.

T_m values were calculated for GlpF in LMPC from the fits of the band intensities in the presence and absence of 4 M TMAO to a two-state thermal transition, and this data is shown in Table 18. The determined values are 77 ± 3°C in 0 M TMAO and 83.5 ± 0.3°C in 4 M TMAO, showing that 4 M TMAO enhances the thermal stability of GlpF in LMPC by 6.5 degrees. This difference is smaller than was measured in any of the other

three detergents where an increase in the stability caused by 4 M TMAO of 9 or 10 degrees is measured (Table 18). Table 18 also shows the increased thermal stability of GlpF solubilized in LLPC and LMPC in the absence of TMAO as compared to analogous experiments in DDM and TDM indicating that GlpF is more thermal stable in detergents with a phosphatidylcholine headgroup. The greater stability of the protein in LLPC than in LMPC, both in the presence and absence of TMAO, suggests that the protein is more stable in a 12 carbon detergent than a 14 carbon detergent.

Table 18: T_m values in different concentrations of TMAO

Detergent	**DDM**	**TDM**	**LLPC**	**LMPC**
0 M TMAO	69 ± 5°C	70± 1°C	82 ± 4°C	77 ± 3°C
4 M TMAO	80 ± 1°C	81 ± 2°C	91 ± 2°C	83.5 ± 0.3°C

3.4.4 Dynamic Light Scattering Heat Denaturations on GlpF in the Absence and Presence of TMAO.

Thermal denaturations of GlpF in LMPC were performed in the presence and absence of TMAO to monitor the quaternary structure of a membrane protein and to compare the results with those measured in other detergents. At 20°C (Figure 68, orange curve), only one peak is observed indicating particles with an average diameter of 8.8

nm. There is currently no literature on the size of LMPC micelles, so no comparisons could be made on the accuracy of the measurement. As the temperature is increased this peak decreases in both diameter and intensity until at 80°C the average particle diameter is 2.5 nm. At 50°C a new peak appears indicating the presence of particles with a diameter of about 165 nm. This large particle peak increases in intensity and diameter with increasing temperature, until at 80°C it has a diameter of 190 nm. These results are similar, though not identical, to those measured for DDM (see Figure 26).

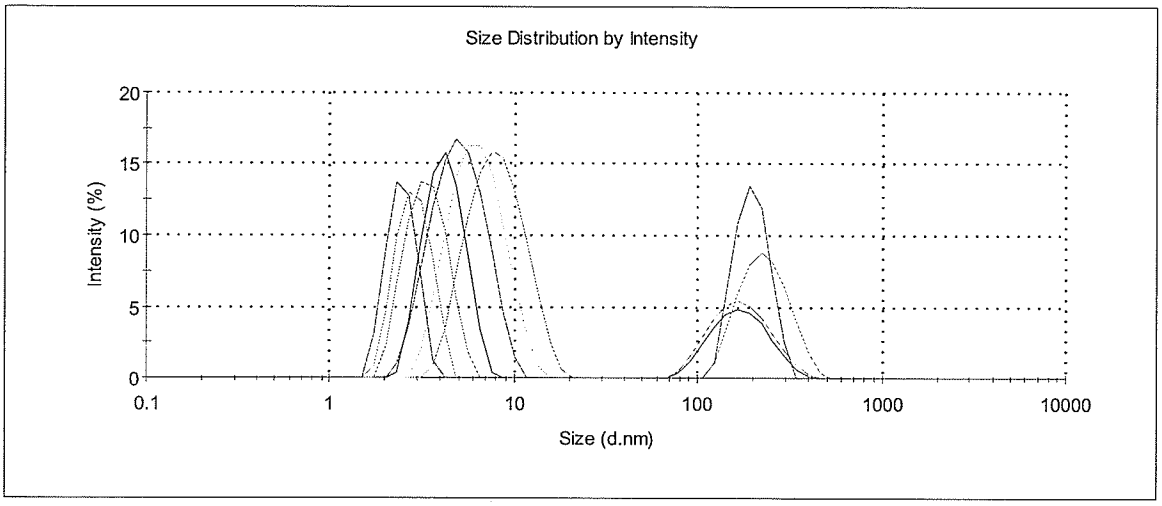

Figure 68: DLS of LMPC at various temperatures. The temperatures shown are 20°C (orange), 30°C (green), 40°C (blue), 50°C (black), 60°C (red), 70°C (purple), and 80°C (brown).

Figure 69 shows a DLS spectrum of GlpF solubilized in LMPC. At 20°C (orange curve) the average diameter of the particles is 12.0 nm, about 3.2 nm bigger than in the detergent alone (Table 19). As the temperature is increased the peak diminishes in intensity only slightly and moves to a lower diameter until particles of about 3.4 nm are observed at 80°C; those particles are about 1 nm larger than the empty LMPC micelles

perhaps indicating the presence of detergent-solubilized monomers and dimers. Similar to the observations made of LMPC in the absence of GlpF (Figure 68, black curve) at 50°C a new peak with a diameter of about 122 nm appears in the spectrum (Figure 69, black curve). Further increases in temperature increase the height and narrow the width of the large diameter particle distribution. Table 20 shows the differences in diameter between the large diameter particles in the presence and absence of protein. At 50°C and 80°C the empty micelles actually appear larger than the protein-containing micelles, whereas at 60°C the opposite is observed. It is not evident that the high diameter peaks contain protein and thus the nature of these peaks is uncertain. In contrast to the observations made in DDM (Figure 28) no intermediate diameter peak is formed in LMPC at 70°C that was attributed to the aggregation of GlpF in DDM. That the unfolding process is not identical in LMPC and DDM is also indicated by the fact that the small diameter particle peak does not greatly diminish in intensity in LMPC (Figure 69) as it does in DDM (Figure 28). One possible explanation for both of these observations is that the higher GlpF melting point in LMPC compared to DDM precludes the observation of significant amounts of aggregated protein at 70°C and 80°C by DLS.

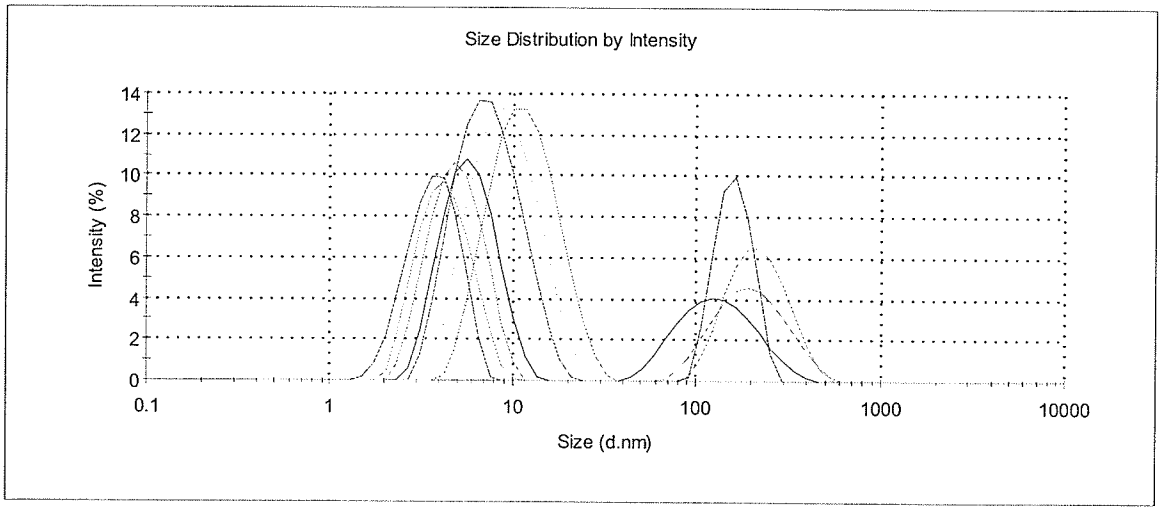

Figure 69: DLS of GlpF in LMPC at several temperatures. The temperatures shown here are 20°C (orange), 30°C (green), 40°C (blue), 50°C (black), 60°C (red), 70°C (purple), and 80°C (brown). The GlpF concentration is 5 μM.

Table 19: LMPC Small Particle Diameters at Different Temperatures

Temperature (°C)	**20**	**30**	**40**	**50**	**60**	**70**	**80**
Detergent diameter (nm)	8.8	6.5	5.2	4.3	3.4	2.9	2.5
Diameter of detergent and GlpF (nm)	12.0	10.2	7.5	5.8	4.8	4.1	3.4
Difference caused by presence of GlpF (nm)	3.2	3.7	2.3	1.5	1.4	1.2	0.9

Table 20: LMPC Large Particle Diameters at Different Temperatures

Temperature (°C)	**50**	**60**	**70**	**80**
Detergent diameter (nm)	164	164	220	190
Diameter of detergent and GlpF (nm)	122	190	220	164
Difference caused by presence of GlpF (nm)	-42.0	26.0	0.0	-26.0

Figure 70 shows the effects of 4 M TMAO on the particle sizes in LMPC at various temperatures. TMAO increases the size of the small particles from about 9 nm (Figure 66 orange curve and Table 18) to about 33 nm. When the temperature is increased to 40°C the particles appear to increase to about 91 nm (Figure 70, green

curve). Further increases in temperature decrease the sizes and, after 50°C, the intensities of the small diameter peaks and increase the sizes and intensities of the large diameter particles. The large diameter peaks appear in the spectrum at 20°C with a diameter of about 250 nm, but are not present between 30°C and 60°C and then reappear at 70°C (purple curve) with a diameter of about 165 nm. When the temperature is increased to 80°C (brown curve), both the diameter and intensity of the peak increase to a size of 295 nm.

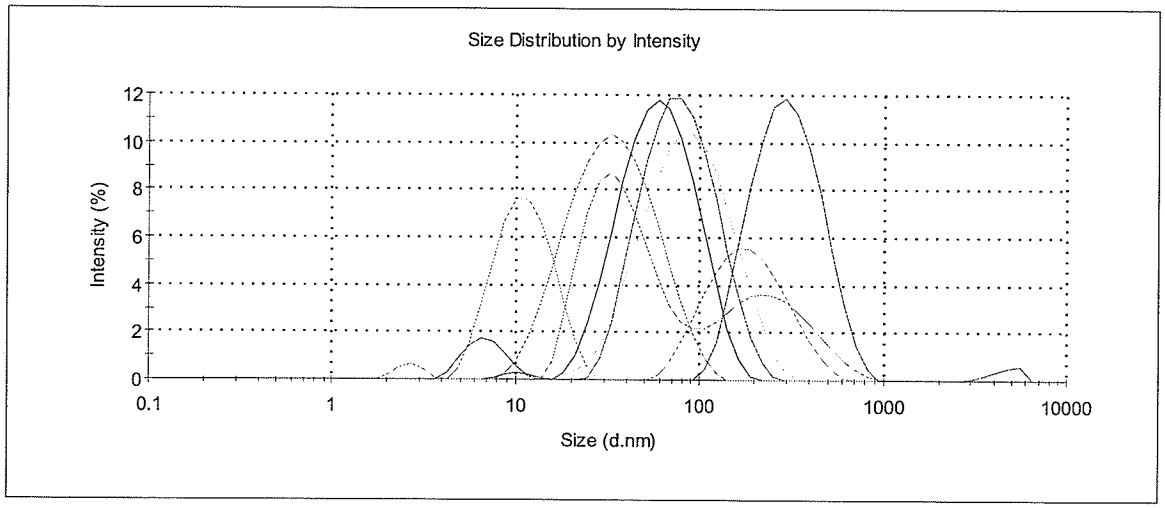

Figure 70: DLS of LMPC in the presence of 4 M TMAO. The temperatures shown here are 20°C (orange), 30°C (green), 40°C (blue), 50°C (black), 60°C (red), 70°C (purple), and 80°C (brown).

When GlpF and TMAO are present together in LMPC (Figure 71) at 20°C most of the scattering intensity resides in a peak indicating a particle diameter of about 37.8 nm, which is about 5.2 nm larger than that observed in GlpF and LMPC alone (Figure 69). As the temperature of the mixture is increased the smaller diameter peaks move to smaller diameters and intensities, and the larger diameter peaks move to smaller diameters until

40°C where they become more intense and move to larger diameters (Figure 71). The changes are not easily comparable to those taking place in the absence of protein (Figure 70). However, it is interesting to note that a weak peak of intermediate diameter (30 – 40 nm, Figure 71, purple and brown curves) appears in the spectrum at 70°C and 80°C, temperatures at which SDS-PAGE experiments show the development of high molecular weight oligomers (Figure 67, Lanes 6-8). This peak might indicate the presence of early oligomers in the unfolding process.

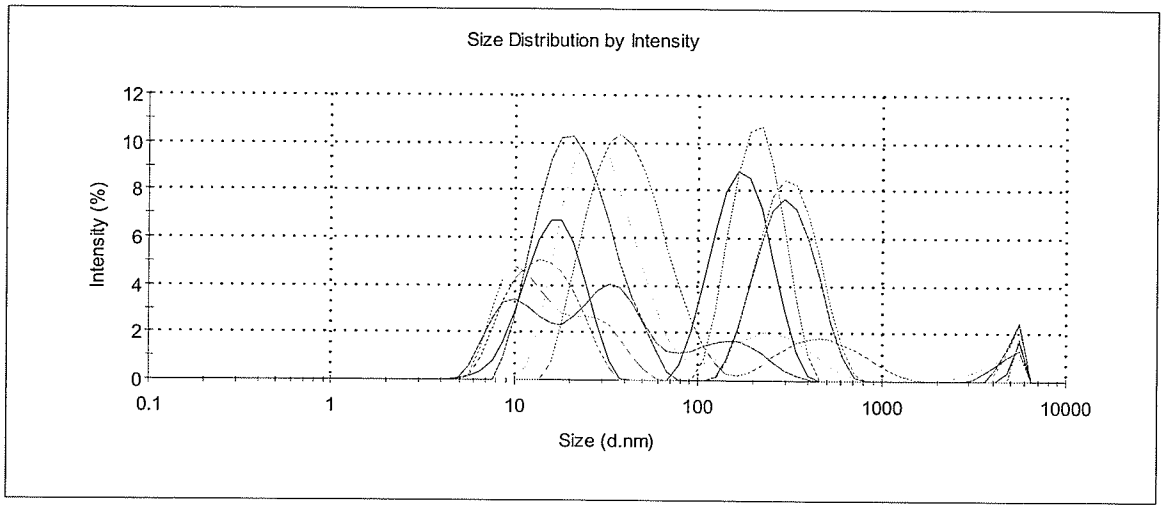

Figure 71: DLS thermal denaturation in the presence of GlpF and 4 M TMAO in LMPC. The temperatures shown here are 20°C (orange), 30°C (green), 40°C (blue), 50°C (black), 60°C (red), 70°C (purple), and 80°C (brown). The GlpF concentration is 5 μM.

The differences caused by the presence of GlpF in LMPC and TMAO are compared in Tables 21 to 23. There is a large increase in the small particle size difference when the temperature is increased from 20°C to 30°C, and a trend of decreasing size difference is observed as the temperature is increased further. It must

also be noted that it is the peaks in the absence of GlpF that are bigger than the peaks in the presence of GlpF, and this result is similar to the DLS data from TDM (Table 12). It is hypothesized that the changes in the aggregation state of the detergent are significantly masking the changes in the protein in LMPC.

Table 21: Small Particle Diameters at Different Temperatures in LMPC with 4 M TMAO

Temperature (°C)	**20**	**30**	**40**	**50**	**60**	**70**	**80**
Diameter in absence of GlpF (nm)	32.7	91.3	78.8	58.8	32.7	11.7	6.5
Diameter in presence of GlpF (nm)	37.8	28.2	21.0	15.7	13.5	10.1	10.1
Difference caused by presence of GlpF (nm)	5.1	-63.1	-57.8	-43.1	-19.2	-1.6	3.6

Table 22: Intermediate Particle Diameters at Different Temperatures in LMPC with 4 M TMAO

Temperature (°C)	**70**	**80**
Diameter in absence of GlpF (nm)	ND	ND
Diameter in presence of GlpF (nm)	24.4	32.7
Difference caused by presence of GlpF (nm)	ND	ND

Table 23: Large Particle Diameters at Different Temperatures in LMPC with 4 M TMAO

Temperature (°C)	**20**	**30**	**40**	**50**	**60**	**70**	**80**
Diameter in absence of GlpF (nm)	ND	ND	ND	ND	ND	164	295
Diameter in presence of GlpF (nm)	458	255	141	164	220	295	295
Difference caused by presence of GlpF (nm)	ND	ND	ND	ND	ND	131	0.0

Chapter IV: Discussion

4.1 Chemical Stability of Membrane Proteins.

True thermodynamic data on the folding of α-helical membrane proteins is scarce in the literature because of the inherent difficulty of working with this class of proteins. In most cases, membrane proteins aggregate as soon as they unfold, precluding the measurement of thermodynamic parameters that require the folded and unfolded proteins to be in equilibrium. With the exception of bacteriorhodopsin [49, 50], diacylglycerol kinase [89], and a few others (for a review see [2]), the barriers to overcoming the experimental problems associated with the true unfolding and refolding of α-helical membrane proteins have fettered progress in this field. To gain more knowledge on membrane protein stability and folding, and to try and find new methods to study this group of proteins, SDS chemical denaturations at different temperatures, in different detergents, and in the presence and absence of the osmolyte TMAO were performed on GlpF.

The interactions between lysozyme and SDS at low concentrations have been observed and indicate that the ionic surfactant (SDS) interacts with the positively-charged, solvent-exposed residues and neutralizes their charge [90]. This reduction in the net charge of the surface of the protein allows for the insertion of the hydrophobic tail of SDS into the protein's core, which then disrupts the protein-protein hydrophobic interactions causing the full denaturation of the protein [90]. The capacity of SDS to denature proteins is well-established, and it has numerous advantages over the

denaturants traditionally used for soluble proteins such as guanidine hydrochloride and urea.

The interactions between SDS and α-helical membrane proteins have been shown to be very different depending on the protein in question. In many cases, SDS has been shown to provide a native-like environment, and in fact there are about 40 NMR structures in the Protein Data Bank of small α-helical proteins and peptides solubilized in SDS [82]. On the other hand, numerous membrane proteins have been denatured by SDS and the highly cooperative spectroscopic changes that occur with increasing amounts of SDS added have been interpreted as protein unfolding [91]. The effects of SDS on the structures of membrane proteins have been shown to range widely. In some cases proteins with structures in SDS very similar to the native helix-helix interactions [92] have been observed; in others, stable oligomers with proper native interactions result [93]; and in other cases the complete disruption of helix-helix interactions takes place [94]. Small increases in the volume of a protein have been observed in SDS solubilized bacterio-opsin, which is a necessary condition for protein unfolding [82], although the increase was not as large as was expected, suggesting that the protein is not completely unfolded by SDS. Because high α-helical content is commonly preserved in SDS [50, 82, 95-100], it has been argued that SDS does not generally yield a random coil denatured state such as that produced by guanidine hydrochloride and/or urea [97]. This suggests that a conformation which maintains most of the native helical structure will likely be a more appropriate model for an unfolded protein within a membrane.

Despite the fact that SDS rarely results in complete denaturation of membrane proteins to the random coil state it is an attractive chemical denaturant for membrane

protein folding studies. Unlike guanidine hydrochloride and urea, SDS is able to form mixed micelles with other detergents. As a result, guanidine hydrochloride and urea are less effective at denaturing membrane proteins than water-soluble proteins and are less able to solubilize the unfolded states of membrane proteins than is SDS. Denaturations in SDS may also provide insight into events relating to the insertion by the translocon of partially folded membrane proteins during translation. Furthermore, the high helical propensity of transmembrane α-helices in micellar and bilayer environments suggests that α-helical membrane proteins may never exist in a fully denatured random coil.

The osmolyte 2-methyl-2, 4-pentanediol (MPD) has been shown to increase the resistance to denaturation by SDS and promote the refolding from a denatured state of the membrane proteins Bacteriorhodopsin (α-helical), and PagP (a bacterial outer membrane protein composed of an eight-stranded β-barrel), and several water-soluble proteins such as egg white lysozyme (α-helical), and human carbonic anhydrase II (HCAII – a β-sheet soluble protein) [101]. The method by which MPD and similar alcohol osmolytes work is that instead of destabilizing the unfolded state (as is found in TMAO), MPD interacts directly with the hydrophobic portions of the protein and causes the displacement of water molecules from the grooves and cavities, thus stabilizing the native folded state [102, 103]. The presence of MPD in solution lowers the number of interactions between SDS and the hydrophobic core of the protein [103]. MPD has also been found to prevent thermal denaturation of PagP in the presence of SDS sample treatment buffer [101].

TMAO is a very well studied osmolyte and it is commonly found in marine organisms [52, 58]. It is believed to stabilize proteins through the strong interactions between itself and water, which results in TMAO being excluded from the hydration

layers of the peptide backbone. This causes the unfolded state of the protein to be entropically very unfavourable [58, 63, 64]. The stabilizing effects of TMAO have been shown to protect proteins from high hydrodynamic pressure, chemical denaturation, thermal denaturation, and anhydrobiotic stresses, and TMAO has even been shown to induce folding in an intrinsically unfolded protein [68].

In bacteriorhodopsin, the paradigm of α-helical membrane protein studies, reversible SDS denaturations have produced valuable information on the thermodynamics and kinetics involved in membrane protein folding. Bacteriorhodopsin is a seven transmembrane α-helical protein that is the principal component found in the 2-D crystalline lattice of the purple membrane of *Halobacterium salinarum* and is usually observed as a trimer, but it is also stable as a monomer [104]. It has been shown that the unfolding transition is a reversible two-state process where a large change in the free energy (20.57 ± 0.20 kcal/mol), and a significant decrease in the α-helical component of the protein from 78 to 53% occurs above a SDS molar fraction of 0.73 [95]. The unfolding proceeds from the native purple state through intermediates which represent isomerisations of the retinal with minor perturbations in the protein structure, to an unfolded state in which the retinal is still loosely bound, but most other interactions in the protein are lost [95, 96, 99].

A member of the potassium channel family, KcsA, has been characterized in *E .coli* by monitoring the unfolding and refolding of the secondary, tertiary, and quaternary structure. In its native form, KcsA has two transmembrane spanning α-helical segments with a short α-helix that confers channel selectivity. The protein oligomerizes into a homotetramer in the membrane, forming the active pore [105]. The denaturation of

KcsA has been performed with trifluoroethanol (TFE) because of the intrinsic resistance of the protein to denaturation by SDS (1 M), urea (7 M), guanidine hydrochloride (8 M), and guanidine isothiocyanate (5 M). This protein is a unique example of membrane protein unfolding because it proceeds through a three-state transition. In the first transition, the protein loses some of its native structure and dissociates into a monomeric form. It is only after this first step that refolding of the protein can reconstitute the protein's active form and oligomeric structure. In the second step, the partially unfolded protein is irreversibly denatured into large protein aggregates [106].

The protein diacylglycerol kinase (DGK) is a member of the membrane protein family which possesses three α-helical transmembrane domains, two cytoplasmic α-helical domains, and has been characterized by reversible SDS denaturation experiments [97]. Similar to the unfolding of KcsA, the unfolding of DGK produces a stable intermediate. The first unfolding event corresponds to a denaturation in the cytoplasmic domain of the protein. In the second unfolding event at a higher concentration of SDS, a denaturation in the transmembrane segment of the protein occurs. The authors conclude that this illustrates the frequent increased stability of transmembrane proteins or transmembrane segments of proteins, as compared to soluble proteins or soluble segments of proteins [97]. The whole process of denaturation is reversible and full activity of DGK is recovered if proper refolding techniques are employed.

4.2 Chemical Stability of GlpF in the Presence and Absence of TMAO.

SDS denaturations were executed at a range of temperatures in DDM. A temperature (40°C) was found at which there was a very reliable, reproducible, and clear transition of the unfolding of the GlpF tetramer. Not knowing what effect, if any, TMAO has on a membrane protein, numerous concentrations of TMAO were tested until it was found that at 4 M TMAO, the stability of the protein conferred by TMAO has reached a maximum. An interesting finding from this work is that in DDM the preferred oligomeric form of the protein in 4 M TMAO is an octamer and this oligomeric form of the protein is also protected from denaturation by SDS (Figure 15). The octamer is dissociated into tetramer with increasing concentration of denaturant, but even at 98% SDS there is still a significant amount of octamer present with the rest of the protein being in a stable tetrameric form. TMAO protects the quaternary structure of GlpF in DDM from denaturation, protecting both the transition of tetramer to monomer/aggregate, and the transition from octamer to tetramer.

In the other three detergents (TDM, LLPC, and LMPC), there is no evidence of a TMAO-induced change in the oligomeric structure. Although the protein was most stable in the detergents with a phosphatidylcholine headgroup (LLPC and LMPC), there was no protection of the tetramer by way of promotion to octamer caused by TMAO. Even in TDM, which is a DDM molecule with 2 extra carbons on its alkyl chain, there was no octamer found. This suggests that the octamer may be a conformation that helps bury some of the hydrophobic surface of the protein left exposed by the shorter 12 carbon hydrocarbon chain. This structure may not form in the 12 carbon LLPC because of

charge repulsion between the detergent-solubilized tetramers. An example of protection of the oligomeric form of a protein by an osmolyte is revealed by the oligomeric form of the DNA-binding protein ClpA which has been shown to be protected from high-stress environments (high KCl concentration or high temperature), by the osmolyte glycine-betaine [107], whereas the monomeric form dominates in the absence of the osmolyte and in high concentrations of denaturant. Despite extensive literature searches however, there seems to be no research showing that osmolytes induce and stabilize oligomeric forms of membrane proteins in different detergents.

Several lines of evidence have shown that TMAO stabilizes protein structure by forming very strong H-bonds with water, thus preventing water from interacting with the protein backbone [71, 108]. It has also been shown to have even stronger interactions with the known protein denaturant urea [71]. Molecular dynamics simulations suggested that TMAO does not strengthen the hydrophobic effect and thereby stabilize proteins, rather TMAO disrupts hydrophobic interactions between neopentanes (a model compound) [72]. The Gibbs free energy of the of SDS micelle formation has been shown through conductivity measurements to not be affected by adding TMAO to the solution [109]. The same author reported that the hydration number of a protein is almost independent of the concentration of TMAO, so the hydrophobic effect will play a minimal role in the stabilization of protein structure by TMAO [110]. It is therefore hypothesized that TMAO is preventing GlpF denaturation by interacting with the SDS molecules, thus preventing SDS-protein interactions. However, it has been shown here by DLS studies that TMAO increases the size of the micelles in all the detergents tested (DDM, TDM, LLPC, and LMPC), suggesting that the hydrophobic environment is

strengthened by TMAO. However, strengthening the hydrophobic effect is not the only mechanism by which micelles can grow in size. For example, any effect that reduces head group repulsion will also promote the growth of micelles. At high salt concentrations a sphere-to-rod transition occurs in the micellar structure of the detergent sodium sulfopropyl octadecyl maleate [111], and the rod-like micellar growth also increases with increasing temperature [88]. A possibility that this rod-like environment in DDM facilitates the octameric form of the protein once TMAO has been added to the solution is also reasonable. It is likely that TMAO increases the free energy penalty for protein unfolding, and prevents any interaction between SDS and GlpF. The main contribution to the prevention of denaturation is suspected to be the strong interaction between TMAO and SDS.

It is hypothesized that the high concentration of TMAO causes two tetramers to associate in a "face-to-face" orientation giving rise to a well folded octamer in DDM. A face-to-face orientation would form when the cytoplasmic (or periplasmic) faces of the protein interact in a mutually beneficial way such that the protein becomes more stable from the interaction. If the tetramers oriented themselves in a cytoplasmic face to periplasmic face fashion, there would be opportunity for an almost limitless stacking of the tetramers, one on top of the other. The fact that, other than the octamer, no other higher oligomeric form is found supports the face-to-face hypothesis. The presence of an octameric form of GlpF has been found previously in small and unpredictable quantities in previous work from our lab [47]. Octamers were also observed in GlpF using cryoelectron microscopy where a unit cell was found to be comprised of two tetramers in a side-on orientation [112]. Another member of the Aquaporin family observed to have

octameric structure is AQP0, and a "face-to-face" orientation is found between tetramers by X-ray crystallography at a resolution of 7.0 Å [113]. AQP0 is the most abundant protein in the plasma membrane of the eye lens and has been shown to facilitate water [114] and glycerol [115] transport.

Glycerol kinase (GlpK) is known to exist in both dimeric and tetrameric forms [116] in the *E. coli* membrane [117]. This coupling facilitates glycerol transport across the membrane by GlpF, and then the coupled GlpK phosphorylates glycerol trapping it inside the cell as *sn*-glycerol-3-phosphate [117], and preventing the membrane permeable glycerol from diffusing back across the membrane [118]. The heterologous association of a GlpF and GlpK tetramer would seem to represent the most efficient way to transport glycerol from GlpF to GlpK, and this type of association has been found in glucose and fructose transport and phosphorylation mechanisms in yeast [119, 120]. GlpK is allosterically regulated by several molecules and changes its oligomeric state in response to effector binding so it is interesting to speculate what role a GlpF octamer might play in altering the oligomeric state and activity of GlpK.

The octameric "face-to-face" orientation is found in other proteins, such as the *T. thermophilus* protein RuvA, which binds DNA Holliday junctions and recruits RuvB which then makes more DNA junctions depending on ATP hydrolysis [121], and in the purified S100B protein [122] which is a member of the largest family of EF-hand Ca^{2+} binding proteins which regulate cell processes such as differentiation, transcription, and cell growth and motility.

In comparing the different stabilities of GlpF to unfolding by SDS in the four different detergents (see Table 17), it is observed that at 0 M TMAO there is no

statistically significant difference in GlpF stability, but that the protein is slightly more stable in LLPC and LMPC than in DDM and TDM. In the presence of 1 M TMAO the differences in stability are much more pronounced and the stability in the PC detergents is much greater than in the neutral detergents. Also, the effect of detergent chain length is much more significant for the PC detergents than for the neutral detergents. It is hypothesized that because the phosphatidylcholine (PC) head group is charged, there is a stabilizing effect between the detergent head group and the hydrophilic amino acids in the loops and turns that connect the hydrophobic α-helices. Hydrogen bonding between protein side chains and the PC headgroup has been found to stabilize membrane-associated proteins [123] and the extracellular loops in the outer membrane protein OmpA [124].

To understand one reason why GlpF is more stable in the phosphatidylcholine detergents compared to the neutral detergents, one must consider the types of phospholipids that GlpF has evolved to be most stable in. The most common phospholipid in the *E. coli* inner membrane is phosphatidylethanolamine (PE), and it constitutes 70 – 80% of the phospholipids in the membrane [125]. PE it has a headgroup that is iso-electronic with PC at neutral pH. It is therefore reasonable to suggest that GlpF is in a more stable state in LLPC and LMPC because of the detergent's similarity to the protein's native environment in the *E. coli* membrane.

Another factor possibly contributing to the stability of GlpF in solution is the length of the detergent tail and its corresponding match to the length of the hydrophobic transmembrane region of GlpF. DDM and LLPC both have a 12 carbon chain length, and TDM and LMPC have a 14 carbon chain length. Table 17 shows that there is a slight

increase in stability of GlpF when solubilized in the detergents with a 12 carbon chain (DDM and LLPC). Molecular dynamics simulations [126] and X-ray diffraction [21] have estimated the hydrophobic transmembrane length of GlpF to be roughly 25 Å. An overall length of 14.6 – 14.8 Å for the detergent n-octyl-β-D-glucopyranoside (OG) and 8.2 – 8.3 Å for the detergent chain has been found through molecular dynamics calculations [87], and it was shown that each carbon in the detergent tail contributes about 1 Å to the total length of the molecule. Therefore, two molecules of detergent with a tail length of 12 – 13 carbons, such as DDM or LLPC, would match the 25 Å hydrophobic stretch of GlpF very well. This is in excellent agreement with our results. Obviously the hydrophobic mismatch for TDM and LMPC would be small and one would expect only a slight decrease in the stability of GlpF in the 14 carbon detergents. Again, this is in excellent agreement with our results. This observation illustrates that although the difference in GlpF stability between the protein dissolved in detergents with PC vs. neutral headgroups is very considerable and the dominant force in the stability of the protein, the hydrophobic matching of detergent length is important to the overall stability of the protein as well, and is very important in choosing the correct detergent for solubilization of a membrane protein.

Although the yield of protein when the membranes are extracted with LMPC or LLPC is lower than in DDM or SDS, it seems as though there is a correlation between the yield of protein that can be harvested from protein preparations, and the stability of the protein. When SDS is used to solubilize GlpF, the protein yields are the highest compared to all other detergents tested (10 ± 1 mg, per litre of culture), but the protein is monomeric, with little or no tertiary structure. When DDM is used to solubilize GlpF,

the quaternary and tertiary structure is present, but if the near UV CD spectrum for the protein in DDM is compared to that in LMPC, the tertiary structure in LMPC is more defined, with less noise, and with stronger bands suggesting a more stable fold and less conformational flexibility [47, 48]. This result shows that the harsher detergents are better at solubilizing the largest amount of protein, but they do not produce an environment that is ideal for maintaining the native GlpF structure.

4.4 Thermal Stability of Membrane Proteins.

The thermal stability of membrane proteins has been studied much less than for their water-soluble counterparts. As was stated earlier, this is due to the intrinsic difficulty in the amplification, isolation, and characterization of a group of proteins which have great difficulty existing outside of their native membrane environments. Unlike water-soluble proteins, the thermal unfolding of membrane proteins does not proceed to a state in which there is little or no residual structure still intact. Much of the secondary structure is not completely denatured at elevated temperatures in membrane proteins, and this has been hypothesized to be due to their evolutionary stability in a membrane environment [127, 128]. Because of this inherent stability in membrane proteins, the need to study and understand the processes and contributing factors governing this stability is essential.

As a protein solution is heated, more energy is given to the system causing the protein to sample different folded states, and Van der Waals and hydrogen bonding networks to become reduced or eliminated. From previous studies on GlpF in LMPC it is

shown that at high temperatures, about 75% of the secondary structure is still present at 80°C [48]. As sections of protein become denatured from their 4° and 3° structures, the α-helices that have been liberated from their inter-protein 3° structural contacts can interact with other proteins' unfolded sections and cause large scale aggregation.

The thermal stability of bacteriorhodopsin has been extensively studied and it is observed to have a T_m near 100°C with an unfolding enthalpy of approximately 3.7 cal/g at neutral pH in native purple membranes [127]. This value is substantially lower than a typical value of about 12 cal/g obtained for soluble proteins. The protein can exist as a stable monomer, but its native form is trimeric. The denaturation of the trimer occurs at a temperature 20°C higher than the monomer, although the enthalpies of unfolding are comparable between the two oligomeric forms [129, 130]. This suggests that the trimeric form of the protein is entropically stabilized through increased disorder in the solvent. The entropy term of the Gibbs free energy equation contributes about 5 kcal/mol to the overall free energy of stabilization, as compared to the monomer [128].

Cytochrome-*c* oxidase is a predominantly α-helical membrane protein composed of three subunits in which all three possess transmembrane sections. It has been reported to retain as much as 45% of its α-helical structure upon thermal denaturation [131]. The unfolding enthalpy for cytochrome-*c* oxidase is about 2.4 to 2.9 cal/g, which is very similar to bacteriorhodopsin, and again much less than that for soluble proteins [128]. Several studies have shown that the in vitro stability of cytochrome-c oxidase is highly dependent on the reconstitution protocol [131-134]. When solubilized in endogenous lipids, there is a 5°C increase in the T_m when compared to delipidated protein, and the

enthalpy of denaturation is highly variable depending on the detergent used to solubilize the protein [134].

Several investigations on the thermal stability of Photosystem II have been performed. Photosystem II is an α-helical membrane protein with several different subunits. It has a denaturation enthalpy of about 5 to 6 cal/g and the calorimetric denaturation profiles are extremely sensitive to the concentration of detergent used in the solubilization of the protein [135]. The sensitivity to the detergent used in the preparation of similar membrane proteins has been studied and the results suggest that the concentration and characteristics of the surfactant play an important role in the stability of membrane proteins [136].

4.4 Thermal Stability of GlpF in the Presence and Absence of TMAO.

From previous experiments in our lab, it was observed that GlpF is more thermally stable in LMPC ($T_m = 74.9 \pm 1.5°C$) than in DDM ($T_m = 71 \pm 2°C$) or OG (GlpF is unstable in OG and therefore a T_m value could not be measured) [48]. This investigation extends these results to include the effects of two new solubilising detergents (TDM and LLPC) and the naturally-occurring osmolyte TMAO on the thermal stability of GlpF. SDS-PAGE and DLS were used to monitor the quaternary structures and particle sizes for the thermal denaturations in all four detergents in the presence and absence of TMAO.

In DDM and TDM, the thermal stability as monitored by SDS-PAGE in the absence of TMAO was very similar with a denaturation occurring at 69 ± 5°C and 70 ± 1°C for DDM and TDM, respectively (Figures 18 and 41, and Table 18). This transition temperature is in close agreement with a previous T_m value of 71 ± 2°C for the tertiary structure which was obtained in our lab [48] for DDM. This agreement in T_m values suggests that the tertiary and quaternary structures unfold at the same time, without the formation of a folded monomeric intermediate. Upon the addition of TMAO to the solution, there is about a 10°C increase in the stability of tetramer in both detergents and denaturation occurs at 80 ± 1°C and 81 ± 2°C (Figures 19 and 42, and Table 18). The foremost difference between the protein stability in the two detergents is the fact that an octamer is observed in DDM with 4 M TMAO but no octamer is observed in TDM. It is this oligomeric form of the protein that predominates and there is no denaturation of the octamer to tetramer as is found in the SDS denaturations. The octamer exhibits a cooperative denaturation to aggregate at 80 ± 1°C (Figure 20 – lane 7).

The SDS-PAGE thermal denaturations of GlpF in LLPC and LMPC were very similar to each other, and comparable to the similarities between DDM and TDM. It is found that there is a significant amount of tetramer present in both detergents at 80°C, and by 85°C the protein is completely denatured into higher molecular weight aggregates. There is a large amount of aggregates in both detergents that just enter the running gel, with a smaller amount that did not even enter the stacking gel at 80°C and 85°C. This illustrates that in LLPC and LMPC the tetramer unfolds at a temperature between 80°C and 85°C, and the calculated T_m values for LLPC and LMPC are 82 ± 4°C and 77 ± 3°C, respectively. A T_m of 74.9 ± 1.5°C for the tertiary structure of GlpF in LMPC was

obtained from previous research in our lab with an unfolding of the quaternary structure around 80°C [48]. The previously obtained T_m value is in close agreement with our results, and again suggests that the thermal denaturation of GlpF does not proceed through an intermediate. At 80°C it is observed that in both detergents there is a significant portion of the tetramer present, but there is a considerable amount of aggregate at this temperature and at all temperatures above 60°C. When TMAO is added to the solution the stability of GlpF in both detergents increases significantly. The T_m values obtained from the TMAO data are 91 ± 2°C and 83.5 ± 2°C for LLPC and LMPC, respectively, which is an increase of 9°C for LLPC and 6.5°C for LMPC in the stability of GlpF caused by TMAO. There is a considerable amount of very high molecular weight aggregates that do not enter the stacking gel in the presence of TMAO at 80°C and 85°C. A smaller amount of aggregates are also observed that just enter the running gel at 80°C and 85°C than is observed at the same temperatures in the absence of TMAO. This may indicate that the types of aggregated GlpF in the presence of TMAO are different than in the absence of TMAO. Note that TMAO causes the unfolded state of the protein to be very unfavourable entropically because of its very strong interactions with water.

There appears to be much larger aggregates in all detergents tested when TMAO is in the solution and this is confirmed with the DLS data that show much larger diameter particles in solution at high temperatures in the presence of TMAO. TMAO may facilitate the aggregation of larger particles by preventing the SDS inherent in SDS-PAGE from breaking up portions of the very large protein aggregates.

The data presented in Table 18 confirm that GlpF is more heat stable in detergents with a charged phosphatidylcholine headgroup (LLPC and LMPC), than in non-ionic

detergents with neutral headgroups (DDM and TDM) both in the presence and absence of TMAO. Interestingly, the length of the hydrocarbon chain appears to have no effect on the stability of the protein in neutral detergents, but the protein is significantly more stable in LLPC than in LMPC. The same differences in thermal stability are retained in 4 M TMAO indicating that the difference in stability measured in TMAO are intrinsic to the hydrocarbon chain. These observations are generally in agreement with the findings in the previous section which showed that GlpF is more stable to SDS in detergents with PC head groups and 12 carbon chains.

4.5 Dynamic Light Scattering Investigations of GlpF in Detergent Micelles

An important goal of the present research was to examine Dynamic Light Scattering as a tool for following the unfolding of a membrane protein in solution. It is a non-invasive technique that provides a means to determining the hydrodynamic diameter of the particles that are in the solution. This method is uniquely suited for detecting and characterizing soluble protein aggregation. Because larger particles in solution scatter light strongly, it is much easier to detect small amounts of aggregates using DLS than with other techniques. It should be noted that several attempts were made in all four detergents to separate the empty detergent micelles from the detergent-solubilized proteins by using size-exclusion chromatography and UV-spectroscopy to detect the amount of protein eluting from the column, but all attempts were unsuccessful. Possible explanations include dilution of the protein that was added to the column, thus yielding negligible amounts of purified protein-detergent micelles. It is also possible that the

protein came out of solution as detergent free buffer was added to the column and that the protein stuck to the chromatographic resin.

Studies into the effects of detergent chain length and salt concentration on the ionic detergent alkyltrimethylammonium bromide using DLS have been published. The investigations have found that the value of the critical micellar concentration (CMC) exhibits a minimum at a certain temperature, T_{min}, and this value shifts to lower temperatures as the detergent chain length increases, or with increasing salt concentration [137, 138]. To state this principle another way, as the temperature is increased the sizes of the micelles in solution decrease to a minimum which is characteristic of the detergent, after which the micelle sizes increase with increasing temperature [138]. Sphere-to-rod transitions in ionic surfactants have been observed in solutions with increasing temperature, salt concentration, and surfactant concentration [111, 139-141]. Studies on sodium alkyl sulphates have shown that the longer the alkyl chain length, the slower the transition from sphere to rod [141].

Investigations using DLS into the effects of concentration and temperature on the aggregation state of non-ionic detergents have been reported in the literature [142]. In these pioneering investigations it was shown that the detergent micelles made from $C_{12}E_5$ and $C_{12}E_6$ both grow strongly with increasing temperature, and through self-diffusion data it was shown that the micelles grow into rod-like micelles as the temperature increases [142]. Numerous more recent studies have also shown sphere-to-rod transitions using DLS in non-ionic detergents [86, 140, 143, 144].

The effects of an osmolyte on the micellarization of SDS have been studied using DLS in the literature [109, 110, 145]. In one case, an increase in the detergent micelle

aggregation number with increasing concentration of the osmolyte mannitol is witnessed, and the interaction between SDS and mannitol was found to be stronger than that between SDS and water [145]. The increase in the aggregation number due to the increase in mannitol was hypothesized to be caused by the penetration of the mannitol molecules between the detergent headgroups resulting in the increased stability of the detergent aggregate, and this had been observed for sucrose previously in the literature [146].

The DLS studies conducted at 20°C on DDM micelles (Figure 26) yielded average diameters of 8.1 nm, which is in excellent agreement with the diameter of 7 – 8 nm measured by DLS that is reported in the literature and is also in excellent agreement with the known size of the detergent [86]. In TDM (Figure 43), the measured average micelle diameter is 11.3 nm which compares to a value of about 8 nm measured by Ericsson et al., [88] by DLS. The measured average diameters observed in LLPC (Figure 56) and LMPC (Figure 68) are 7.7 nm and 8.8 nm, respectively. This is the first time that micelle diameters have been measured in LLPC and LMPC, therefore no comparisons could be made to the literature. However, the diameters of the micelles are close to what would be predicted on the basis of detergent size.

When the temperature is increased in 10°C steps from 20°C to 80°C in DDM and TDM, the average particle sizes decrease suggesting that the micelles are getting smaller with increasing temperature. In DDM, a second peak corresponding to very large particles forms at 50°C, which then grows in intensity with increasing temperature. This result suggests that very large micelles are forming at higher temperatures and there is a sphere-to-rod transition that begins at 50°C in DDM micelles. Sphere-to-rod transitions

have been observed in detergents many times [86, 111, 139-144], and it is reasonable to assume that a similar transition is occurring in DDM considering that a spherical particle 255 nm in diameter composed of DDM molecules would not be possible based on the known size of the detergent. In TDM however, there is no large diameter peak that is formed at higher temperatures, demonstrating that sphere-to-rod transitions may not occur in all detergents. Decreasing particle size as temperature is increased is observed in the small diameter peaks in LLPC and LMPC. Large particles are observed in LLPC at all temperatures tested, and only at temperatures above 40°C in LMPC. This demonstrates that the thermal behaviour of detergents with a PC headgroup are different than those with a maltoside headgroup, and that large aggregations of detergent are more favoured in LLPC and LMPC, as compared to DDM and TDM. In the reference Heerklotz et al. [86], it was reported that there is no sphere-to-rod transition observed at increased temperatures greater than or equal to 35°C in DDM as observed by DLS. This is contrary to what was observed in Figure 26 where a very significant peak corresponding to very large particles is observed at higher temperatures. However, it should be noted that our experiments matched the results from 20 to 35°C and were conducted over a much wider range of temperatures as compared to Heerklotz et al. [86]. The temperature range in Figure 26 is 20°C to 80°C, and Heerklotz et al. presented a range of measurements from 0°C to 35°C [86]. There was indication of micellar growth reported by Heerklotz et al. at higher temperatures as observed by pressure perturbation calorimetry (PPC), but the result was very weak using this technique and its significance was reported as questionable [86]. The diameters of the large particles in Figure 26 are

more than 200 nm and the peaks grow with increasing temperature. It is extremely improbable that these particles are huge spherical micelles [140].

When 4 M TMAO is added to detergent solutions at room temperature the effect is an increase in the size of the micelles in all detergents tested. Increases of 18.4 nm in DDM (Figure 28), 130.4 nm in TDM (Figure 45), 16.3 nm in LLPC (Figure 58), and 23.9 nm in LMPC (Figure 70) were observed. These results suggest that the effect of TMAO on micelle diameter is more pronounced in detergents possessing a maltoside head group, and in detergents with a longer alkyl chain.

When the detergent solution is heated in the presence of 4 M TMAO, the result in DDM is similar to its corresponding spectrum in the absence of TMAO in that the trend of decreasing size is observed, but the particles begin at a larger size. There are also peaks corresponding to large particles that are present throughout the experiment in DDM and TMAO that are not observed in the absence of TMAO. In TDM and TMAO, large particle peaks appear at temperatures above 60°C, and the smaller diameter particles follow a similar trend of decreasing size as the temperature is increased as compared to TDM in the absence of TMAO. LLPC shows a trend of decreasing size of both the large and small particle peaks as the temperature is increased, but the particles are much larger than those observed in the absence of TMAO. In LMPC large diameter peaks are only observed at temperatures higher than 60°C, and the small diameter peaks show an initial increase in size from 20°C to 30°C, but further increases in temperature decrease the size of the particles.

When GlpF is added to the detergent solutions at 20°C, small increases in micelle size are observed in all detergents (Tables 2, 10, 13, and 19). Other than the increase of

0.8 nm observed in TDM, all other detergents show an increase in size that is almost what is predicted for the addition of GlpF to the corresponding micelle. The size of the GlpF tetramer as determined by X-ray crystallography is 4.5 nm [21], and diameter increases of 3.5 nm, 4.1 nm, and 3.2 nm were observed in DDM, LLPC, and LMPC, respectively. These results are in agreement with the SDS-PAGE data which show that GlpF is in a tetrameric form at 20°C. In TDM, the increase in size is smaller than expected suggesting that there may displacement of detergent when the protein is solubilized by the micelle. It may also be possible that the presence of an abundance of empty micelles along with protein-containing micelles yields an average micelle size that does not reflect the true size of the protein-containing micelles.

Increased temperature on the protein-detergent particle sizes in DDM leads to a peak that does not appear in the detergent-only experiment suggesting that we can observe irreversibly unfolded GlpF at 70°C (Figure 27). This result is in close agreement with the GlpF thermal denaturation results observed in SDS-PAGE (Figure 18), where the tetramer is unstable at temperatures above 65°C. Unfortunately, no evidence of irreversibly unfolded GlpF is found in TDM, LLPC, or LMPC. The large diameter peaks of GlpF in TDM, GlpF in LLPC, and GlpF in LMPC observed at high temperatures are also observed in the absence of GlpF, therefore it is not clear what the nature of the protein is in the peaks with GlpF and detergent. Thus, similar to the case of TMAO, GlpF most likely alters the micelle size and structure preventing calculation of the size of the protein aggregate by subtracting the size of the empty-detergent particle from the protein-detergent particle.

When 4 M TMAO is added to a solution of protein and detergent at 20°C, the sizes of the particles in all detergents tested, that are observed are much larger than those predicted by SDS-PAGE. This result suggests that the protein has a tendency to self associate into large oligomers in the presence of TMAO. Octamers have been previously observed in GlpF (Figures 15 and 16) [47, 112], and AQP0 [113], therefore the appearance of higher oligomeric forms of GlpF is not improbable. Conversely, it is also possible that TMAO rearranges the micellar structure, which makes valid conclusions about the state of the protein solubilized in detergent in the presence of TMAO difficult to establish. Regardless of this, my observations suggest that the preferred oligomeric state of the protein is a tetramer in TDM, LLPC, and LMPC, but an octamer in DDM and TMAO.

The DLS data presented here are preliminary work using such a system, and it is believed that through further experimentation, characterization of GlpF and similar membrane proteins can be achieved using DLS.

4.6 Future Work

Here I have presented a study on the conformational stability of GlpF in several different detergents and in the presence of the osmolyte TMAO. This research contributed to an improved understanding of membrane protein folding and a better methodology for studying these proteins. DLS has never been used before to study an α-helical membrane protein in detergent and the present study has shown that valuable information on the effects of temperature and TMAO on a membrane protein and the detergents that are used to solubilize them can be gained from this line of research.

However, the presence of scattering from detergent micelles made some of the results difficult to interpret. Future directions in this research would benefit from the ability to produce 200 μM or higher quantities of ^{13}C, ^{15}N, and deuterium-labelled protein for multidimensional NMR studies into structure and dynamics of GlpF. The way that this appears to be possible is through cell-free protein expression which has been shown to be effective for over-expressing membrane proteins [147]. If high levels of labelled protein can be achieved, then high-resolution studies into the effects of TMAO on membrane protein structure and stability, including the effects of SDS, pH, and temperature could be investigated.

Bibliography

1. Singer, S.J. and G.L. Nicolson, *The fluid mosaic model of the structure of cell membranes.* Science, 1972. **175**(23): p. 720-31.
2. Mackenzie, K.R., *Folding and stability of alpha-helical integral membrane proteins.* Chem Rev, 2006. **106**(5): p. 1931-77.
3. Devaux, P.F., *Static and dynamic lipid asymmetry in cell membranes.* Biochemistry, 1991. **30**(5): p. 1163-73.
4. Rothman, J.E. and J. Lenard, *Membrane asymmetry.* Science, 1977. **195**(4280): p. 743-53.
5. Hemker, H.C., et al., *Platelet membrane involvement in blood coagulation.* Blood Cells, 1983. **9**(2): p. 303-17.
6. Edidin, M., *Shrinking patches and slippery rafts: scales of domains in the plasma membrane.* Trends Cell Biol, 2001. **11**(12): p. 492-6.
7. Nelson, D.L., Cox, M.M., *Lehninger Principles of Biochemistry.* Third ed. 2000, New York, New York: Worth Publishers. 1152.
8. Voet, D., Voet, J.G., Pratt, C.W., *Fundamentals of Biochemistry: Life at the Molecular Level.* 2 ed. Fundamentals of Biochemistry. 2006, Hoboken, NJ: John Wiley & sons, Inc. 1130.
9. Tristram-Nagle, S., C.P. Yang, and J.F. Nagle, *Thermodynamic studies of purple membrane.* Biochim Biophys Acta, 1986. **854**(1): p. 58-66.

10. White, S.H. and W.C. Wimley, *Membrane protein folding and stability: physical principles.* Annu Rev Biophys Biomol Struct, 1999. **28**: p. 319-65.
11. Engelman, D.M., T.A. Steitz, and A. Goldman, *Identifying nonpolar transbilayer helices in amino acid sequences of membrane proteins.* Annu Rev Biophys Biophys Chem, 1986. **15**: p. 321-53.
12. Kyte, J. and R.F. Doolittle, *A simple method for displaying the hydropathic character of a protein.* J Mol Biol, 1982. **157**(1): p. 105-32.
13. von Heijne, G., *Membrane protein structure prediction. Hydrophobicity analysis and the positive-inside rule.* J Mol Biol, 1992. **225**(2): p. 487-94.
14. Aidley, D.J., Stanfield, P.R., *Ion Channels: Molecules in Action.* 1996: Cambridge University Press. 324.
15. Mahalakshmi, R. and F.M. Marassi, *Orientation of the Escherichia coli Outer Membrane Protein OmpX in Phospholipid Bilayer Membranes Determined by Solid-State NMR.* Biochemistry, 2008.
16. Jiang, Y., et al., *X-ray structure of a voltage-dependent K+ channel.* Nature, 2003. **423**(6935): p. 33-41.
17. Yellen, G., *The voltage-gated potassium channels and their relatives.* Nature, 2002. **419**(6902): p. 35-42.
18. Preston, G.M. and P. Agre, *Isolation of the cDNA for erythrocyte integral membrane protein of 28 kilodaltons: member of an ancient channel family.* Proc Natl Acad Sci U S A, 1991. **88**(24): p. 11110-4.
19. Moon, C., et al., *The human aquaporin-CHIP gene. Structure, organization, and chromosomal localization.* J Biol Chem, 1993. **268**(21): p. 15772-8.
20. Preston, G.M., et al., *Appearance of water channels in Xenopus oocytes expressing red cell CHIP28 protein.* Science, 1992. **256**(5055): p. 385-7.
21. Fu, D., et al., *Structure of a glycerol-conducting channel and the basis for its selectivity.* Science, 2000. **290**(5491): p. 481-6.
22. Agre, P. and D. Kozono, *Aquaporin water channels: molecular mechanisms for human diseases.* FEBS Lett, 2003. **555**(1): p. 72-8.
23. Stroud, R.M., et al., *Glycerol facilitator GlpF and the associated aquaporin family of channels.* Curr Opin Struct Biol, 2003. **13**(4): p. 424-31.
24. de Groot, B.L. and H. Grubmuller, *Water permeation across biological membranes: mechanism and dynamics of aquaporin-1 and GlpF.* Science, 2001. **294**(5550): p. 2353-7.
25. Tajkhorshid, E., et al., *Control of the selectivity of the aquaporin water channel family by global orientational tuning.* Science, 2002. **296**(5567): p. 525-30.
26. Murata, K., et al., *Structural determinants of water permeation through aquaporin-1.* Nature, 2000. **407**(6804): p. 599-605.
27. Agre, P., *The aquaporin water channels.* Proc Am Thorac Soc, 2006. **3**(1): p. 5-13.
28. Chakrabarti, N., B. Roux, and R. Pomes, *Structural determinants of proton blockage in aquaporins.* J Mol Biol, 2004. **343**(2): p. 493-510.
29. Sui, H., et al., *Structural basis of water-specific transport through the AQP1 water channel.* Nature, 2001. **414**(6866): p. 872-8.

30. Heller, K.B., E.C. Lin, and T.H. Wilson, *Substrate specificity and transport properties of the glycerol facilitator of Escherichia coli.* J Bacteriol, 1980. **144**(1): p. 274-8.
31. Nollert, P., et al., *Atomic structure of a glycerol channel and implications for substrate permeation in aqua(glycero)porins.* FEBS Lett, 2001. **504**(3): p. 112-7.
32. Sela, M., F.H. White, Jr., and C.B. Anfinsen, *Reductive cleavage of disulfide bridges in ribonuclease.* Science, 1957. **125**(3250): p. 691-2.
33. Anfinsen, C.B., et al., *The kinetics of formation of native ribonuclease during oxidation of the reduced polypeptide chain.* Proc Natl Acad Sci U S A, 1961. **47**: p. 1309-14.
34. Haber, E. and C.B. Anfinsen, *Side-chain interactions governing the pairing of half-cystine residues in ribonuclease.* J Biol Chem, 1962. **237**: p. 1839-44.
35. White, F.H., Jr. and C.B. Anfinsen, *Some relationships of structure to function in ribonuclease.* Ann N Y Acad Sci, 1959. **81**: p. 515-23.
36. Epstein, C.J., Goldberger, R.F., Anfinsen, C.B., in *Cold Spring Harbor Symp. Quant, Biol.* 1963: Cold Spring Harbor. p. 439.
37. Goldberg, M.E., *The second translation of the genetic message: protein folding and assembly.* Trends in Biochemical Sciences, 1985. **10**: p. 388 - 391.
38. Baker, D. and A. Sali, *Protein structure prediction and structural genomics.* Science, 2001. **294**(5540): p. 93-6.
39. Jaenicke, R., *How do proteins acquire their three-dimensional structure and stability?* Naturwissenschaften, 1996. **83**(12): p. 544-54.
40. Dempsey, C.E., *The actions of melittin on membranes.* Biochim Biophys Acta, 1990. **1031**(2): p. 143-61.
41. Cramer, W.A., et al., *Structure-function of the channel-forming colicins.* Annu Rev Biophys Biomol Struct, 1995. **24**: p. 611-41.
42. Zhan, H., et al., *Interaction of the isolated transmembrane domain of diphtheria toxin with membranes.* Biochemistry, 1995. **34**(14): p. 4856-63.
43. Song, L., et al., *Structure of staphylococcal alpha-hemolysin, a heptameric transmembrane pore.* Science, 1996. **274**(5294): p. 1859-66.
44. Johnson, A.E. and M.A. van Waes, *The translocon: a dynamic gateway at the ER membrane.* Annu Rev Cell Dev Biol, 1999. **15**: p. 799-842.
45. White, S.H. and G. von Heijne, *Transmembrane helices before, during, and after insertion.* Curr Opin Struct Biol, 2005. **15**(4): p. 378-86.
46. Yano, Y., *[Fundamental studies on membrane protein folding using model transmembrane helices].* Yakugaku Zasshi, 2005. **125**(9): p. 725-32.
47. Galka, J.G., *Solution State Characterization of the E. coli Inner Membrane Protein Glycerol Facilitator*, in *Chemistry*. 2008, University of Manitoba: Winnipeg. p. 166.
48. Galka, J.J., et al., *Stability of the glycerol facilitator in detergent solutions.* Biochemistry, 2008. **47**(11): p. 3513-24.
49. Huang, K.S., et al., *Refolding of an integral membrane protein. Denaturation, renaturation, and reconstitution of intact bacteriorhodopsin and two proteolytic fragments.* J Biol Chem, 1981. **256**(8): p. 3802-9.

50. London, E. and H.G. Khorana, *Denaturation and renaturation of bacteriorhodopsin in detergents and lipid-detergent mixtures.* J Biol Chem, 1982. **257**(12): p. 7003-11.
51. Yancey, P.H., et al., *Living with water stress: evolution of osmolyte systems.* Science, 1982. **217**(4566): p. 1214-22.
52. Yancey, P.H., *Organic osmolytes as compatible, metabolic and counteracting cytoprotectants in high osmolarity and other stresses.* J Exp Biol, 2005. **208**(Pt 15): p. 2819-30.
53. Shen, B., et al., *Roles of sugar alcohols in osmotic stress adaptation. Replacement of glycerol by mannitol and sorbitol in yeast.* Plant Physiol, 1999. **121**(1): p. 45-52.
54. Schaffer, S., et al., *Why is taurine cytoprotective?* Adv Exp Med Biol, 2003. **526**: p. 307-21.
55. Brown, A.D. and J.R. Simpson, *Water relations of sugar-tolerant yeasts: the role of intracellular polyols.* J Gen Microbiol, 1972. **72**(3): p. 589-91.
56. Pruski, A.M., Fiala-Médioni, A., Fisher, C. R. and Colomines, J. C., *Composition of free amino acids and related compounds in invertebrates with symbiotic bacteria at hydrocarbon seeps in the Gulf of Mexico.* Mar. Biol., 2000. **136**: p. 411-420.
57. Wolfe, G.V., *The chemical defense ecology of marine unicellular plankton: constraints, mechanisms, and impacts.* Biol Bull, 2000. **198**(2): p. 225-44.
58. Yancey, P.H., *Water stress, osmolytes and proteins.* AMERICAN ZOOLOGIST 2001. **41**(4): p. 699-709.
59. Singer, M.A. and S. Lindquist, *Thermotolerance in Saccharomyces cerevisiae: the Yin and Yang of trehalose.* Trends Biotechnol, 1998. **16**(11): p. 460-8.
60. Storey, K.B., Storey, J. M., *Natural freezing survival in animals.* Ann. Rev. Ecol. Syst., 1996. **27**: p. 365-386.
61. Tunnacliffe, A. and J. Lapinski, *Resurrecting Van Leeuwenhoek's rotifers: a reappraisal of the role of disaccharides in anhydrobiosis.* Philos Trans R Soc Lond B Biol Sci, 2003. **358**(1438): p. 1755-71.
62. Siebenaller, J.F., Somero, G. N., *Biochemical adaptation to the deep sea.* CRC Crit. Rev. Aq. Sci., 1989. **1**: p. 1-25.
63. Bolen, D.W., *Protein stabilization by naturally occurring osmolytes.* Methods Mol Biol, 2001. **168**: p. 17-36.
64. Bolen, D.W. and I.V. Baskakov, *The osmophobic effect: natural selection of a thermodynamic force in protein folding.* J Mol Biol, 2001. **310**(5): p. 955-63.
65. Raymond, J.A., *Trimethylamine oxide and urea synthesis in rainbow smelt and some other northern fishes.* Physiol Zool, 1998. **71**(5): p. 515-23.
66. Yancey, P.H., et al., *Trimethylamine oxide counteracts effects of hydrostatic pressure on proteins of deep-sea teleosts.* J Exp Zool, 2001. **289**(3): p. 172-6.
67. Yancey, P.H. and J.F. Siebenaller, *Trimethylamine oxide stabilizes teleost and mammalian lactate dehydrogenases against inactivation by hydrostatic pressure and trypsinolysis.* J Exp Biol, 1999. **202**(Pt 24): p. 3597-603.
68. Kumar, R., *Osmolyte-induced folding of an intrinsically disordered activation function subdomain of glucocorticoid receptor.* J Recept Signal Transduct Res, 2008. **28**(5): p. 465-74.

69. Bennion, B.J. and V. Daggett, *Counteraction of urea-induced protein denaturation by trimethylamine N-oxide: a chemical chaperone at atomic resolution.* Proc Natl Acad Sci U S A, 2004. **101**(17): p. 6433-8.
70. Mukherjee, A., et al., *A natural osmolyte trimethylamine N-oxide promotes assembly and bundling of the bacterial cell division protein, FtsZ and counteracts the denaturing effects of urea.* FEBS J, 2005. **272**(11): p. 2760-72.
71. Paul, S. and G.N. Patey, *Structure and interaction in aqueous urea-trimethylamine-N-oxide solutions.* J Am Chem Soc, 2007. **129**(14): p. 4476-82.
72. Paul, S. and G.N. Patey, *The influence of urea and trimethylamine-N-oxide on hydrophobic interactions.* J Phys Chem B, 2007. **111**(28): p. 7932-3.
73. Ford, N.C.J., *Dynamic Light Scattering: Applications of Photon Correlation Spectroscopy*, ed. R. Pecora. 1985, New York, NY: Plenum Press.
74. Malvern, *Zetasizer Nano User Manual.* 2007, Worcestershire, UK: Malvern Instruments Ltd.
75. Miroux, B. and J.E. Walker, *Over-production of proteins in Escherichia coli: mutant hosts that allow synthesis of some membrane proteins and globular proteins at high levels.* J Mol Biol, 1996. **260**(3): p. 289-98.
76. Manley, D. and J.D. O'Neil, *Preparation of glycerol facilitator for protein structure and folding studies in solution.* Methods Mol Biol, 2003. **228**: p. 89-101.
77. Manley, D.M., et al., *Secondary structure and oligomerization of the E. coli glycerol facilitator.* Biochemistry, 2000. **39**(40): p. 12303-11.
78. Morein, S., D. Henricson, and L. Rilfors, *Separation of Inner and Outer-Membrane Vesicles from Escherichia-Coli in Self-Generating Percoll Gradients.* Analytical Biochemistry, 1994. **216**(1): p. 47-51.
79. Laemmli, U.K., *Cleavage of structural proteins during the assembly of the head of bacteriophage T4.* Nature, 1970. **227**(5259): p. 680-5.
80. O'Neil, J.D., *Fitting SDS-Induced Protein Unfolding Measurements to a Two-State Transition.* 2006: Winnipeg.
81. Sehgal, P., J.E. Mogensen, and D.E. Otzen, *Using micellar mole fractions to assess membrane protein stability in mixed micelles.* Biochim Biophys Acta, 2005. **1716**(1): p. 59-68.
82. Renthal, R., *An unfolding story of helical transmembrane proteins.* Biochemistry, 2006. **45**(49): p. 14559-66.
83. Yancey, P.H. and G.N. Somero, *Counteraction of urea destabilization of protein structure by methylamine osmoregulatory compounds of elasmobranch fishes.* Biochem J, 1979. **183**(2): p. 317-23.
84. Forster, R.P. and L. Goldstein, *Intracellular osmoregulatory role of amino acids and urea in marine elasmobranchs.* Am J Physiol, 1976. **230**(4): p. 925-31.
85. Henkels, C.H. and T.G. Oas, *Thermodynamic characterization of the osmolyte- and ligand-folded states of Bacillus subtilis ribonuclease P protein.* Biochemistry, 2005. **44**(39): p. 13014-26.
86. Heerklotz, H., et al., *Structural, volumetric, and thermodynamic characterization of a micellar sphere-to-rod transition.* J Am Chem Soc, 2004. **126**(50): p. 16544-52.

87. Konidala, P., L. He, and B. Niemeyer, *Molecular dynamics characterization of n-octyl-beta-d-glucopyranoside micelle structure in aqueous solution.* J Mol Graph Model, 2006. **25**(1): p. 77-86.
88. Ericsson, C.A., et al., *Effects of temperature, salt, and deuterium oxide on the self-aggregation of alkylglycosides in dilute solution. 2. n-Tetradecyl-beta-D-maltoside.* Langmuir, 2005. **21**(4): p. 1507-15.
89. Sanders, C.R., 2nd, et al., *Escherichia coli diacylglycerol kinase is an alpha-helical polytopic membrane protein and can spontaneously insert into preformed lipid vesicles.* Biochemistry, 1996. **35**(26): p. 8610-8.
90. Behbehani, G.R., A.A. Saboury, and E. Taleshi, *A direct calorimetric determination of denaturation enthalpy for lysozyme in sodium dodecyl sulfate.* Colloids Surf B Biointerfaces, 2008. **61**(2): p. 224-8.
91. Turro, N.J., Lei, X.G., *Spectroscopic Probe Analysis of Protein-Surfactant Interactions: The BSA/SDS System.* Langmuir, 1995. **11**(7): p. 2525-2533.
92. Howell, S.C., M.F. Mesleh, and S.J. Opella, *NMR structure determination of a membrane protein with two transmembrane helices in micelles: MerF of the bacterial mercury detoxification system.* Biochemistry, 2005. **44**(13): p. 5196-206.
93. Laubinger, W. and P. Dimroth, *Characterization of the ATP synthase of Propionigenium modestum as a primary sodium pump.* Biochemistry, 1988. **27**(19): p. 7531-7.
94. Pervushin, K.V., et al., *Three-dimensional structure of (1-71)bacterioopsin solubilized in methanol/chloroform and SDS micelles determined by 15N-1H heteronuclear NMR spectroscopy.* Eur J Biochem, 1994. **219**(1-2): p. 571-83.
95. Curnow, P. and P.J. Booth, *Combined kinetic and thermodynamic analysis of alpha-helical membrane protein unfolding.* Proc Natl Acad Sci U S A, 2007. **104**(48): p. 18970-5.
96. Booth, P.J., *Unravelling the folding of bacteriorhodopsin.* Biochim Biophys Acta, 2000. **1460**(1): p. 4-14.
97. Lau, F.W. and J.U. Bowie, *A method for assessing the stability of a membrane protein.* Biochemistry, 1997. **36**(19): p. 5884-92.
98. Faham, S., et al., *Side-chain contributions to membrane protein structure and stability.* J Mol Biol, 2004. **335**(1): p. 297-305.
99. Riley, M.L., et al., *Slow alpha helix formation during folding of a membrane protein.* Biochemistry, 1997. **36**(1): p. 192-6.
100. Reynolds, J.A. and C. Tanford, *The gross conformation of protein-sodium dodecyl sulfate complexes.* J Biol Chem, 1970. **245**(19): p. 5161-5.
101. Michaux, C., N.C. Pomroy, and G.G. Prive, *Refolding SDS-denatured proteins by the addition of amphipathic cosolvents.* J Mol Biol, 2008. **375**(5): p. 1477-88.
102. Anand, K., D. Pal, and R. Hilgenfeld, *An overview on 2-methyl-2,4-pentanediol in crystallization and in crystals of biological macromolecules.* Acta Crystallogr D Biol Crystallogr, 2002. **58**(Pt 10 Pt 1): p. 1722-8.
103. Michaux, C., et al., *Protecting role of cosolvents in protein denaturation by SDS: a structural study.* BMC Struct Biol, 2008. **8**: p. 29.
104. Subramaniam, S., et al., *Electron diffraction analysis of structural changes in the photocycle of bacteriorhodopsin.* EMBO J, 1993. **12**(1): p. 1-8.

105. Doyle, D.A., et al., *The structure of the potassium channel: molecular basis of K+ conduction and selectivity.* Science, 1998. **280**(5360): p. 69-77.
106. Barrera, F.N., et al., *Unfolding and refolding in vitro of a tetrameric, alpha-helical membrane protein: the prokaryotic potassium channel KcsA.* Biochemistry, 2005. **44**(43): p. 14344-52.
107. Diamant, S., et al., *Dicarboxylic amino acids and glycine-betaine regulate chaperone-mediated protein-disaggregation under stress.* Mol Microbiol, 2003. **49**(2): p. 401-10.
108. Zou, Q., et al., *The molecular mechanism of stabilization of proteins by TMAO and its ability to counteract the effects of urea.* J Am Chem Soc, 2002. **124**(7): p. 1192-202.
109. Freda, M., G. Onori, and A. Santucci, *Hydrophobic hydration and hydrophobic interaction in aqueous solutions of tert-butyl alcohol and trimethylamine-N-oxide: a correlation with the effect of these two solutes on the micellization process.* Phys. Chem. Chem. Phys., 2002. **4**: p. 4979–4984.
110. Di Michele, A., et al., *Modulation of hydrophobic effect by cosolutes.* J Phys Chem B, 2006. **110**(42): p. 21077-85.
111. von Berlepsch, H., Dautzenberg, H., Rother, G., Jager. J., *An Investigation of the Micellar Phase of Sodium Sulfopropyl Octadecyl Maleate in Aqueous Sodium Chloride Solutions by Light Scattering Techniques. Evidence of Nearly Rodlike Micelles.* Langmuir, 1996. **12**: p. 3613-3625.
112. Braun, T., et al., *The 3.7 A projection map of the glycerol facilitator GlpF: a variant of the aquaporin tetramer.* EMBO Rep, 2000. **1**(2): p. 183-9.
113. Palanivelu, D.V., et al., *Co-axial association of recombinant eye lens aquaporin-0 observed in loosely packed 3D crystals.* J Mol Biol, 2006. **355**(4): p. 605-11.
114. Chandy, G., et al., *Comparison of the water transporting properties of MIP and AQP1.* J Membr Biol, 1997. **159**(1): p. 29-39.
115. Varadaraj, K., et al., *The role of MIP in lens fiber cell membrane transport.* J Membr Biol, 1999. **170**(3): p. 191-203.
116. Koga, Y., et al., *Crystal structure of highly thermostable glycerol kinase from a hyperthermophilic archaeon in a dimeric form.* FEBS J, 2008. **275**(10): p. 2632-43.
117. Voegele, R.T., G.D. Sweet, and W. Boos, *Glycerol kinase of Escherichia coli is activated by interaction with the glycerol facilitator.* J Bacteriol, 1993. **175**(4): p. 1087-94.
118. Hill, W.G., R.L. Rivers, and M.L. Zeidel, *Role of leaflet asymmetry in the permeability of model biological membranes to protons, solutes, and gases.* J Gen Physiol, 1999. **114**(3): p. 405-14.
119. Jaspers, H.T. and J. van Steveninck, *Transport-associated phosphorylation of 2-deoxy-D-glucose in Saccharomyces fragilis.* Biochim Biophys Acta, 1975. **406**(3): p. 370-85.
120. Bisson, L.F. and D.G. Fraenkel, *Involvement of kinases in glucose and fructose uptake by Saccharomyces cerevisiae.* Proc Natl Acad Sci U S A, 1983. **80**(6): p. 1730-4.

121. Fujiwara, Y., K. Mayanagi, and K. Morikawa, *Functional significance of octameric RuvA for a branch migration complex from Thermus thermophilus.* Biochem Biophys Res Commun, 2008. **366**(2): p. 426-31.
122. Ostendorp, T., et al., *Structural and functional insights into RAGE activation by multimeric S100B.* EMBO J, 2007. **26**(16): p. 3868-78.
123. Psachoulia, E. and M.S. Sansom, *Interactions of the pleckstrin homology domain with phosphatidylinositol phosphate and membranes: characterization via molecular dynamics simulations.* Biochemistry, 2008. **47**(14): p. 4211-20.
124. Bond, P.J. and M.S. Sansom, *Membrane protein dynamics versus environment: simulations of OmpA in a micelle and in a bilayer.* J Mol Biol, 2003. **329**(5): p. 1035-53.
125. Cronan, J.E. and P.R. Vagelos, *Metabolism and function of the membrane phospholipids of Escherichia coli.* Biochim Biophys Acta, 1972. **265**(1): p. 25-60.
126. Jensen, M.O. and O.G. Mouritsen, *Lipids do influence protein function-the hydrophobic matching hypothesis revisited.* Biochim Biophys Acta, 2004. **1666**(1-2): p. 205-26.
127. Haltia, T. and E. Freire, *Forces and factors that contribute to the structural stability of membrane proteins.* Biochim Biophys Acta, 1995. **1228**(1): p. 1-27.
128. Minetti, C.A. and D.P. Remeta, *Energetics of membrane protein folding and stability.* Arch Biochem Biophys, 2006. **453**(1): p. 32-53.
129. Brouillette, C.G., et al., *Structure and thermal stability of monomeric bacteriorhodopsin in mixed phospholipid/detergent micelles.* Proteins, 1989. **5**(1): p. 38-46.
130. Heyes, C.D. and M.A. El-Sayed, *The role of the native lipids and lattice structure in bacteriorhodopsin protein conformation and stability as studied by temperature-dependent Fourier transform-infrared spectroscopy.* J Biol Chem, 2002. **277**(33): p. 29437-43.
131. Haltia, T., et al., *Thermodynamic and structural stability of cytochrome c oxidase from Paracoccus denitrificans.* Biochemistry, 1994. **33**(32): p. 9731-40.
132. Morin, P.E., D. Diggs, and E. Freire, *Thermal stability of membrane-reconstituted yeast cytochrome c oxidase.* Biochemistry, 1990. **29**(3): p. 781-8.
133. Rigell, C.W. and E. Freire, *Differential detergent solubility investigation of thermally induced transitions in cytochrome c oxidase.* Biochemistry, 1987. **26**(14): p. 4366-71.
134. Yu, C.A., S.H. Gwak, and L. Yu, *Studies on protein-lipid interactions in cytochrome c oxidase by differential scanning calorimetry.* Biochim Biophys Acta, 1985. **812**(3): p. 656-64.
135. Thompson, L.K., J.M. Sturtevant, and G.W. Brudvig, *Differential scanning calorimetric studies of photosystem II: evidence for a structural role for cytochrome b559 in the oxygen-evolving complex.* Biochemistry, 1986. **25**(20): p. 6161-9.
136. Kleinschmidt, J.H., *Membrane protein folding on the example of outer membrane protein A of Escherichia coli.* Cell Mol Life Sci, 2003. **60**(8): p. 1547-58.
137. Zielinski, R., *Effect of Temperature on Micelle Formation in Aqueous NaBr Solutions of Octyltrimethylammonium Bromide.* J Colloid Interface Sci, 2001. **235**(2): p. 201-209.

138. Gorski, N., Kalus, J., *Temperature Dependence of the Sizes of Tetradecyltrimethylammonium Bromide Micelles in Aqueous Solutions.* Langmuir, 2001. **17**: p. 4211-4215.
139. Reiss-Husson, F.L., V., The Journal of Physical Chemistry, 1964. **68**: p. 3504.
140. Tanford, C., *The Hydrophobic Effect: Formation of Micelles and Biological Membranes*. 1973.
141. Zhang, J., et al., *Stopped-flow kinetic studies of sphere-to-rod transitions of sodium alkyl sulfate micelles induced by hydrotropic salt.* J Colloid Interface Sci, 2007. **316**(2): p. 796-802.
142. Lindman, B., *Non-Ionic micelles Grow with Increasing Temperature.* The Journal of Physical Chemistry, 1991. **95**(15): p. 6053-6054.
143. Briganti G, B.A., *Interfacial composition as a function of temperature in C12E6 and C12E8 micellar solutions.* Journal of Non-Cystalline Solids 1998. **235**: p. 704-708.
144. Grell E, L.E., Schneider R, Ilgenfritz G, Grillo I, von Raumer M *Phase Transitions in Non-Ionic Detergent Micelles.* Journal of Thermal Analysis and Calorimetry, 2002. **68**(2): p. 469-478.
145. Inayathullah, N.M., Jasmine, G.J., Jayakumar, R., *Effect of Osmolyte on the Micellization of SDS at Different Temperatures.* Langmuir, 2003. **19**: p. 9545-9547.
146. Lonostro, P., Gabrielli, G, *Temperature and Subphase Effects on Aliphatic Alcohol Films at the Air-Water-Interface* Langmuir, 1993. **9**(11): p. 3132-3137
147. Klammt, C., et al., *Cell-free production of integral membrane proteins on a preparative scale.* Methods Mol Biol, 2007. **375**: p. 57-78.